NBS SPECIAL PUBLICATION 683

U.S. DEPARTMENT OF COMMERCE / National Bureau of Standards

Technical Digest - Symposium on Optical Fiber Measurements, 1984

Sponsored by the National Bureau of Standards
in cooperation with the
IEEE Optical Waveguide Communications Committee
and the Optical Society of America.

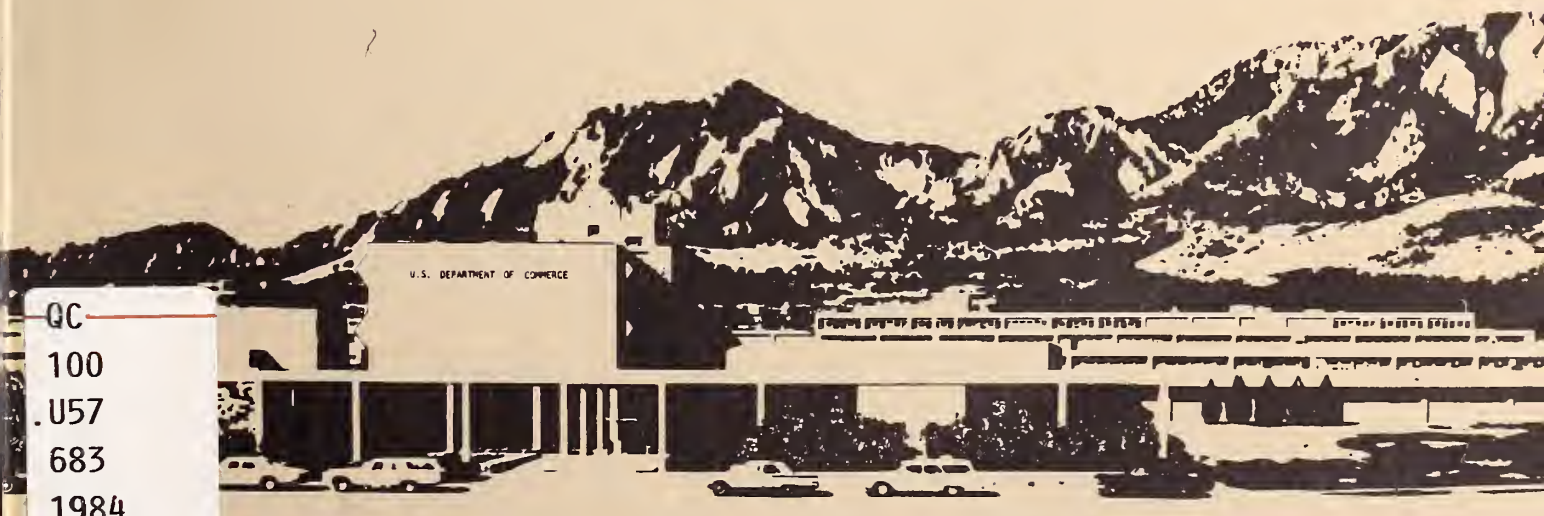

NATIONAL BUREAU OF STANDARDS

The National Bureau of Standards[1] was established by an act of Congress on March 3, 1901. The Bureau's overall goal is to strengthen and advance the Nation's science and technology and facilitate their effective application for public benefit. To this end, the Bureau conducts research and provides: (1) a basis for the Nation's physical measurement system, (2) scientific and technological services for industry and government, (3) a technical basis for equity in trade, and (4) technical services to promote public safety. The Bureau's technical work is performed by the National Measurement Laboratory, the National Engineering Laboratory, and the Institute for Computer Sciences and Technology.

THE NATIONAL MEASUREMENT LABORATORY provides the national system of physical and chemical and materials measurement; coordinates the system with measurement systems of other nations and furnishes essential services leading to accurate and uniform physical and chemical measurement throughout the Nation's scientific community, industry, and commerce; conducts materials research leading to improved methods of measurement, standards, and data on the properties of materials needed by industry, commerce, educational institutions, and Government; provides advisory and research services to other Government agencies; develops, produces, and distributes Standard Reference Materials; and provides calibration services. The Laboratory consists of the following centers:

Absolute Physical Quantities[2] — Radiation Research — Chemical Physics — Analytical Chemistry — Materials Science

THE NATIONAL ENGINEERING LABORATORY provides technology and technical services to the public and private sectors to address national needs and to solve national problems; conducts research in engineering and applied science in support of these efforts; builds and maintains competence in the necessary disciplines required to carry out this research and technical service; develops engineering data and measurement capabilities; provides engineering measurement traceability services; develops test methods and proposes engineering standards and code changes; develops and proposes new engineering practices; and develops and improves mechanisms to transfer results of its research to the ultimate user. The Laboratory consists of the following centers:

Applied Mathematics — Electronics and Electrical Engineering[2] — Manufacturing Engineering — Building Technology — Fire Research — Chemical Engineering[2]

THE INSTITUTE FOR COMPUTER SCIENCES AND TECHNOLOGY conducts research and provides scientific and technical services to aid Federal agencies in the selection, acquisition, application, and use of computer technology to improve effectiveness and economy in Government operations in accordance with Public Law 89-306 (40 U.S.C. 759), relevant Executive Orders, and other directives; carries out this mission by managing the Federal Information Processing Standards Program, developing Federal ADP standards guidelines, and managing Federal participation in ADP voluntary standardization activities; provides scientific and technological advisory services and assistance to Federal agencies; and provides the technical foundation for computer-related policies of the Federal Government. The Institute consists of the following centers:

Programming Science and Technology — Computer Systems Engineering.

[1]Headquarters and Laboratories at Gaithersburg, MD, unless otherwise noted; mailing address Washington, DC 20234.
[2]Some divisions within the center are located at Boulder, CO 80303.

Technical Digest - Symposium on Optical Fiber Measurements, 1984

Digest of a Symposium sponsored by the
National Bureau of Standards
in cooperation with the
IEEE Optical Waveguide Communications Committee
and the Optical Society of America

October 2-3, 1984
National Bureau of Standards
Boulder, Colorado 80303

Edited by
G.W. Day
D.L. Franzen

Electromagnetic Technology Division
National Engineering Laboratory
National Bureau of Standards
Boulder, Colorado 80303

U.S. DEPARTMENT OF COMMERCE, Malcolm Baldrige, Secretary

NATIONAL BUREAU OF STANDARDS, Ernest Ambler, Director

Issued October 1984

Library of Congress Catalog Card Number: 84-601092

National Bureau of Standards Special Publication 683
Natl. Bur. Stand. (U.S.), Spec. Publ. 683, 148 pages (Oct. 1984)
CODEN: XNBSAV

U.S. GOVERNMENT PRINTING OFFICE
WASHINGTON: 1984

For sale by the Superintendent of Documents, U.S. Government Printing Office, Washington D.C. 20402

PREFACE

The optical fiber industry continues to evolve and with it, research on the characterization of fiber and related components. The Digests of this Symposium and its predecessors in 1980 and 1982 reflect these changes.

In 1980 about 12 percent of the program dealt with singlemode fibers. In 1982 it was 25 percent and this year about 75 percent. Attenuation measurements appear to have been the major concern at the first meeting. Two years later the problem of predicting the bandwidth of concatenated links drew a large number of contributed papers. This year the measurement of chromatic dispersion is obviously a topic of prime concern. Several talks related to the use of fiber in coherent communications systems and in sensing applications point to the future.

The Symposium continues to draw contributions from around the world. The 25 contributed papers accepted by the committee come from 8 countries, as follows:

U.S.A. - 10,
U.K. - 5,
Finland - 2,
France - 2,
Germany - 2,
Japan - 2,
Italy - 1, and
The Netherlands - 1.

These represent about two-thirds of the papers submitted.

The National Bureau of Standards is indebted to the IEEE Optical Waveguide Communications Committee, the Optical Society of America, and members of the committee for their continued assistance in organizing this Symposium.

G. W. Day
D. L. Franzen
Boulder, Colorado
October 1984

Symposium Committee

D. L. Franzen, NBS, General Chairman
G. W. Day, NBS, Program Chairman
R. L. Gallawa, NBS
W. A. Gambling, Univ. of Southampton
W. B. Gardner, AT&T Bell Laboratories
M. C. Hudson, Raycom Systems
F. P. Kapron, ITT
W. F. Love, Corning Glass Works
S. Shimada, NTT
G. H. Sigel, Jr., NRL

CONTENTS

Measurements on Multimode Fibers

Instrumentation and Field Measurements

Single Mode Fiber Measurements, III

Single Mode Fibre Specification and System Performance

D B Payne, M H Reeve, C A Millar, C J Todd.

British Telecom Research Laboratories, Martlesham Heath, Ipswich, UK.

It can now be safely stated that single mode fibre is established as a viable transmission medium for communications networks.

The fibre types being adopted around the world as 'standard' have a nominal step index profile and are either of the matched cladding or depressed cladding designs. During the research and development phase of these fibres many different parameters, using a wide range of measurement techniques, were used to characterise the behaviour and increase our understanding of these fibre types. From this plethora of measured characteristics and measurement techniques it was necessary to distill the few essential characteristics and simplest measurement techniques necessary to ensure reliable and acceptable performance of the fibre in systems.

Two parameters are emerging that appear to be very good for specification purposes, these are a measurement of mode width and the cut off wavelength of the LP_{11} mode. These two parameters define a plane as in figure 1. Each point in the plane defines uniquely a fibre with nominal step index profile behaviour. As we move about the plane in any direction, problems of one sort or another can arise that will impair system performance. By measurement of such parameters as cabling loss susceptibility [1,2], dispersion characteristics [3,4] and fibre loss [5,6], together with splice loss analyses [7,8] and the need to avoid bimoded operation [9], bounds can be placed on the W, λco plane which will define a safe operating regime for this fibre type.

It is still a matter of some debate as to which measurement techniques and definitions should be used for the mode width and cut off parameters. At British Telecom we have favoured the offset splice technique [10] as a single measurement for both parameters. This technique has been adopted as one of two possible test methods in the draft CCITT recommendation [11] for the mode width parameter. However in order to obtain a measure of cut off wavelength it is necessary to use an offset splice technique that will measure mode width as a function of wavelength. Because it is obviously possible to set up an offset splice measurement system to measure the width parameter at the single wavelength required for the 'specification diagram' (the W, λco plane at 1300nm) alternative techniques may be desirable for the measurement of cut off wavelength. Because of this the CCITT recommendation proposes a method not involving the offset splice technique for cut off measurement, this method being instead based on power transmission techniques.

Fundamentally it does not matter which definition or measurement technique is used for mode width and cut off as long as they are self consistent. For example the measurement of mode width as made by the offset splice technique is a measure of the width of the field overlap integral. This measurement and definition of W is a measurement of a real physical parameter, no approximation is made at this stage. If the functional form of the field is known then this measured parameter can

be related to a width parameter of the real field and, for simple fibre structures, to models of the profile (when combined with the cut off measurement). As an example for fibres with near step index profile behaviour the fibre can be modelled via the width of the overlap integral (as measured by the offset splice technique) and cut off wavelength using the Marcuse relationship:

$$W = a(0.65 + 1.619V^{-1.5} + 2.879V^{-6})$$

$$\text{and } V = 2.405\lambda_{co}/\lambda = ka(N1^2 - N2^2)^{1/2}$$

From this relationship an equivalent step index profile can be derived in terms of the so called ESI parameters 'a' and 'Δn'. The measured parameters and measurement technique are a self consistent set linked via the ESI model of the fibre profile.

Theoretically there is only one defined value for the cut off wavelength of the second mode, that is when the mode index equals the cladding index. Unfortunately this theoretical cut off cannot be determined for a real fibre without recourse to some measurement technique eg. a measurement of the refractive index profile. Because different measurement techniques can give significantly different results for cut off wavelength the measurement has become somewhat controversial. However because there is only one value of cut off wavelength for the fibre it should be possible to relate all the various measurement methods to one reference method (regardless which one) via a definition of cut off, appropriate to the measurement method being employed.

The mode width and cut off wavelength parameters are being successfully used for the specification of near step index profile fibre. The use of the parameters could be extended to other profiles as long as W and λ_{co} are single valued functions of the parameters determining the fibre profile. This requirement of single valued functions for specification purposes could be used to define a class of fibre. Indeed if a fibre profile was sufficiently complex that normal manufacturing tolerances caused the general specification parameters (eg W and λ_{co}) to become multi-valued, then the fibre could be deemed to be unspecifiable interms of these general parameters. In this case it may be necessary to specify (and measure) the specific performance parameters for which the fibre was designed.

So far we have considered the fibre specification in isolation from the system specification. A fibre user is ultimately interested in minimising system cost consistent with adequate system performance. A notable feature of optical systems is that the parameters affecting system performance are all random variables with variances significant compared with means. This can mean that system performance and probabilities of system failure can be considerably influenced by different purchasing and planning strategies without recourse to any fine tuning of component specifications. This will be discussed further at the conference with examples, using a statistical model of the system, illustrating possible effects of different purchasing stategies.

If we consider the trends in optical technology and speculate about possible system requirements five to ten years hence one or two features of a future fibre begin to emerge.

It is very likely in the future that single mode fibre technology will reach into all parts of communications networks, from

long haul submarine and trunk systems to small networks within a single building. It would be desirable, though not essential, if the same fibre was used for all these networks, simply to increase economy of scale. On long haul systems there will be a continuing demand to increase range and capacity. Range could be limited by the power budget available and the system loss or dispersion problems. On short distance 'local' systems, range is not important but high channel number could be. To achieve this high channel number extensive wavelength multiplexing may be used. Also future systems, both long and short distance, may exploit coherent optical technology.

Dispersion effects were given a considerable amount of attention during the design of the 'first generation' monomode fibres (primarily single window fibre with nominal step index profile). It is more questionable that it will be an important system parameter for the next generation fibre. If the transmitted optical line width is determined by the message bandwidth then several Gb/s data rates are possible over 200-300 km of fibre even in the 1550 window, using present day fibre. For the forseeable future, dispersion is a device problem not a fibre problem. On the time scale of 5-10 years it is not unreasonable to postulate spectral control of sources with (if necessary) external modulation, giving line widths determined by the modulation applied. The necessity for exotic fibres with a primary aim of controlling dispersion properties, can therefore be considered unlikely. However beyond 'second generation' fibre when very high bit rate systems over very long distances could become practical, dispersion control in fibres may again intrude.

The more important parameters in a future fibre will have more to do with loss and possible power budgets, the latter being determined ultimately by non-linear effects limiting optical power densities in the fibre. The loss of the link will be determined by a combination of fibre loss, splice loss, and cabling loss. Fibre designs that reduce simultaneously all these component losses would be of interest, for example profiles that increase the width of the overlap integral while constraining the field shape to minimise cabling loss would be valuable. If the profiles required to achieve these results are complex then it may well be that simple two parameter specifications will not be adequate and specification of the variables of interest will have to be made separately.

For multi-channel coherent systems polarisation maintaining fibres may be necessary. It may well be that this requirement will be the most important in determining a new fibre design if dispersion is not important and loss can only be marginally reduced by fibre design. This will add a whole new dimension to the fibre specification.

The near step index profile fibre is now being installed in quantity into various communications networks around the world and unless there is a very clear overiding advantage the administrations involved will be very unwilling to consider changing to a new fibre design for some considerable time (except maybe for small specialist requirements). When considering totally new fibres therefore, we are probably thinking in terms of systems application at least five to ten years hence. On this time scale it is unlikely that the system requirements that determined the current fibre specification will still apply.

Acknowledgements.

The authors wish to thank J V Wright and K Blow for useful discussions and the Director of Research, British Telecom for permission to publish this work.

References.

1. S Hornung and M H Reeve Elec. Lett 17, 774 (1981)

2. A D Pearson, F D Lazay, W A Reed, M J Saunders Proceedings ECOC Canes 1982.

3. B P Nelson and S Hornung Elec Lett 18, 270 (1982)

4. U C Peak, G E Peterson, A Carvale Applied Optics Vol 21, No.19 1 Oct 1982

5. M H Reeve, C A Millar Proceedings ICC 1984, Amsterdam, Vol 3, p1056

6. P D Lazay and A D Pearson Technical Digest, OFC 1982, Phoenix, THCC2

7. D Marcuse, Bell Sys. Tech. Journal, Vol 56, No.5, May/June 1976.

8. D B Payne and D J McCartney Proceedings ICC 1984, Amsterdam, Vol 3, p1075

9. K Petermann Elec Lett 15, 706 (1979)

10. C A Millar Technical Digest, OFC 1982, phoenix, THEE3

11. CCITT Recommendation G652, Study Grp xv, Geneva, May 1984.

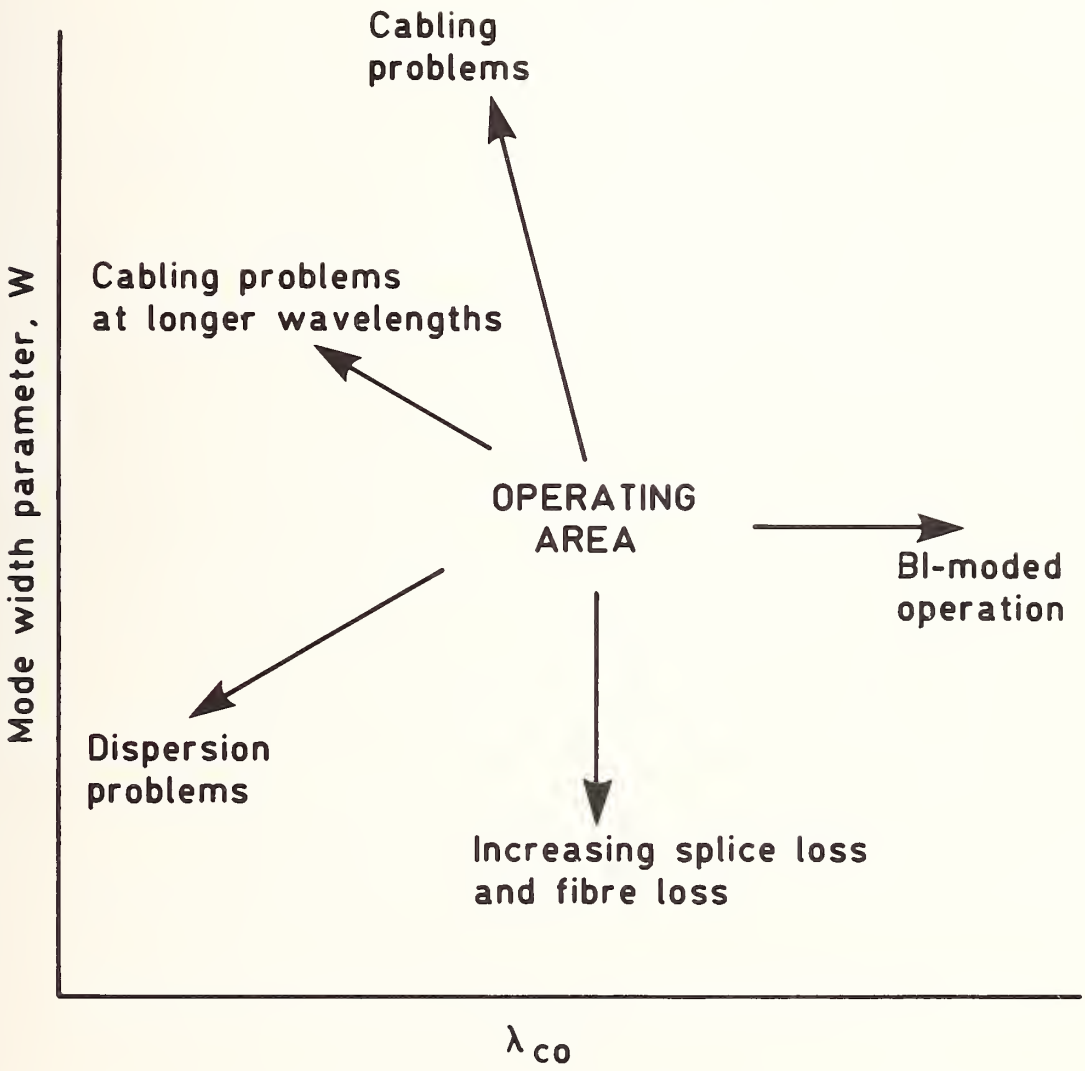
Cabling
problems
Cabling problems
at longer wavelengths
OPERATING
AREA
Bi-moded
operation
Dispersion
problems
Increasing splice loss
and fibre loss
Mode width parameter, W
λco

FIGURE 1

Effective Cut-Off Wavelength for Single-Mode Fibers: The Combined Effect of Curvature and Index Profile.

V. S. Shah
Bell Communications Research, Inc.
Crawfords Corner Road
Holmdel, New Jersey 07733

SUMMARY

In single mode transmission systems, the effective cut-off wavelength is an important design parameter separating the single-modal and bi-modal regime in an optical fiber. Controlling the effective cut-off wavelength instead of the theoretical cut-off wavelength makes the design less sensitive to the various loss mechanisms which always exist in a practical system. In general, the effective cut-off wavelength is found to be somewhat shorter than the theoretically predicted value, [1-3] resulting in a more robust design that allows the system to operate at a higher V value and thereby confining the fundamental mode more tightly to the core. The effective cut-off wavelength for use in the system should be short enough to attenuate the higher-order mode sufficiently to preclude modal noise so as not to degrade the signal-to-noise ratio of the system. [4]

One of the methods being used to determine the effective cut-off wavelength is the bend induced loss [5] (transmitted power) method. Since in this method, the results depend upon the length of the fiber as well as the bend diameter, CCITT study group XV recently recommended that 2 meter length of fiber with a single loop of 28 cm diameter be used.

In light of the importance of the effective cut-off wavelength in system design and the need to standardize its range, a study program is in progress in our Laboratory to gain further understanding of the dependence of the effective cut-off wavelength on various parameters. Initial results of the measurement of the effective cut-off wavelength (with the bend diameter as a parameter) on three fibers are reported here. One fiber is of matched cladding design while the other two fibers are of depressed cladding design (Figure 1). The measurements were made using a

2 meter long fiber. For each fiber , the transmitted power levels for several radii of curvature R are compared with that for the fiber with a small single loop 2.5 cm in diameter. The effective cut-off wavelength is determined to be the wavelength above which the small loop introduces a loss of less than .1db in the output power.

Figure 2 shows the results of the above measurement made on the fibers. The result for fiber #1 (matched cladding design) shows that as expected, the effective cut-off wavelength shifts towards smaller values (due to the increasing radiation loss) as the radius of curvature R=D/2 decreases. However, for the other two fibers, (depressed cladding design) the effective cut-off wavelength increases at first and then decreases as R decreases from an initial large value.

Using the procedure similar to that employed by Marcuse [6] to calculate the radiation loss of LP_{01} mode due to a constant curvature in a depressed cladding fiber, a radiation loss formula is being developed for LP_{11} mode in a depressed cladding fiber to explain the experimental observation. We will report and discuss the results of such calculation (which is based on an infinite outer cladding model). Additional measurement data will also be presented.

ACKNOWLEDGEMENT

The author would like to thank P. Kaiser and W. C. Young for their encouragement and helpful discussions.

REFERENCES

[1] W. T. Anderson, "Measuring the Effective Cut-Off Wavelength of a Single-Mode Fiber - The Effect of Fiber Length," Conf. on Precision Electromagnetics Meas. Digest, L-12 (Boulder, June 1982)

[2] P. D. Lazay, "Effect of Curvature on the Cut-Off Wavelength of Single Mode Fibers," Tech Digest Symp. Opt. Fiber Meas., 93 (Boulder, Oct. 1980)

[3] G. W. Tasker, et al., 'Low-Loss Single-Mode Fibers with Different B_2O_3 - SiO_2 Compositions," Appl. Opt., 17, 1836 (1978).

[4] N. K. Cheung and P. Kaiser, 'Modal Noise in Single-Mode Fiber Transmission System," to be published in ECOC on Opt. Comm. '84, Stuttgart.

[5] Y. Katsuyama, et. al. 'New Method for Measuring V-Value of a Single-Mode Optical Fiber," Elect. Lett., 12, 699 (1976)

[6] D. Marcuse, 'Inference of Curvature on the Losses of Double Clad Fibers," Appl. Opt., 21, 4208 (1982).

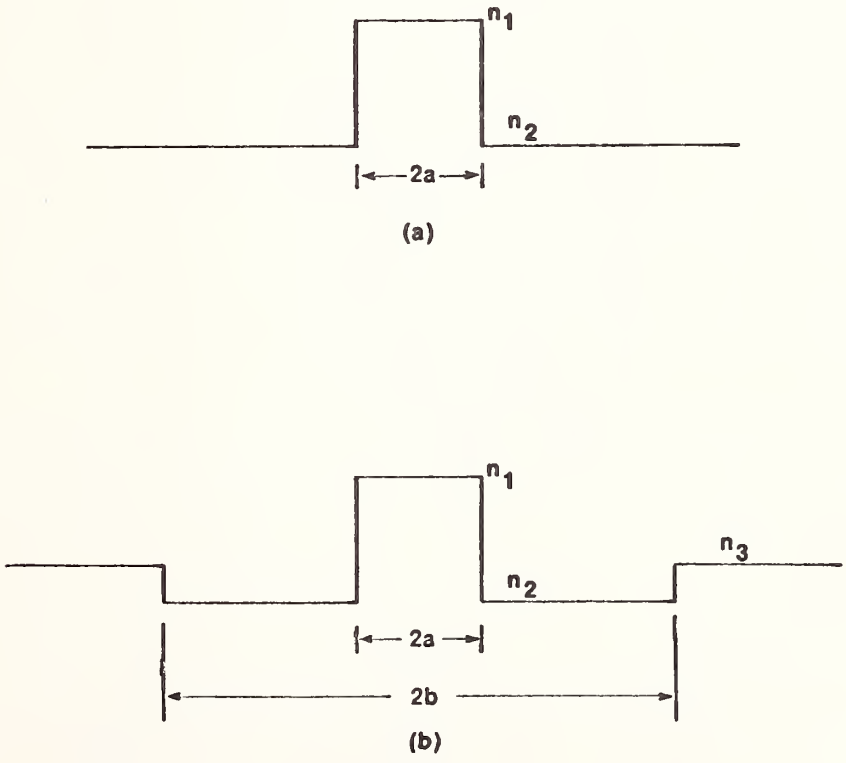

Fig.1 Fiber design (a) Matched cladding; (b) depressed cladding

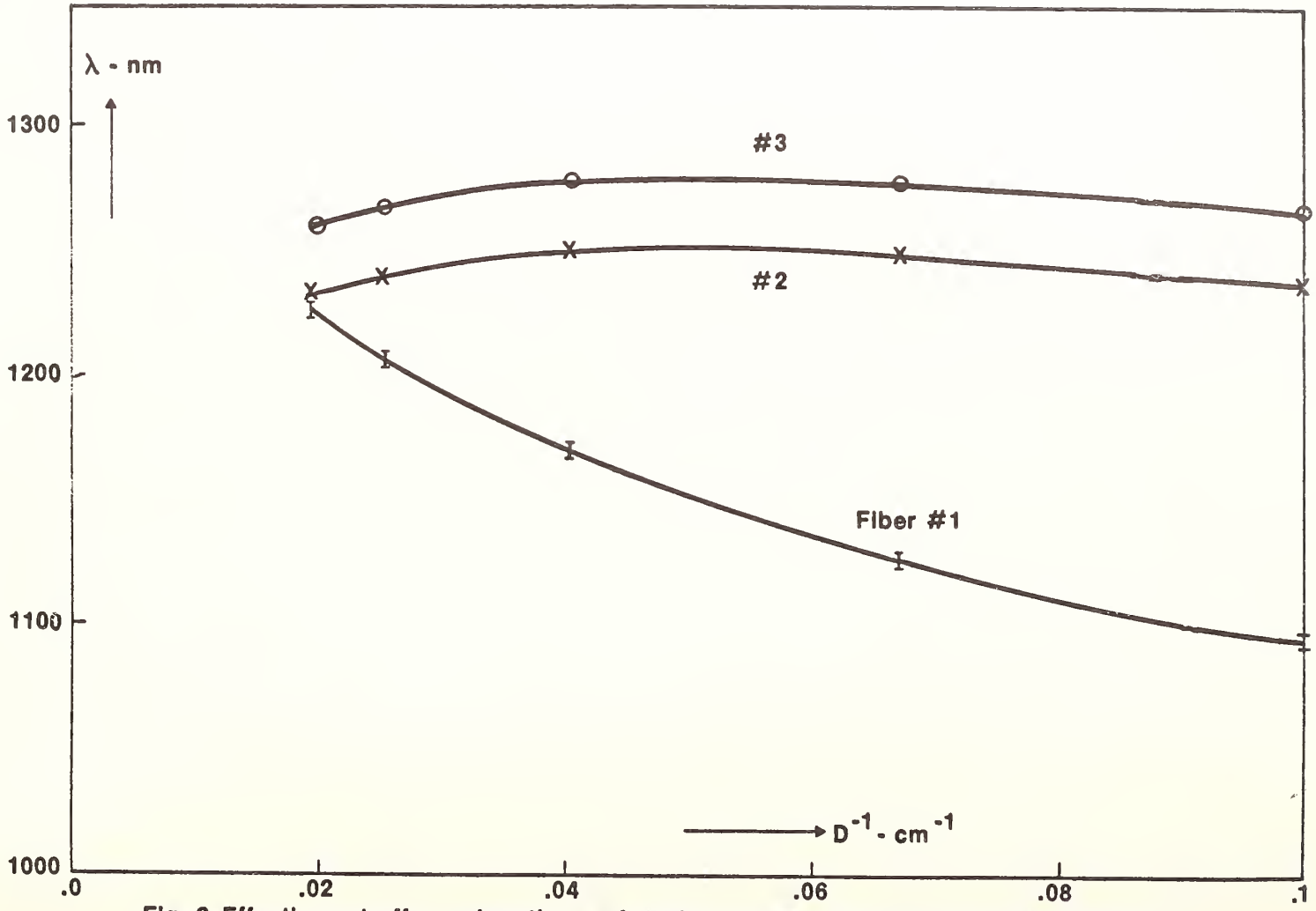

Fig. 2 Effective cut-off wavelength as a function of the reciprocal of the bend diameter.

LENGTH AND CURVATURE DEPENDENCE OF EFFECTIVE CUTOFF WAVELENGTH AND LP_{11}-MODE ATTENUATION IN SINGLE-MODE FIBERS

H.T. Nijnuis, K.A.H. van Leeuwen

Dr. Neher Laboratorium, PTT
P.O. Box 421, 2260 AK Leidschendam
The Netherlands

The cutoff phenomenon of the next higher order (LP_{11}) mode in single-mode fibers is best described by the wavelength-dependent attenuation coefficient of the LP_{11}-mode (α_{11}). This coefficient also depends on the geometrical condition of the section of fiber under consideration. The simple case of a fiber, bent to a constant radius of curvature, is sufficient to model the fiber in most practical applications. Therefore, the specification of α_{11} as a function of wavelength (λ) and radius (R) generally provides a satisfactory operational description of the cutoff behavior.

It is currently common however, to describe the cutoff in terms of an effective cutoff wavelength (λ_{ce}), defined as the wavelength above which there is (practically) no light transmitted in the LP_{11}-mode through a section of fiber. Making this definition strict by requiring a minimum total attenuation of the LP_{11}-mode in the studied fiber section, it is clear that λ_{ce} will depend on the length of the fiber section (L) as well as on its geometrical condition. It can easily be shown that with this definition a description in terms of the function $\lambda_{ce}(L,R)$ is completely equivalent to the description by the function $\alpha_{11}(\lambda,R)$.

The specification of a single number, e.g. the effective cutoff wavelength of a section of fiber of specified length under specified conditions measured according to the CCITT-recommendations[1], usually does not provide enough information to determine e.g. whether modal noise may become a problem in a specific situation. However, determination of the complete function $\lambda_{ce}(L,R)$ (or $\alpha_{11}(\lambda,R)$) for every reel of fiber to be used is, of course, not realistic. Thus it would be attractive to obtain some empirical "rules-of-thumb" giving the length- and curvature dependence of a fiber with a given type of index-profile, leaving only one cutoff wavelength to be determined for each individual reel as is common practice already.

In this contribution we report on measurements of the length and curvature dependence of the effective cutoff wavelength in a number of single-mode fibers

with various types of index-profile, aimed at establishing such empirical rules. The results indicate approximately linear relations between the cutoff wavelength and the logarithm of the fiber length (as has been found before[2]), and between cutoff wavelength and the inverse of the radius of curvature to which the fiber is bent.

The experimental apparatus consists of a standard set-up used for wavelength-dependent attenuation measurements. The light of a filament lamp is filtered by a monochromator and coupled into the test fiber through a microscope objective. Care is taken to overfill both LP_{01} and LP_{11} modes. Light emerging from the far end of the fiber is detected with a pigtailed InGaAs photodiode. For fibers having non-stripping primary coatings, cladding mode strippers are used both at the input- and output end of the test fiber.

The total attenuation of the LP_{11} mode as a function of wavelength is determined from three wavelength scans of the monochromator. First the detector signal is recorded with the test fiber wound a number of turns (1 to 20) around a spool with the desired radius, second, the number of turns is reduced to either 0 or 1, the excess fiber removed and the signal is again recorded as a function of wavelength and third, a few small loops (1 to 2 cm radius) are inserted in the fiber at the detector end and the last scan is made. The number and radius of these loops are chosen so as to remove all light in the LP_{11} mode in the wavelength region of interest.

Designating the three recorded detector signal vs. wavelength curves $P_1(\lambda)$, $P_2(\lambda)$ and $P_3(\lambda)$ respectively, the attenuation of the LP_{11} mode (in dB) is calculated:

$$-10\ ^{10}\log((P_1(\lambda)-P_3(\lambda))/(P_2(\lambda)-P_3(\lambda)))\quad .$$

Dividing the attenuation by the length of the fiber section that has been removed in the second step of the procedure, $\alpha_{11}(\lambda)$ curves result. An effective cutoff wavelength is obtained by determining the wavelength at which the attenuation equals 3 dB (arbitrary value chosen for convenience).

Of the tested fibers, first the cutoff wavelength has been determined at 14 cm radius of curvature for a number of fiber lengths ranging from 1 to 20 meters. Afterwards, the cutoff wavelength for three meters of fiber bent to a number of radii ranging from 2.25 to 14 cm has been determined.

The results for four studied fiber samples are shown in Figs. 1-4, in which the effective cutoff wavelength is plotted against the logarithm of fiber length and against the inverse of the radius of curvature. Best-fit straight lines through the data points are also shown.

The straight lines in Figs. 1-4 correspond to a simple three-parameter empirical formula for the effective cutoff wavelength:

$$\lambda_{ce}(L,R) = \lambda_0 - a \log(L) - b/R$$

with λ_0 the cutoff wavelength of 1 meter of stretched fiber, and a and b coefficients representing the length-dependence and bending-sensitivity of the cutoff wavelength respectively.

Table 1 summarizes the best-fit parameters for the 4 studied fibers.

SAMPLE	PROFILE TYPE	λ_0(nm)	a(nm/decade)	b(nm/cm^{-1})
1	matched cladding	1139(5)	41(5)	617(22)
2	matched cladding	1227(7)	50(12)	564(28)
3	strongly depressed cladding	1282(6)	74(8)	375(14)
4	slightly depressed cladding	1166(12)	35(14)	375(53)

TABLE 1 Best-fit parameters for studied fibers. Errors are statistical.

Both length-dependence and bending-sensitivity are seen to vary by a factor of two between fibers. This stresses the impossibility to describe the cut-off of the LP_{11} mode by a single parameter. It is interesting to note that the coefficients a and b as determined for the two matched-cladding type fibers (supplied by different manufacturers) are nearly equal. This suggests the possibility of estimating these parameters on the basis of the index-profile, which possibility, if confirmed, will be clearly of considerable practical value.

It is obvious from Table 1 that the cutoff wavelength in both depressed-cladding fibers does not depend as strongly on the curvature of the fiber as in both matched-cladding fibers. This can be understood by assuming the dominant loss mechanism for the LP_{11} mode to be different for both types of index-profile ("tunneling" of light from the core to the outer cladding[3] in depressed-cladding fibers, and bending losses in matched-cladding fibers).

A consequence of the weak curvature dependence of the LP_{11}-mode attenuation in depressed-cladding fibers is, that insertion of a single loop of 2 cm radius in the fiber for the removal of the LP_{11} mode as recommended by the CCITT[1] is not sufficient.

References

(1) CCITT - COM XV-289-E - Draft recommendation G.652
(2) Anderson, W.T. and Lenahan, T.A.: J. of Lightwave Technology LT-2, 238 (1984)
(3) Jeunhomme, L.B.: Single-mode fiber optics (1983) (New York: Marcel Dekker)

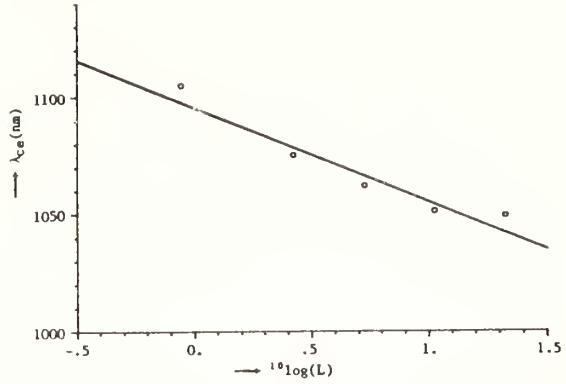

Figure 1[a]: Effective cutoff wavelength vs. the logarithm of fiber length (in meters). Fiber sample 1.

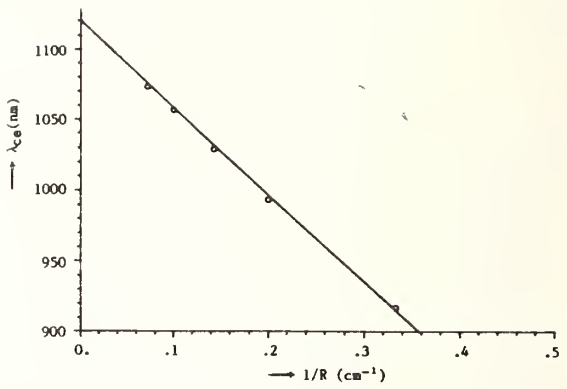

Figure 1[b]: Effective cutoff wavelength vs. the inverse of radius of curvature. Fiber sample 1.

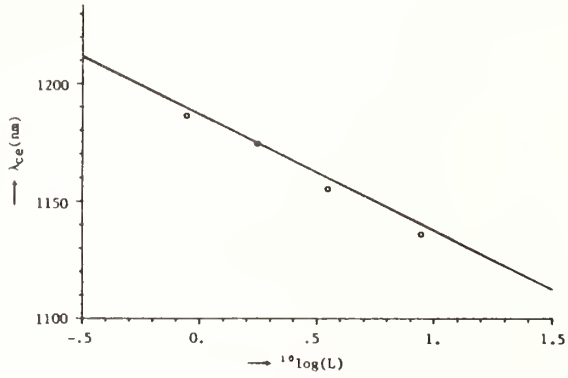

Figure 2[a]: Effective cutoff wavelength vs. the logarithm of fiber length (in meters). Fiber sample 2.

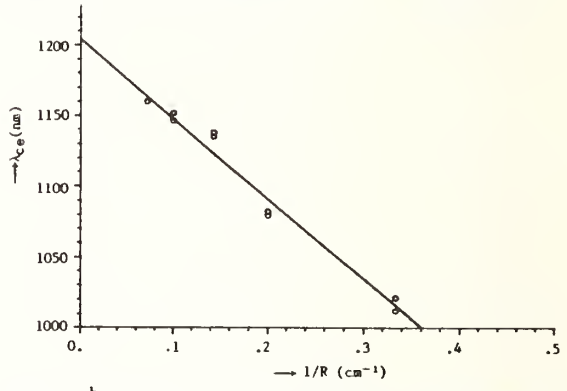

Figure 2[b]: Effective cutoff wavelength vs. the inverse of radius of curvature. Fiber sample 2.

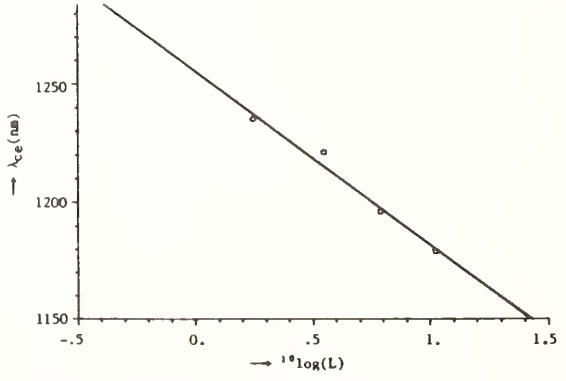

Figure 3[a]: Effective cutoff wavelength vs. the logarithm of fiber length (in meters). Fiber sample 3.

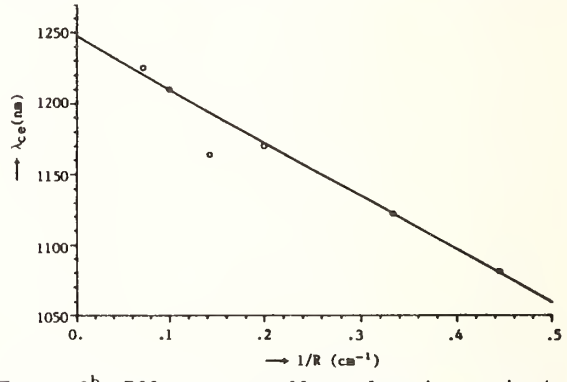

Figure 3[b]: Effective cutoff wavelength vs. the inverse of radius of curvature. Fiber sample 3.

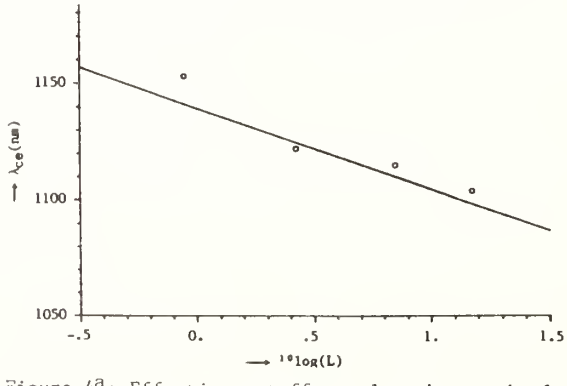

Figure 4[a]: Effective cutoff wavelength vs. the logarithm of fiber length (in meters). Fiber sample 4.

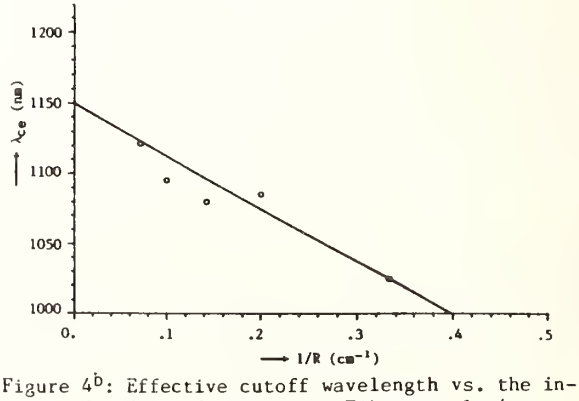

Figure 4[b]: Effective cutoff wavelength vs. the inverse of radius of curvature. Fiber sample 4.

CUTOFF WAVELENGTH AND MODAL NOISE IN SINGLE-MODE FIBER SYSTEMS*

N. K. CHEUNG and P. KAISER

BELL COMMUNICATIONS RESEARCH, INC.,
HOLMDEL, NEW JERSEY 07733 U.S.A.

In practical single-mode fiber communication systems one generally distinguishes between the theoretical cutoff wavelength λ_{th} of the first higher order mode, and the effective cutoff wavelength which may be substantially shorter than λ_{th} by as much as 100 to 200 nm. The theoretical cutoff wavelength is computed from the refractive index distribution of the core, and its value is obtained experimentally with short, straight fiber sections (say, on the order of 1 cm). Near the theoretical cutoff wavelength the LP_{11} mode is highly attenuated, and since its relative intensity depends strongly on fiber length and curvature, single-mode fibers can actually be operated slightly in the multimode domain [1]. The effective cutoff wavelength is therefore defined for a fiber of a specific length deployed with a certain bend radius. While in the past different combinations of such parameters have been used for this purpose [2] -- making a meaningful comparison of cutoff wavelength data originating in different laboratories difficult -- most recently an agreement has been reached to determine the effective cutoff wavelength with a 2 meter long single-mode fiber containing a 28 cm-diameter loop [3].

The challenge arises to properly choose the effective cutoff wavelength relative to the systems operating wavelength, while considering practical cabled-fiber lengths deployed with particular bending radii. In this regard, it should be noted that the effective cutoff wavelength was found to decrease logarithmically with fiber length, with a reduction of 20 to 30 nm per decade of length (in meters) having been observed for certain types of fibers [4] (i.e. the effective cutoff wavelength of a 1 km long fiber is approximately 60 to 90 nm shorter than that of a 1 m fiber section). Similarly, the effective cutoff wavelength typically decreases with curvature for matched-cladding fibers, but has much less dependence on curvature for depressed-cladding fibers [5].

In order to avoid multimode and associated modal noise and systems degradation effects [6], it appears prudent to choose the cutoff wavelength as low as possible with respect to the 1.3 μm operating wavelength region. However, a short

---

*) Part of this work was performed while the authors were with A.T.&T. Bell Laboratories.

cutoff wavelength results in weaker guidance of the fundamental mode in the 1.55 μm wavelength region, with accompanying increased sensitivity of such fibers towards macro-bends and micro-bend-induced cabling losses. Since it is desirable to maintain lowest losses in the 1.55 μm wavelength region, the cutoff wavelength has to be optimized such as to avoid modal noise effects in the 1.3 μm region, and to minimize the sensitivity of the fundamental mode towards macro- and micro-bend-induced excess losses in the 1.55 μm region.

In this paper we report on the observation of modal noise effects for different fiber interconnection schemes containing intentionally overmoded fiber sections [7]. Connectorized fiber sections of length L and cutoff wavelengths λ_{C2} were inserted between the laser pigtail and another jumper cable with cutoff wavelengths λ_{C1} (Fig. 1). λ_{C1} was measured as described above, and was chosen to be 1.24 μm throughout. The laser wavelength λ_L satisfied the condition $\lambda_{C1} < \lambda_L < \lambda_{C2}$. With λ_L = 1.26 μm, modal noise was readily observed for 1 m long interconnection cable sections having λ_{C2} >1.31 μm, and with the overmoded fiber deployed straight (Fig. 1(a)). The noise was due to the mode-partitioning of the multi-longitudinal-mode laser employed resulting in the fluctuation of the coupling between the LP_{01} and LP_{11} modes at the two joints of the central jumper. The modal noise disappeared when a 2.5 cm diameter loop was introduced into the central jumper (Fig. 1(b)), or when the jumper was removed (Fig. 1(c)). A typical power penalty measurement performed for a 1 m long fiber with a cutoff wavelength of 1.46 μm deployed straight is shown in Fig. 2. For a longer fiber section L of 30 m deployed with a diameter of 35 cm or a section L of 1 km wound on a 15 cm spool, no power penalty was observed in spite of the high 1.46 μm cutoff wavelength (Fig. 3). It is important to note that modal noise has also been observed when the fiber used in the laser pigtail has a high cutoff wavelength λ_{C2} relative to λ_{C1} and λ_L as shown in Fig. 1(d).

In conclusion, we have demonstrated that single-mode fiber systems can be operated well above the effective cutoff wavelength provided the fibers are sufficiently long, or are deployed with appropriate bends. Cutoff wavelengths of 1.31 μm have been used successfully in previous single-mode fiber system experiments where the laser wavelength was as low as 1.272 μm [8], and fibers with cutoff values as high as 1.46 μm have been used in conjunction with 1 km long fiber sections in the experiments described in this paper. In order to leave some margin for laser wavelength variations and wavelength measurement tolerances, cutoff

values for outside plant fibers on the order of 1.35 μm are considered to be readily usable. In case of shorter fiber sections such as pigtails, interconnect cables, and repair lengths, mode filters in the form of bends or loops with suitable radii can be introduced to sufficiently attenuate the first higher order mode. On the other hand, mode filters are not required if the cutoff wavelength of short fibers is chosen lower than that of the outside plant fiber, say, by approximately 100 nm.

Acknowledgment is given to P. Glodis of A.T.&T. Bell Laboratories who supplied the fibers used in this experiment.

REFERENCES

[1] P. Kaiser et al, Topical Meeting on Optical Fiber Fiber Transmission, Technical Digest, Williamsburg (1977)
[2] W. T. Anderson, Conference on Precision Electromagnetic Measurements, L-12, Boulder (1982), IEEE Cat. No. 82CH1737-6
[3] CCITT SGXV Recommendation G.652, Geneva (1984)
[4] Y. Kitayama and S. Tanaka, OFC´84, Tun 14, New Orleans (1984)
[5] V. Shah, Symposium on Optical Fiber Measurements, Boulder (1984)
[6] S. Heckmann, Electron Lett., 17, p.499 (1981)
[7] N. K. Cheung and P. Kaiser, ECOC´84, Stuttgart (1984)
[8] P. Kaiser et al, IOOC´83, 27C2-4, Tokyo (1983)

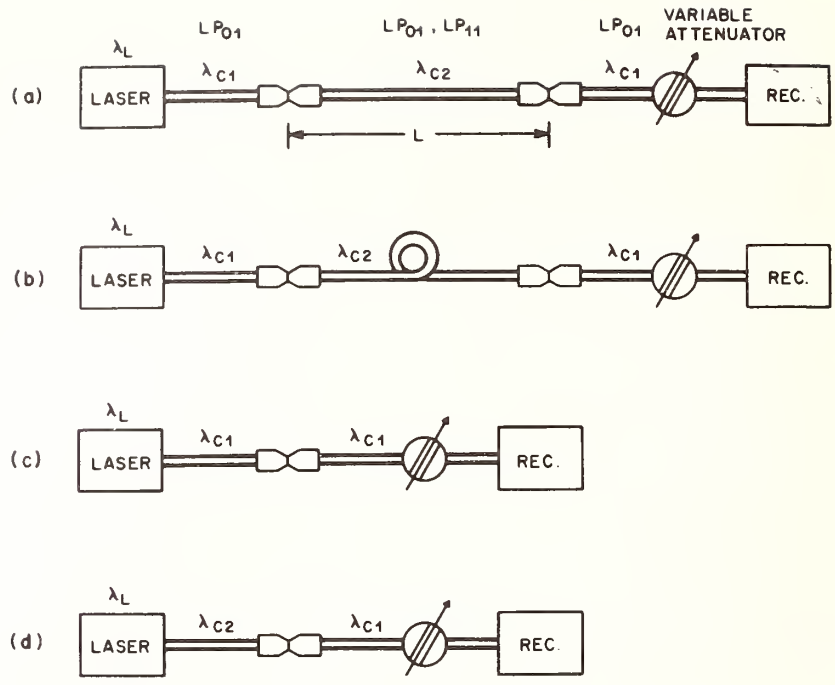

Fig. 1 Different interconnection schemes to study modal noise in single-mode fibers $\lambda_{C1} < \lambda_L < \lambda_{C2}$

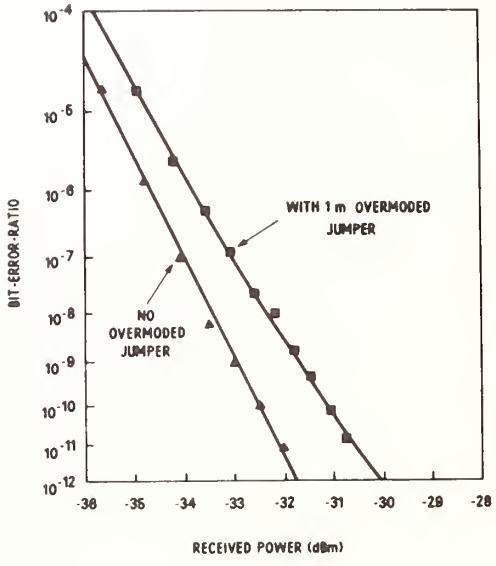

Fig. 2 Bit-error-ratio curves with and without overmoded jumper for config. shown in Fig. 1(a), λ_L= 1.26 μm, λ_{C1}= 1.24 μm, λ_{C2}= 1.46 μm, and L = 1 m

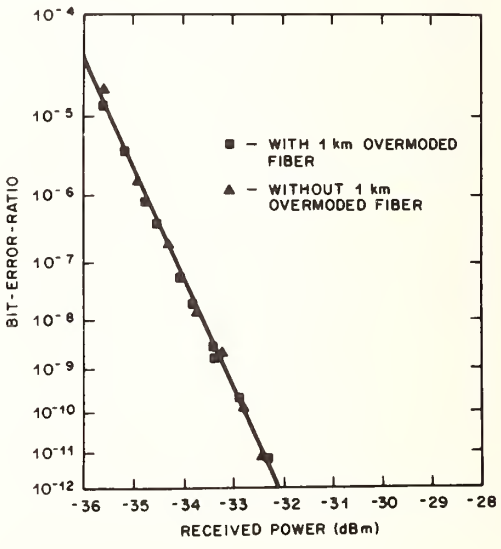

Fig. 3 Bit-error-ratio curves with and without 1 km of overmoded fiber, same wavelength combinations as in Fig. 2

ISSUES IN THE CHARACTERIZATION OF COHERENT OPTICAL COMMUNICATIONS SYSTEMS

Takeshi Ito

Yokosuka Electrical Communication Laboratory, NTT
1-2356 Take, Yokosuka-shi, Japan

These few years, research on coherent optical transmission systems has been prosecuted enthusiastically by a couple of laboratories. It raises up world-widely the "revival" of an interest in coherent systems. The present major interest is to seek ever more sensitive receivers, ever longer repeater spans, ever greater transmission capacities and so on. Laying stress on the sensitivity of a receiver, this paper compares a coherent system with a direct detection system, referring to published or reported experimental data, and describes the future research items.

As well known, theoretical shot-noise bounds for a predetermined error rate are almost equal between coherent and direct detection systems, if a quantum detector is used(1). One of appeals for coherent systems seems that the sensitivity could easily reach the shot-noise bound, compared with direct detection systems. The other is that optical angular modulation(FSK, PSK) suppress the stimulated Brillouin scattering so that a greater power could be launched into a fiber(2).

Receiver sensitivity and transmitting optical power that is obtainable at a 1.5 micron wavelength are shown in Fig.1, including an expected sensitivity and observed data for direct detection systems. Here, photodetector sensitivity is assumed to be close to Si-detector sensitivity at 0.8 micron wavelengths. The PSK modulation-homodyne

detection scheme will improve the sensitivity more than 10dB over the IM direct detection scheme.

Features of coherent transmission experiments conducted so far are summarized in TABLE I (3)-(8). All of fundamental modulation-detection schemes have been examined at a bit rate from 100 to 200Mb/s, at wavelengths from 0.82 to 1.52 microns. The achieved receiver sensitivity ranges from 70 to 1300 photons per bit. Using a He-Ne gas laser as a signal oscillator, its sensitivity reaches nearly the theoretical shot-noise bound. On the other hand, if a laser diode is directly modulated, few differences are found between the results summarized in the table and an attainable sensitivity at the same bit rate in a direct detection system at the present time. In most those experiments, there appears no floor phenomenon in the relationship between the received optical power and a bit error rate. However, a bit error rate less than 10^{-9} has never been measured. More stable operations of oscillators and control systems such as an AFC and a PLL circuit could realize a bit error rate less than the above-mentioned value.

Major research items are summarized in TABLE II. Both a high speed direct detection system and a coherent detection system need stabilized single-frequency light sources. However, the requirement for coherent system light sources is significantly different from the requirement for the light sources in a direct detection system. A 100Mb/s PSK coherent system requires, for example, less than 1MHz light source spectrum width. The above performance is required for a local oscillator in a receiver as well as for a signal oscillator in a transmitter. Against

the above requirement, a conventional single-frequency laser diode, such as a DFB laser diode, has a comparatively wide spectrum width of 50 to 100MHz at 1.3 to 1.55 micron wavelengths(9). An automatic frequency control(AFC) circuit using a Fabry-Perot etalon or moleqular absorption has achieved frequency stability less than 1MHz per a few minutes up to two hours(10). However, a practical coherent system needs long term frequency stability as well as short term stability.

To realize the above-mentioned sophisticated modulation and detection techniques, a coherent system requires modulators, isolators, directional couplers and other components for optical circuitry in addition to single- frequency narrow-spectrum-width laser diodes. It is very important to suppress thoroughly insertion losses of those components in order to establish a repeater gain that could be obtained by sensitivity improvement and transmitting optical power increase.

Polarization holding through transmission medium is desirable because of polarization sensitivity in the detection. Various types of polarization holding fiber have been developed so far(11). On the other hand, polarization control is inevitable if a conventional single-mode fiber is used as a medium, because a polarization state changes due to the variation of circumstances such as an atmospheric temperature. Polarization change, however, is observed to be very slow. For example, polarization axis rotated at maximum at a rate of 20 degrees per minute for a submarine-cabled fiber of 10km layed at the bottom of the sea(12). In fact, polarization is manually compensated to match that the local oscillator in the experiments summarized in TABLE I.

In conclusion, in addition to the characterization of fiber polarization performance and modulation and detection component performance, it is very important, at present, to characterize a fine structure of laser diode spectrum as well as its frequency stability, in order to clarify its residual AM, FM and/or PM noise characteristics and to demonstrate the feasibility of a coherent system using a laser diode. It is because a laser diode seems to be mostly preferable from a practical point of view. The research on these sophisticated optical transmitters and receivers will make clear great scope for ever longer repeater-span transmission systems and/or ever more frequency-division-transmission systems. This may accelerate optical technology towards the shot-noise limit or beyond it.

Acknowledgements The author wishes to gratefully acknowledge the sensible and occasionally shrewd and suggestive comments from Drs. Kiyoshi Nosu, Ikutaro Kobayashi and Yoshihisa Yamamoto. Acknowledgement is also due to Drs. Sadakuni Shimada and Masaki Koyama for their encouragement.

References

(1) Y.Yamamoto, IEEE J.Quantum Electron., vol.QE-16, no.11, Nov. 1980.
(2) D.Cotter, Electronics Letters, vol.18, no.12, June 1982.
(3) M.Shikada et al, Electronics Letters, vol.20, no.4, Feb. 1984.
(4) D.J.Maylon et al, ibid., vol.19, no.4, Feb. 1983.
(5) S.Saito and Y.Yamamoto, presented at 1983 Nat. Conven. IECE Japan (in Japanese), March 1983.
(6) K.Emura et al, ibid. no.14, July 1983.
(7) R.Wyatt, T.G.Hodgkinson and D.W.Smith, Electronics Letters, vol.19,
(8) D.J.Maylon, ibid., vol.20, no.7, March 1984.
(9) Y.Yamabayashi and M.Saruwatari, presented at 1984 Nat. Conven. IECE Japan(in Japanese), March 1984. Aug. 1982.
(10) T.Okoshi, IEEE Trans. Microwave Theory Tech., vol.MTT-30, no.8,
(11) Y.Sasaki and J.Noda, presented at 1983 Nat. Conven. IECE Japan (in Japanese), March 1983. (in Japanese), March 1984.
(12) T.Imai and K.Yanagimoto, presented at 1984 Nat. Conven. IECE Japan

TABLE I FEATURES OF COHERENT TRANSMISSION EXPERIMENTS

Mod. Scheme		ASK		FSK		PSK	
Det. Scheme		Heterodyne	Homodyne	Heterdyne/ Freq. discri.	Heterodyne/ Envelope	Heterodyne	Homodyne
Bit Rate (Mb/s)		100	140	200	100	140	140
Wavelength (microns)		1.3	1.52	0.825	1.28	1.52	1.52
Compo-nent	Medium, Length(km)	SMF, 30	-	-	-	SMF, 109	Cabled SMF, 30
	Sig. Osc.	DFB-LD	He-Ne	LD	DFB-LD	He-Ne	He-Ne
	Modulator	$LiNbO_3$ wave-guide mod.	$LiNbO_3$ wave-guide mod.	(Direct mod. f=400MHz)	(Direct mod. f=1.5GHz)	$LiNbO_3$ wave-guide mod.	$LiNbO_3$ wave-guide mod.
	Loc. Osc., Pow.(dBm)	DFB-LD, -7.3	Branch of S.O. -24	LD, -5	DFB-LD, -3.2	LD, -23	He-Ne, -30
	Detector	Ge-APD	PIN-FET	Si-APD	PIN-FET	PIN-FET	PIN-FET
	Others	Isolator, Pol. contl., Dire. coupl.	Pol. contl., Direc. coupl.	Isolator, Direc. coupl.	Isolator, Direc. coupl.	Pol. contl., Direc. coupl.	Isolator, Pol. contl., Direc. coupl.
Sensitivity* (dBm)		-52	-59	-44.5	-47	-59	-57
Year, Month		1984, Feb.	1983, Feb.	1983, March	1983, March	1983, July	1984, March
Organization (Ref.)		NEC(3)	BTRL(4)	MECL(5)	NEC(6)	BTRL(7)	BTRL(8)

* for a bit error rate of 10^{-8}

TABLE II MAJOR RESEARCH ITEMS FOR DIRECT AND COHERENT DETECTION SYSTEMS

	Direct Detection System	Coherent Detection System
Signal Light Source	Single-frequency oscillation, Self optical injection.	Frequency stabilization, Narrower spectrum-width (Residual AM, FM, PM noise suppression), Self optical injection.
Modulation	Frequency chirping.	external Optical loss reduction, Higher efficient modulation. direct Residual noise suppression.
Detection	APD performance improvement, Lower noise amplifier.	Quantum efficiency improvement, PLL performance improvement, Local osc. frequency control, Same problems of signal source.
Fiber	Non-linear effect, Material dispersion.	Non-linear effect, Polarization axis rotation, Depolarization.

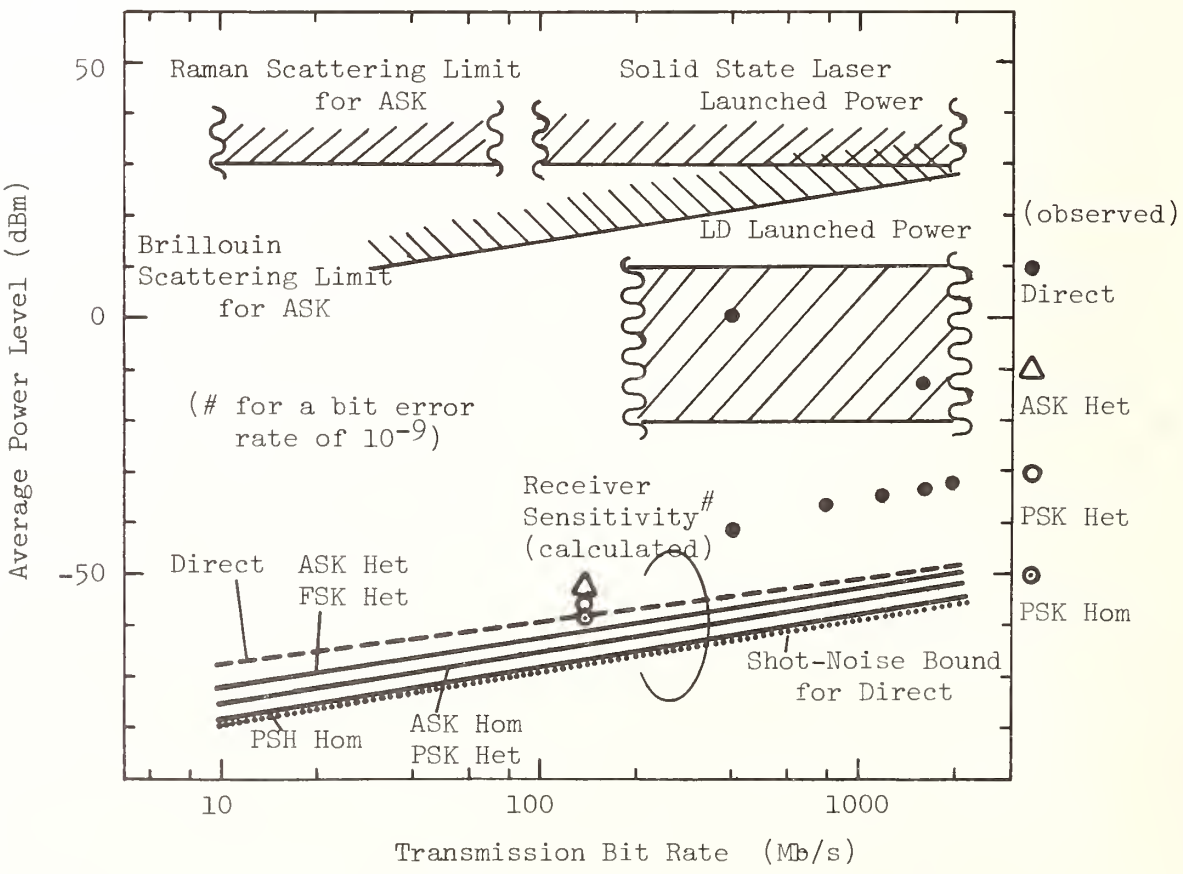

Fig.1 Launched Power and Receiver Sensitivity

BENDING AND MICROBENDING LOSS SENSITIVITY OF STEP INDEX SINGLE MODE FIBERS

-°-

J. AUGE, P. DUPONT, L. B. JEUNHOMME
LABORATOIRES DE MARCOUSSIS, CGE RESEARCH CENTER
91460 MARCOUSSIS - FRANCE

INTRODUCTION

Single-mode optical fibers with step index core and matched index or depressed index claddings are finding an increasingly large variety of applications, in long range transmission, signal processing, and sensing devices. These applications involve very different bending and microbending conditions, and it is therefore necessary to get an in-depth knowledge of bend and microbend losses as a function of fiber parameters. We have used the basket-weave test [1] to experimentally determine the losses in various matched cladding (MC) and depressed cladding (DIC) fibers. The results are found to agree reasonably well with simple loss models, and the behaviour of both fiber types is discussed in some details.

RESULTS ON MATCHED CLADDING FIBERS

Three MC fibers with approximately the same cutoff wavelength of 1.1μm and index differences Δn of 3×10^{-3}, 5×10^{-3}, and 7×10^{-3} were used together with a standard parabolic index multimode fiber (50 μm core dia.; 0.2 NA) serving as a reference. The fibers were first wound on a drum 480 mm in diameter in one layer and without tension, and were then rewound on a 100 mm diameter drum in 15 superposed layers with a tension of 17 g. As can be seen in Fig. 1, the experimental results exhibit for all fibers an almost constant addi-

tional loss at relatively short wavelengths. This part agrees well with the prediction of Petermann's theory [2] which relates the SMF microbend loss $\Delta\alpha_{SM}$ to the multimode microbend loss $\Delta\alpha_{MM}$ (here $\Delta\alpha_{MM} = 1.1 \pm 0.1$ dB/km) :

$$\Delta\alpha_{SM}/\Delta\alpha_{MM} \simeq 2\times10^{-4} \quad r_o^6/\lambda^4 \qquad (1)$$

where r_o is the area-weighted R.M.S. mode intensity diameter (in μm). For the comparison we used for r_o the value measured with the VAL method [3]. The steeply rising loss which occurs at longer wavelengths for the two SMF with the lower index difference is attributed to pure bend loss under a radius of R = 50 mm. It is seen in fig. 1 to agree well with the predictions of a simplified model [4] :

$$\Delta\alpha_R \text{ (dB/m)} \simeq 2.5 \quad V^2 \ (aR)^{-\frac{1}{2}} \exp\left[-9.84 \ (b\Delta n)^{3/2} \ R/\lambda\right] \qquad (2)$$

where R is the radius of curvature, a is the core radius, and b is the normalized propagation constant of the fundamental mode, for which very simple and useful approximations exist [4].

RESULTS ON DEPRESSED CLADDING FIBERS

Similar measurements as above were carried out on depressed cladding fibers having an almost constant total index difference of about 5×10^{-3}. The depressed cladding radius d was varied between d/a = 1.7 and d/a = 8 and the negative index depression Δn_- ranged from $\Delta n_-/\Delta n = 0.25$ to 0.5. The general shape of the curves is very similar to that of MC fibers and we again identify a microbend loss region and a steep rise above a given wavelength called λ_L attributed to pure bend loss.

For the microbend loss, a reasonable agreement is again found between the measurements and the predictions of Eq. (1) with r_o measured by the VAL me-

thod. As can be seen in fig. 2, this agreement occurs regardless of the shape of the depressed cladding, except for one point with a wide and deep cladding for which the microbend sensitivity seems unexpectedly small. For the bend loss which is seen in fig. 1 to increase abruptly above a given wavelength called λ_L, there is no simple model available for DIC fibers. Fig. 3 shows the measured values of λ_L for a set of fibers with $\Delta n = 0.005$ and two values of the winding radius, all fibers but one matched cladding (MC) having $\Delta n_{-}/\Delta n \simeq 0.43$. Other results not shown here indicate that the general evolution of λ_L against d/a is almost independent on Δn (provided V remains the same), and that λ_L increases when $\Delta n_{-}/\Delta n$ decreases for a given d/a. These features and some indications on an empirical model for λ_L (R, d/a, $\Delta n_{-}/\Delta n$) will be discussed at the conference.

REFERENCES

[1] A. Tomita et al., Tech. digest Symp. Opt. Fiber Meas., Boulder (Co), NBS special publication 641, pp. 89-92, 1982.

[2] K. Petermann, Arch. Electron. Uebertrag., 30, pp. 337-342, 1976.

[3] F. Alard et al., Electron. Lett., 17, pp. 958-960, 1981.

[4] L. Jeunhomme, in Single-Mode Fiber Optics, Optic. Eng. Series, Marcel Dekker, New-York, 1983.

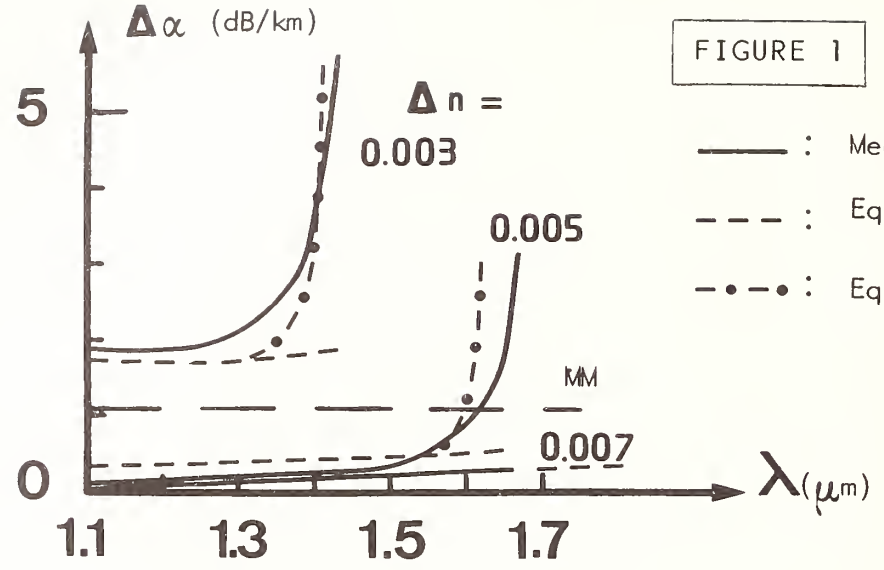

FIGURE 1

——— : Meas.

– – – : Eq. (1)

–•–• : Eq. (1) + Eq. (2)

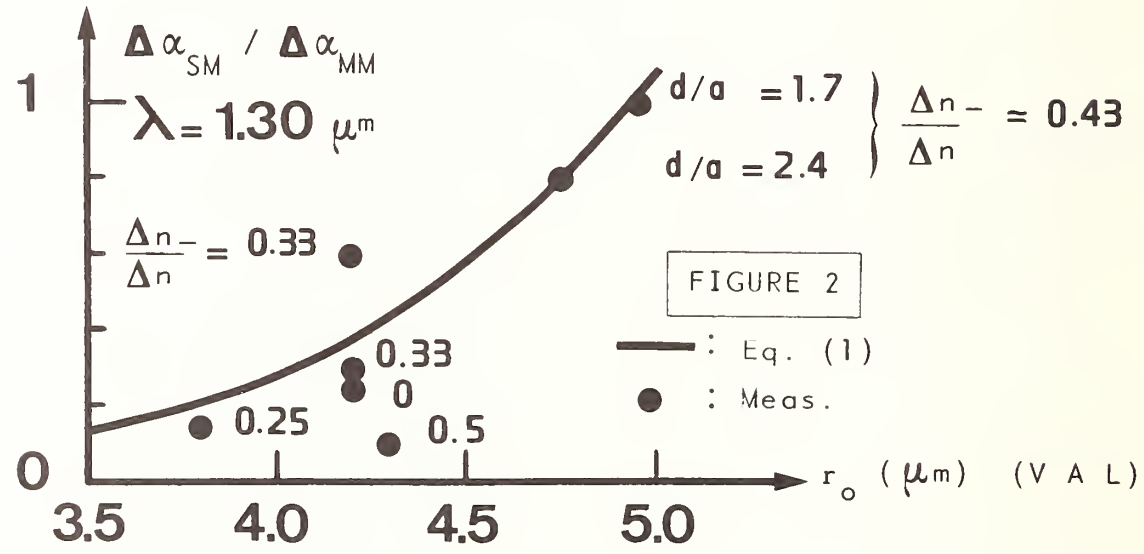

FIGURE 2

——— : Eq. (1)

● : Meas.

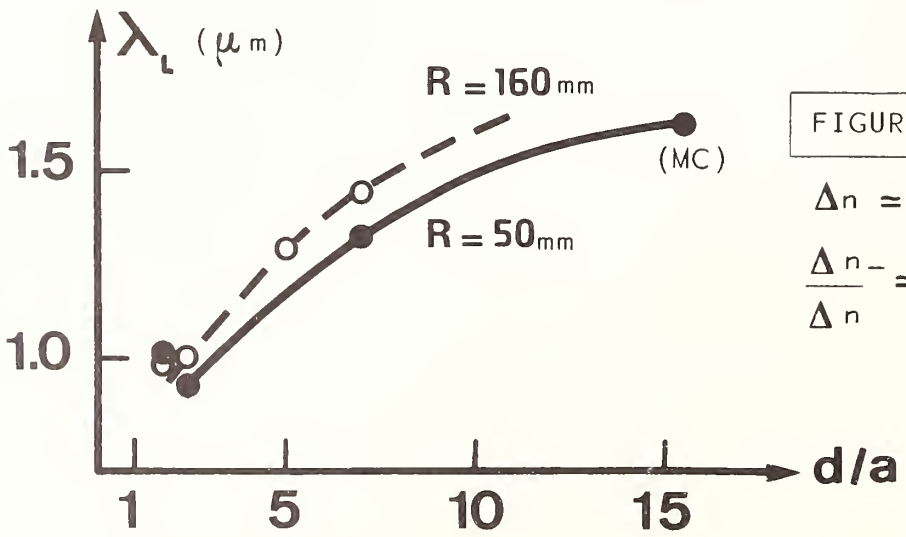

FIGURE 3

$\Delta n \simeq 0.005$

$\frac{\Delta n^-}{\Delta n} \simeq 0.43$

REFRACTIVE-INDEX PROFILE AND MODAL DISPERSION PREDICTION FOR A SINGLE-MODE OPTICAL WAVEGUIDE FROM ITS FAR-FIELD RADIATION PATTERN

W. Freude and A. Sharma*

Institut für Hochfrequenztechnik und Quantenelektronik, Universität Karlsruhe (W.-Germany)

* During this work on leave from Physics Department, Indian Institute of Technology, Delhi (India), as an Alexander von Humboldt fellow.

1. Theory

In a scalar treatment of the single-mode waveguide fields we neglect longitudinal components. Therefore the far-field $\Phi(\gamma,d)$ of a rotational symmetric near-field $\Phi(r)$ is specified by the Kirchhoff integral, and by inversion we find

$$\Phi(r) = -jk_0 d e^{jk_0 d} \int_0^\infty \underset{\sim}{\Phi}(\gamma,d) J_0(k_0 r \sin\gamma) \sin\gamma \, d\gamma \quad , \tag{1}$$

if we detect the far-field power in dependence of the angle γ as measured from the fibre axis in a meridional plane at a distance $d \gg a$, where a is the core radius. J_0 denotes the zeroth order Bessel function of the first kind, λ is the wavelength, and $k_0 = 2\pi/\lambda$ the free space propagation constant. The far-field

$$\underset{\sim}{\Phi}(\gamma,d) = \mathrm{sign}[\underset{\sim}{\Phi}(\gamma,d)]\,\underset{\sim}{\Phi}(0,d)\sqrt{P(\gamma)/P(0)} \tag{2}$$

can be computed from the corresponding measured far-field power $P(\gamma)$. The sign function denotes the polarity of the far-field, which changes sign at each zero of the power. Instead of evaluating Eq.(2) directly [2] we expand $\Phi(\gamma,d)$ in the series

$$\Phi(r) = \sum_{m=1}^{M} c_m G_m^{(0)}(\alpha,r), \quad \frac{\underset{\sim}{\Phi}(\gamma,d)}{\cos\gamma/d} = jk_0 e^{-jk_0 d} \sum_{m=1}^{M} (-1)^{m-1} c_m G_m^{(0)}\left(\frac{1}{\alpha}, k_0 \sin\gamma\right) \tag{3}$$

with the orthonormalized Gauß-Laguerre functions

$$G_\mu^{(\nu)}(\alpha,x) = 2\sqrt{\frac{\mu!}{(\mu+\nu)!}}\,\alpha(\alpha^2x^2)^{\nu/2} e^{-\alpha^2x^2/2} L_{\mu-1}^{(\nu)}(\alpha^2x^2). \tag{4}$$

$L_{\mu-1}^{(\nu)}$ are the generalized Laguerre polynomials. We minimize the sum of the weighted squared differences between the computed and the measured far-field data having chosen the parameter α for our basic system such that the fundamental mode $G_1^{(0)}(1/\alpha, k_0 \sin\gamma)$ approximates the central lobe of the far-field best. The unknown

coefficients $(-1)^{m-1}c_m$ are fast and accurately found by a standard matrix inversion procedure. A renormalisation guarantees $\sum_{m=1}^{M}|c_m|^2=1$. If we insert the fitted near-field into the Helmholtz equation we see that

$$k_0^2 n^2(r) - \beta^2 = -2\alpha^2 - \alpha^4 r^2 + 4\alpha^2 \sum_{m=1}^{M} m c_m G_m^{(0)}(\alpha,r) \Big/ \sum_{m=1}^{M} c_m G_m^{(0)}(\alpha,r), \qquad (5)$$

where $n(r)$ is the refractive-index profile, β the propagation constant, and M the maximum number of coefficients. The resulting near-field resolution δ_B depends on the maximum measured far-field angle γ_m and on M by

$$\delta_B \approx 0.610\ \lambda/\sin\gamma_m \quad , \quad \delta_B \approx \frac{\sqrt{2}}{\alpha}(1.23/M)^{0.472} \qquad (6)$$

where for the second formula the largest zero of $G_M^{(0)}(\alpha,r)$ (as approximated by McMahon's expansion [4]) divided by M-1 was given in terms of an empirical function with an error smaller than 3 % for $3 \le M \le 100$.

The dispersion properties of the waveguide may be derived adopting a formula [3] which can be safely applied to weakly guiding single-mode structures. Whether the newly developed doubly and quadruply clad broad-band fibers do allow the underlying assumptions has not yet been verified. Some algebra leads to the dispersion factor $T(\lambda) = T_M(\lambda) + T_W(\lambda)$ as a sum of material and waveguide dispersion,

$$T(\lambda) \approx \frac{1}{c}\frac{dn_{2g}}{d\lambda} + \frac{\lambda I(\lambda)}{8\pi^2 c n_2}\left[1 + \frac{\lambda}{I(\lambda)}\frac{dI(\lambda)}{d\lambda}\right], \quad I(\lambda) = \alpha^2 \int_0^\infty e^{-x} f(x)\,dx\,,$$
$$f(x) = \frac{1}{x}\left\{\sum_{m=1}^{M} c_m\left[(2m-2-x)L_{m-1}^{(0)}(x) - (2m-2)L_{m-2}^{(0)}(x)\right]\right\}^2 \qquad (7)$$

where n_2 is the refractive-index, n_{2g} the group index of the cladding, and c the vacuum velocity of light. $I(\lambda)$ may be evaluated exactly by a Laguerre integration [4].

2. Experiment

We tested our method by comparison to published data [2] and found that in sharp contrast to previous methods [2] we could tolerate random errors in $P(\gamma)$ of at least 20 % without changing the computed refractive-index profile significantly, Fig.1: We weight

all relevant data according to their largely varying absolute values (a dynamic power range D of 60 to 90 dB is typical), while the direct use of Eq.(1) implies the summation of widely varying numbers, so that the highest valued $P(\gamma)$ have to be measured with a relative power accuracy of about $A = 10^{-4}$ if the side-lobe information is not to be covered by the measuring uncertainty. In fact we estimated $D/dB \approx -20 \log A$, which limits the useful angle range and therefore the near-field resolution.

We carried out own experiments with a single-mode fiber at $\lambda = 632.8$ nm and found a refractive-index profile with $M = 10$ coefficients as in Fig.2. Because of the required resolution the dynamic range amounted to $D = 60$ dB, so the use of a laser source was mandatory.

In measuring the waveguide dispersion where resolution is not as important, D may be reduced to 20 dB which allows for an incoherent light source. Fig.3a shows the measured far-field powers along with the calculated near-field intensities $I(r)$, Fig.3b, from which the waveguide dispersion evaluates to $T_W(\lambda = 632.8\,\text{nm}) = -3.5\,\text{ps}\,\text{km}^{-1}\,\text{nm}^{-1}$. A least-squares error Gaussian fit does not show a good agreement, therefore an estimate of $T_W(\lambda)$ using only the wavelength dependent change of the fitted spot size [3] is 2.3 times larger.

If in the expansion Eq.(3) unsymmetric Gauß-Laguerre modes are included one could detect the content of the higher-order LP_{11} mode thereby finding the single mode operating range of the waveguide.

3. Conclusion

We expanded measured far-fields in M Gauß-Laguerre functions, the coefficients of which are determined with a least relative-error squares fit by matrix inversion. Thereby the near-field is given, from which the refractive-index profile can be calculated. Using wavelength dependent far-field data measured with an incoherent source the waveguide dispersion may be deduced.

Besides the general benefits of far-field measurements (uncritical mechanical and optical setup) the advantage of our method

lies in its inherent insensitivity against noise, so that the practical resolution limit is only given by the amount to which cladding modes and stray light can be reduced.

Acknowledgement

We thank Prof. Dr. techn. G. K. Grau for discussions.

References

[1] Born, M. and Wolf, E., Principles of optics. Pergamon Press, Oxford, 1980.
[2] Hotate, K. and Okoshi, T., Measurement of refractive-index profile and transmission characteristics of a single-mode optical fiber from its exit radiation pattern. Appl. Optics 18 (1979), 3265 - 3271.
[3] Sansonetti, P., Modal dispersion in single-mode fibres: Simple approximation issued from mode spot size spectral behaviour. Electron. Lett. 18 (1982), 647-648.
[4] Abramowitz, M. and Stegun, I., Handbook of mathematical functions. Dover Publications, New York, 1970.

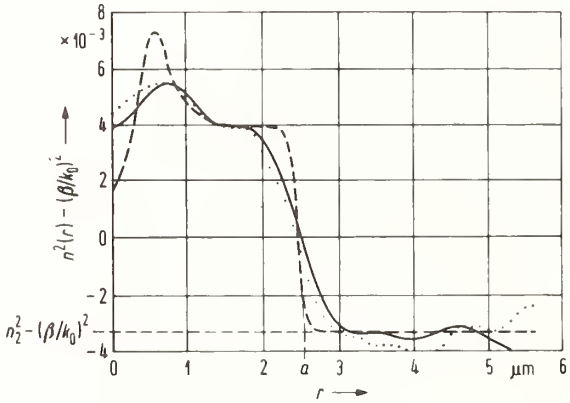

Fig.1. Refractive index profile, computed by the present method with M = 31 (—) and by direct Fourier inversion [2] (···), or measured by an interference technique using a Q fibre (---)[2].

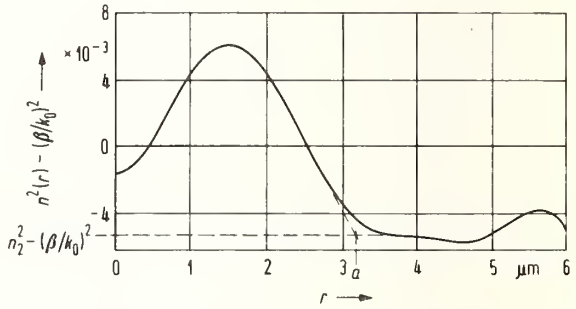

Fig.2. Refractive-index profile of single-mode fiber L137/II with M = 10.

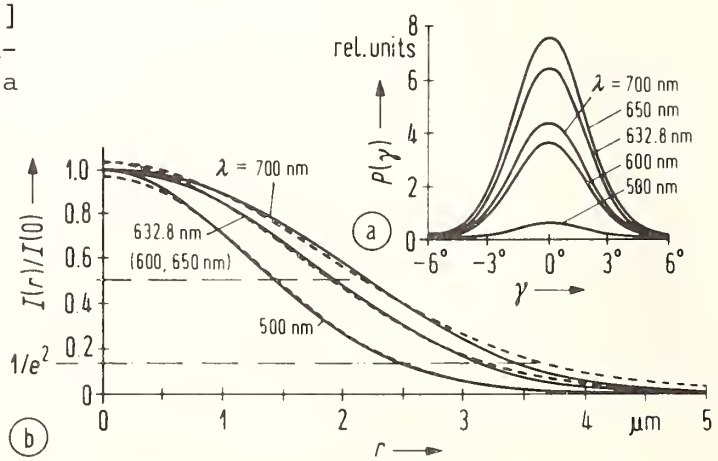

Fig.3.
a Far-field power P(γ) of single-mode fiber L137/II for different wavelengths λ.

b Computed near-field power I(r) (—); fitted Gaussian function (---).

A SIMPLE NEAR-FIELD SCANNING SYSTEM FOR REFRACTIVE INDEX PROFILES AND MODE SPOT SHAPE.

C A Millar

British Telecom Research Laboratories, Martlesham Heath, Ipswich, UK.

Introduction

Measurements of refractive index profile and mode spot intensity distribution are fundamentally important for singlemode fibre characterization. Using the Transmitted Near Field (TNF)[1][2] technique, the two measurements are essentially the same, but with different sources and detectors in place. This paper describes a straightforward apparatus which, when appropriate sources and detectors are used, permits high-resolution, real-time near field scanning.

Measurement system

The apparatus may be divided into three distinct parts, the optical system, the mechanical system and the electronic system (fig 1). The optical system comprises, for TNF profiling, a tungsten lamp, diffuser, condenser and a X60 coupling lens. Care was taken to minimize leaky mode excitation by restricting the launch NA to 0.05 and preparing low cleave-angle fibre ends. For mode spot distribution measurement, the test fibre was butt-coupled, using a diffraction alignment device[3], to a pigtail fibre from a 1.32um or 1.55um wavelength laser. The other end of this short length of test fibre is placed in a V-groove clamp and the image of the near field is projected by a microscope objective onto a slit placed immediately in front of a mechanical chopper blade. Alternatively, a chopper disc with circumferential photochemically-etched slits may be used. Light passing through the slit and chopper arrangement is collected by a large-area photodiode; Si or Ge as appropriate. The slit, which selects a radial sample of the TNF along its length, is sequentially scanned by the chopper blades. The photodiode voltage V_p is proportional to the sum of all the light intensity at any chopper blanking position r', ie

$$V_p \propto \int_{r'}^{\infty} E^2(r)\, dr$$

Since

$$v_{chop} = dr'/dt = Rw$$

analogue differentiation of this signal gives

$$V_d(t) \propto Rw\, d/dr' \int_{r'}^{\infty} E^2(r)\, dr \propto E^2(r)$$

which represents recovery of the radial variation of the intensity distribution as a time-dependent voltage. The advantage of the method is that it is repetitive and synchronous, allowing (a) real-time viewing of the TNF on an oscilloscope (b) signal averaging to reduce noise and (c) digitization of waveforms for immediate processing of the fibre properties. Positioning the fibre in the object plane enables sequential scans to provide complete cross-sectional near field information.
The key mechanical component is the chopper motor, which must maintain constant angular velocity, w, to ensure temporal stability. The number of

chopper blades determines the repetition rate of the signal, whereas the linear velocity at the slit (at radius R) is a compromise between the provision of adequate signal from the differentiator (higher speed) and the bandwidth of the detector and analogue electronics (lower speed).

Calibration

Knowing the oscilloscope timebase speed, the chopper velocity and the spatial magnification of the optics, it is possible to calibrate the radial dimension as a time interval. Alternatively, a fibre of known dimensions may be used as a reference. For mode spot intensity distributions, the peak level is set to unity and the pattern scaled accordingly. For refractive index profiling, however, the scaling procedure for absolute index is more involved, and methods of doing so will be presented in detail at the conference.

Results

Figure 2(a) shows the TNF refractive index profile of a singlemode fibre, using a low magnification objective lens to enable the cladding depression to be identified. Using a higher magnification lens the core profile shown in figure 2(b) results. Direct comparison with the refracted near field profile for the same fibre indicates that a spatial resolution of $\sim$ 0.5um is achieved for both. Changing the source and detector provides the TNF mode spot distribution shown in figure 2(c), for the same fibre at 1.32um wavelength. The spot shape is very similar to that predicted from a finite-element analysis[4] of the digitized refracted near field index profile, with an e^{-2} width of 3.72um as compared with 3.9um respectively. Transverse offset measurement of e^{-1} power transmission width gave a value of 4.0um. The resolution of the scanning system is not likely to change with wavelength, but the optical resolution of the objective lens may result in a degradation in the infrared, which is governed by the transfer function of the lens. By removing the objective lens, the scanning system may be applied with equal effect to the measurement of far field intensity distributions.
Experience of this near field, the transverse offset, and numerical methods of fibre characterization will be discussed, with particular reference to current CCITT deliberations and to the problem of specifying advanced singlemode fibres.

Conclusions

A simple scanning system has been used for TNF refractive index profiling and mode spot intensity distribution measurement. A resolution of $\sim$ 0.5um has been obtained for profiles, and good agreement for spot shape and width by two alternative methods has been achieved.

Acknowledgements

Thanks are due to B Nelson and G Warnes, and the Director of Research of British Telecom is gratefully acknowledged for permission to publish this work.

References

1 D H Irving, El Letts, 19, p190, 1983.
2 Y Murakami, A Kawana, H Tsuchiya, Appl Opt, 18, p1101, 1979.
3 C A Millar, paper IV-A5, 9th ECOC, Geneva, 23-26 Oct, 1983.
4 B Nelson, private communication, BTRL.

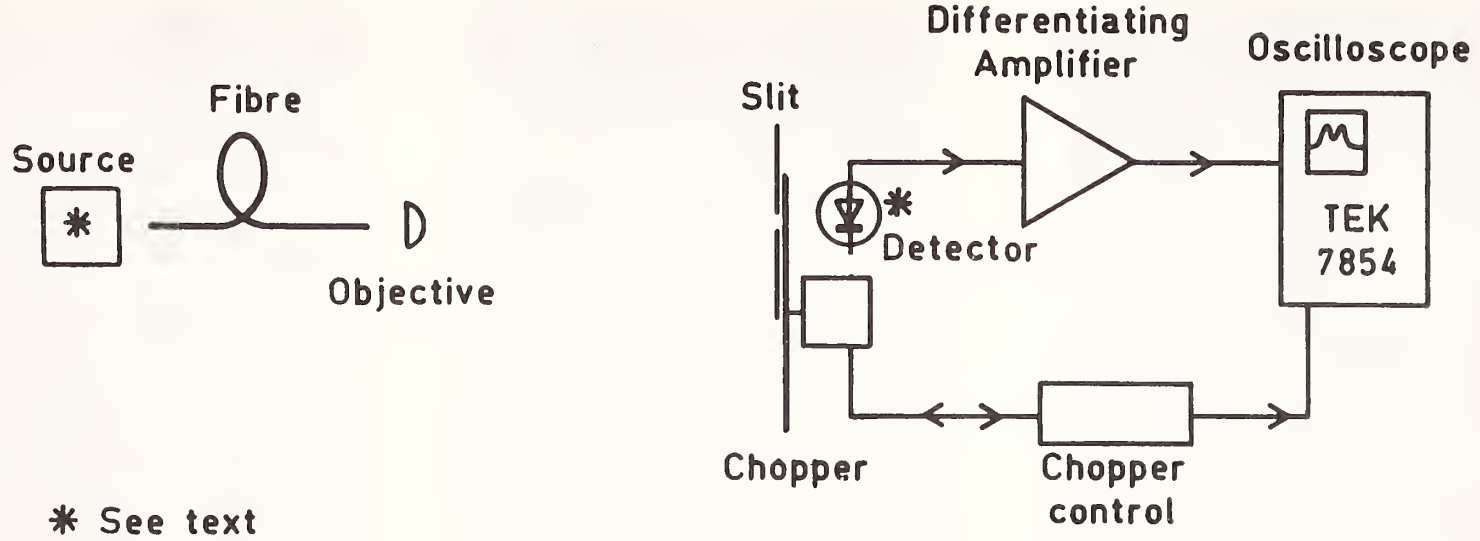
Fibre
Source
Objective
* See text
Differentiating
Amplifier
Oscilloscope
Slit
Detector
TEK
7854
Chopper
Chopper
control

FIGURE 1

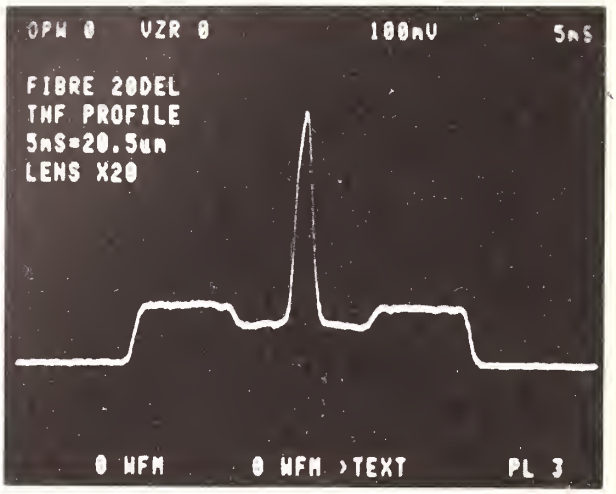

Figure 2a

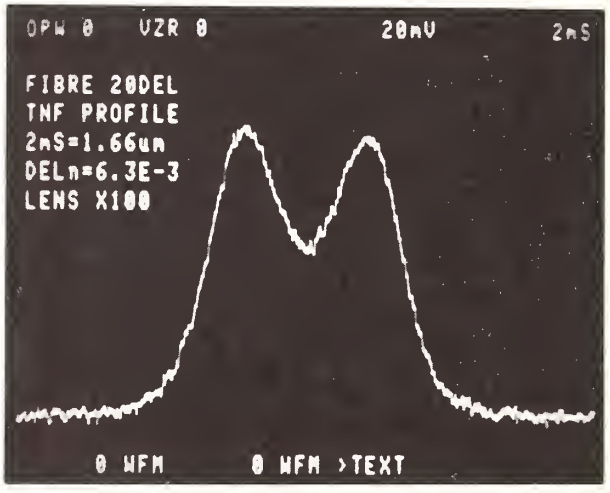

Figure 2b

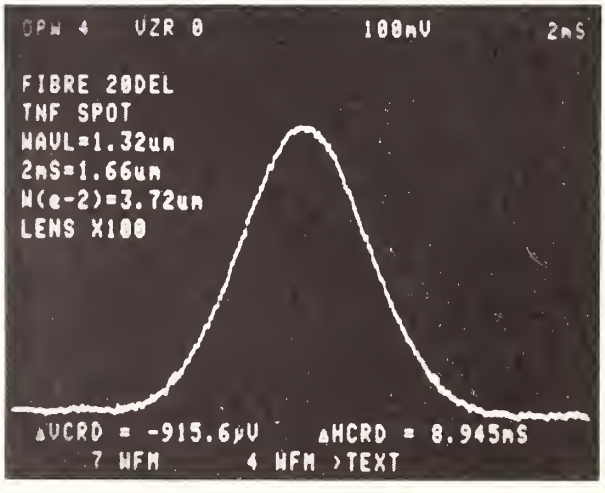

Figure 2c

SPOT-SIZE MEASUREMENTS IN SINGLE-MODE FIBRES

R. Caponi, G. Coppa, P. Di Vita, U. Rossi
CSELT - Via G. Reiss Romoli, 274 - 10148 Torino (Italy)

It is known that the dimensional specification of single-mode fibres is performed on the basis of the so-called mode field diameter. It has not been possible, up to now, to agree (e. g., in the CCITT) an acceptable definition of such a parameter, and the matter is presently strongly debated. In order to clarify the situation, it seems convenient firstly to review some definitions of parameters related to the mode field diameter and successively to discuss various techniques proposed recently for its measurement. It is not our aim to penetrate the measurement problems of each proposed method, but we want to analyze them critically in order to understand what actually is being measured and how useful that quantity can be. Finally we expose a novel and very promising technique that permits a direct measurement of the mode field diameter making use of suitable masks.

In the following we will refer to the so-called spot-size w, simply related to the corresponding mode field diameter d by $d=2\sqrt{2}\,w$.

If the mode field is (as practically happens) circularly symmetric, two parameters are of relevant physical significance. The first one is defined as:

$$(1) \qquad w_m=\{\int E^2 r^3 dr / \int E^2 r dr\}^{1/2},$$

E(r) being the field amplitude of the fibre versus the radial coordinate r. w_m is an important quantity, since **microbending losses** [1] and **joint losses due to small tilts** [2] depend on this parameter. The second quantity is defined as:

$$(2) \qquad w_j=\{\int E^2 r dr / \int (dE/dr)^2 r dr\}^{1/2}$$

it is analogously important too, since the **joint losses due to small lateral offsets** [2,3] and the **waveguide dispersion** [3,4] depend on it. Note that these two parameters coincide if the field distribution is Gaussian, and in general very rarely differ by more than 10 %, for fibres with conventional profiles.

Thus, it is easy to understand the importance of specifying and characterizing the fibre by a certain mode field dimension. A first approach consists simply in taking the 1/e radius of the near-field intensity distribution. Such an evaluation coincides with w_m and w_j for rigorously Gaussian E(r), but

generally gives only a too rough estimate of such parameters [5,6]. Their evaluation can be obtained more reliably from a transmitted near-field scanning, by applying directly Eqs. (1) and (2), but a considerable dynamic range (> 20 dB) is required in the measurement in order to avoid truncation errors in the tails [5,6].

Such problems can be overcome (as proposed recently [5,6]) by a suitable analytic extrapolation of the tails of the near-field pattern with simple exponentially decaying function. This technique provides immediate and accurate evaluations of both w_m and w_j, directly from the defining equations (1) and (2), and could be useful particularly for fibres with non-conventional profiles (multicladding, segmented core, etc) at higher wavelenghts, where the difference between w_m and w_j could be so cospicuous to indicate, in the future, the need of providing both parameters.

A different elaboration of near-field measurements [7] (applicable also to the far-field) permits to deduce a further parameter, w_b. It is defined as the 1/e width of the Gaussian power distribution that maximizes the coupling efficiency in the considered fibre. An implicit definition of w_b is the following:

$$(3) \qquad w_b=\{ \int E(r)\exp[-r^2/(2w_b^2)]r^3dr/ \int E(r)\exp(-r^2/(2w_b^2)]rdr\}^{1/2}.$$

It can be demonstrated that it is always: $w_j \leqslant w_b \leqslant w_m$ (the equal being valid only for Gaussian E(r)). This means that if a single kind of mode field diameter should be adopted, w_b could represent a good compromise between the two relevant parameters: w_m and w_j.

A further parameter, w_a, based on a completely different measurement procedure, is defined as the lateral offset value that reduces the coupling efficiency between two fibre samples to 1/e of the maximum [8]. Notwithstanding its euristic definition, w_a provides a surprisingly good evaluation of w_m, particularly around the cut-off wavelength of the LP_{11} mode. Such a coincidence is better for monotonical profiles and for W-type fibres than for dipped or segmented core fibres. The evaluation of w_a thus permits often a good estimate of w_m, but replacing the problems arising from the limited dynamic range of common near-field technique with the typical problems of an offset measurement apparatus (sub-micron displacements are involved and particular care should be devoted to the quality of the end faces of the fibres).

This transverse offset technique is an example of integral measurement of the field dimensions. Different methods are now under development. Let us

consider, e. g., Eq. (1) for w_m. The denominator within brackets is simply proportional to the whole power at the output of the single-mode fibre that can be obtained by a simple integral measurement. The numerator can also be obtained by a single integral measurement, by using a mask [9] in the near-field plane whose transmittivity is proportional to r^2. In this way two integral measurements permit to derive w_m. Also w_j can be measured by the mask method since it has been recently shown that it is inversely proportional to the far-field width, a quantity that can be written as Eq. (1) but replacing the near-field pattern $E^2(r)$ by the far-field one and the radial coordinate by the angular one [10]. In this case a third integral measurement, interposing the mask in the far-field plane, permits to derive w_j immediately. The mask can be obtained in various ways, examples of which are: a dark zone delimited by portions of Fermat's spiral (Fig. 1a) or a grey distribution (Fig. 1b).
A schematic set-up for this measurement is shown in Fig. 2. A first spectral scanning is performed without mask, a second one with the mask in the far-field plane, F.F., in order to obtain w_j, a third one with the mask in the near-field plane, N.F., in order to obtain w_m. The results of a preliminar measurement of the quantity w_j are reported in Fig. 3. Although a certain refinement in our preliminary experimental apparatus is needed, a substantial agreement with the data obtained by a precise and high dynamic range near-field measurement is obtained. Considering that such similar data have been obtained with quite completely different techniques, that exploit different effects, such early results are very encouraging, since this "mask" technique is much more immediate with respect to different techniques and can be suited for factory or field measurements. Refinements are now in progress to improve the precision of the measurement, and further results will be presented at the Conference.

References

1. K. Petermann, Opt. Quamtum Electron, **9** (1977) 176.
2. G. Coppa, P. Di Vita, CSELT Rapp. Tecn., **11** (1983) 427.
3. K. Petermann, Electron. Lett., **19** (1983) 712.
4. G. Coppa et al., Electron. Lett., **19** (1983) 731.
5. G. Coppa et al., CSELT Rapp. Tecn., **12** (1984) 109.
6. G. Coppa et al., Proc. of ICC '84, Amsterdam (NL), May 14-17, 1984.
7. W. T. Anderson, D. L. Philen, IEEE J. Lightwave technol., **LT-1** (1983) 20.
8. C. A. Millar, Electron. Lett., **17** (1981) 458.
9. G. Coppa et al., Patent pending, 1983.
10. C. Pask, Electron. Lett., **20** (1984) 144.

a)

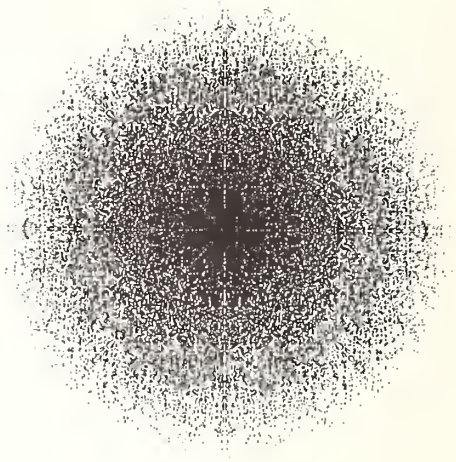

b)

Fig. 1 - Examples of masks used for spot-size measurements.

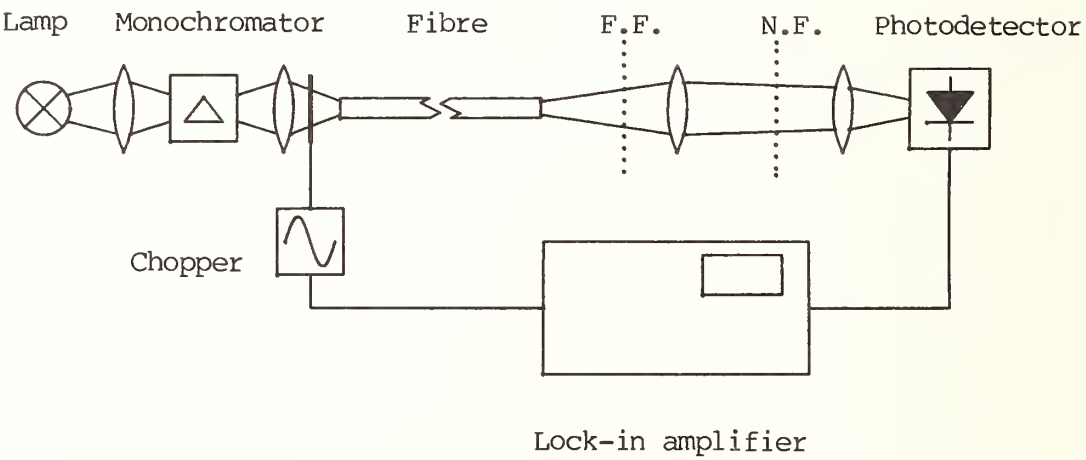

Fig. 2 - Experimental apparatus.

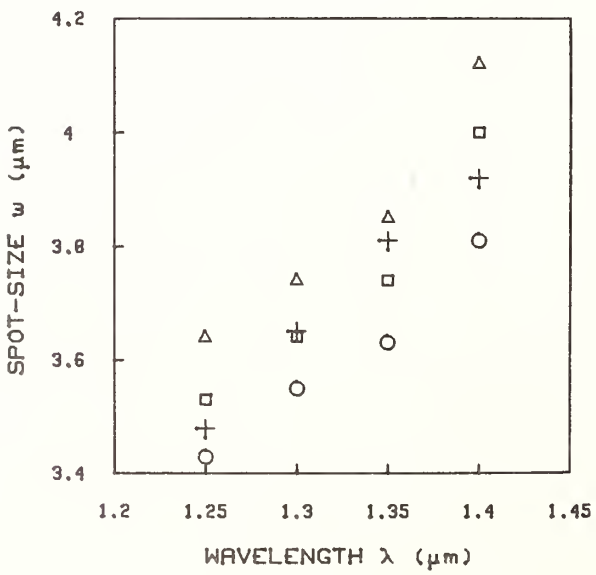

Fig. 3 - Experimental results of spot-size: w_m (triangles), w_j (circles), w_b (squares), obtained with the near-field technique, compared with w_j obtained with the mask technique (crosses).

COMPATIBILITY OF NATIONAL AND INTERNATIONAL STANDARDS FOR OPTICAL FIBER

P. R. Reitz, Corning Glass Works, Corning, NY 14831

INTRODUCTION

Worldwide standardization activities for telecommunications-grade optical fibers and cables have been underway for the better part of a decade. Because the various organizations represent diverse interests, it is to be expected that their efforts will sometimes lead to conflicting test methods. For companies wishing to participate fully in this new industry, it is of paramount importance to understand the details of the various requirements in a manner that can maximize product conformance.

NATIONAL AND INTERNATIONAL STANDARDS ORGANIZATIONS

The bulk of international optical fiber standardization effort rests in two organizations, the International Electrotechnical Commission (IEC) and the International Telegraph and Telephone Consultative Committee (CCITT). A description of the general work of these organizations can be found in Reference 1. In the United States, the primary source of optical fiber standards is the Electronic Industries Association (EIA), which works in cooperation with the American National Standards Institute (ANSI).

To understand the difficulty involved in creating compatible standards, it is helpful to review the goals and expectations of these separate entities. Both IEC and EIA exist to promote trade and commerce, and as a consequence use a particular hierarchy of generic, sectional, and detail specifications (known as the IEC-Q system) to foster an exact means of specifying characteristics of components like optical fibers and cables. As a result, IEC and EIA are generally interested in a broad range of product specifications and in test methods that can be effectively applied to manufacturing a product under the IEC-Q system.

The CCITT involvement in optical fibers and cables is to promote the establishment of standard fiber types for use in public networks, and the test methods to characterize these fibers. It reflects the viewpoint of

those government telecommunication administrations and operating agencies of which it is composed, and focuses upon developing reference test methods (RTMs) to be used for product specification and resolution of disputes. It also sometimes acknowledges acceptable practical factory measurements in the form of alternative test methods (ATMs).

STANDARD MEASUREMENT METHODS FOR MULTIMODE FIBERS

Attenuation

The unanimously preferred procedure for attenuation measurement is the two-point cutback method. It has been recognized as the most accurate and precise method, and is the CCITT RTM. CCITT and IEC also allow insertion loss (substitution) and backscattering methods as alternatives. Although EIA is currently reviewing backscatter measurement methods, use of these methods for attenuation has not generally been accepted in the U.S. due to the uncertainties contained in the interpretation of the results. Further, most use of the technique is made with commercial instruments that generally have no provision for controlled launching conditions. Consequently, OTDR measurements are most often used as a process check, for example in cable manufacturing where cutback measurements have already been performed in fiber manufacturing.

Insertion loss (substitution) measurements are currently under study in the EIA because of a need for non-destructive testing of connectorized cables, and as a basic method for measurement of installed repeater sections. There is some debate as to whether this test can fairly apply to the common practice of mandrel wrapping, since the mandrel cannot be well applied to the cable, and the reference length of cable may often be a different structure. Neither CCITT nor IEC methods address this point. While IEC and CCITT insertion loss measurements agree almost verbatim, there is a small difference. While it is agreed that insertion loss measures both the (cabled) fiber and connection device attenuation, the IEC procedure allows correction for the loss of the connection while there is no mention of this in the CCITT document.

Launching Conditions For Attenuation

A very strong correlation exists between IEC and CCITT documents, so agreement between these organizations is apparently complete. However, one should note that neither provides a particular definition for achieving proper launch conditions. This has proven to be a difficult task, as is evidenced by the complex procedure described in EIA FOTP-50, where launching conditions for attenuation measurements are addressed. EIA specifies an approach to define a steady-state mandrel based upon creating a somewhat smaller angular distribution at the input than the actual far-field pattern of the fiber under test, and also specifies the 70/70 LPS launch. The "dummy fiber" method, also specified in FOTP-50, is qualified by the same procedure as for the mandrel.

These launch conditions were formulated with the same general intent, to achieve steady-state loss values, but before it was recognized that launch conditions for attenuation generally only need to avoid exciting the highest order guided modes. Because any of several means can be used for this purpose, it becomes a question mainly of preference, until bandwidth measurements are considered.

Bandwidth Measurements

Bandwidth, or baseband response measurements, have been the focus of much attention, particularly with respect to launching conditions. Because of the effectiveness of restricting the launch for prediction of link attenuation, some have hoped that the same launch conditions would yield consistent system predictions of bandwidth from individual fiber measurements. Many have therefore proposed using the same launch restriction for bandwidth as has been used for attenuation, but improvement in predictability has not occurred. Further, those different launching conditions that produced equivalent loss values now can be seen to produce varied bandwidth values because the launch restrictions are sufficient to attenuate some modes that propagate even over several kilometers. EIA, in contrast, has specified the use of uniformly overfilled launch conditions - the so-called

full launch - mainly for reproducibility. Since the predominant transient loss mechanisms occur within the first one or two kilometers, the measured power distribution for bandwidth using full launch nearly approximates steady-state conditions. Thus, if the test fiber is sufficiently long the bandwidth measurement with full launch can be considered to be a steady-state measurement. In this manner, the intent of IEC, CCITT and EIA may be reconcilable on this principle.

With respect to measurement methods for bandwidth, complete agreement now exists on the equivalence of time and frequency domain techniques. This has allowed implementation of each technique where its specific strength is required; time domain for interpretation of fiber measurement and frequency domain for dynamic range in field measurements.

Geometrical Measurements

Widespread agreement exists on methods for measuring these characteristics, although some differences are evident. All three organizations either allow or prefer the Refracted Near-Field method for determining core diameter. The core is defined on the basis of the best-fit circle to 5% relative index points in the case of CCITT, while EIA requires only a diameter scan, but with the profile fit by a power law function between 10 and 80% index points. Core diameter is then defined as the intersection of this profile with the zero baseline. The relevant IEC document contains no such details.

All organizations allow transmitted near-field measurements, but again with some differences. CCITT defines core diameter from the best-fit circle to a number of 5% intensity points around the core periphery, whereas EIA allows a single diametrical scan, but with two possible interpretations. One is the distance between 2.5% relative intensity points, the other is a power-law fit between 10-80% relative intensity points extrapolated to the baseline. EIA has determined these relationships by considering consistency between TNF and RNF measurements. This is an area requiring further study, especially when comparing measurements on fiber

lengths differing by several orders of magnitude. This is especially true because of recent proposals in CCITT to do TNFs on very short (2-3cm) fiber samples. The net result is that average differences between techniques and fitting prescriptions can be of the order of 1-2 micrometers, but significantly larger errors can exist for fibers with particular kinds of index profile details that confound some of the test methods, notably the RNF. Thus, the manufacturer who wishes to comply with all techniques will find that a significantly tighter distribution of parameter values may be required to avoid the possibility of rejected ware.

Other geometrical measurements are typically performed with microscope techniques, which by virture of the very rapid contrast changes at the air/clad interface do not seem to be unduly sensitive to interpretation; most test methods do not require the degree of detail that creates incompatibility.

While the main benefit of the RNF method is the convenience of one technique that can apply to both core diameter and numerical aperture, insufficient effort has been expended to address the details necessary to produce reliable NA results from the technique. EIA has no procedure for determining NA from RNF measurements; only short-length overfilled far-field results contain a prescription based upon the half angular extent of the far-field at the 5% relative intensity points, similar to the CCITT ATM. This result is expected to be smaller than RNF results, in part due to the 5% intensity definition and in part due to uncertainty as to what constitutes the peak core and homogenous cladding indices in the RNF. The exact relationship is hard to verify because of the problems just cited, and the fact that RNF absolute index calibration to the accuracy required for comparison to far-field measurements is rather difficult to achieve. Further study by Standards Committee is required. However, at issue here (and in the case of core diameter measurements) is a difference in underlying principle between CCITT and EIA measurements. The former relies heavily upon RNF tests (on sample lengths of 1-2mm) while the latter tends to prefer transmission measurements through a few meters of fiber as being more indicative of functionality.

TEST METHODS FOR SINGLE MODE FIBERS

It is fortuitous that standardization activities were maturing before the widespread introduction of single mode fibers, because this had led to a much higher degree of cooperative effort in the development of consistent and compatible standards. There is basic agreement among EIA, IEC and CCITT for virtually all major parametric tests, including spectral attenuation, cutoff wavelength and fiber dispersion. Since the geometrical properties of single mode fibers can generally be measured by the existing techniques for multimode fibers, the same comparison of methods applies.

One example of the maturation of the standardization process is the decision to allow both time delay and phase shift methods for dispersion measurements in CCITT. In the analogous case of bandwidth measurements of multimode fibers, it took years of discussion to reach the consensus that allowed both time and frequency domain techniques; when this similar situation occurred in single mode fibers it was recognized as the preferred solution almost immediately. This has avoided lengthy debate as to which method should become the "Reference Test Method".

The preferred measurement method of mode field diameter has yet to be resolved in CCITT. In contrast, EIA has begun to develop what is believed to be a set of internally-consistent measurement procedures using all the main methods; near-field, far-field (by two means), and transverse offset. IEC has a draft document for the transverse offset method only. Technical issues related to Gaussion fitting or a newer proposal by Petermann are key to final resolution of this question. With the range of methods considered so far, differences at 1300nm are expected to be on the order of ~ 5%, but may be twice as large at 1550nm.

Conclusions

In the last several years we have witnessed the rapid growth and acceptance of optical fiber communications; this has been accompanied by a noticeable maturation of standards activities. In large measure the existing measure-

ment standards are very similar, particularly considering the diverse frames of reference from which they have been created. There remains, however, a significant number of important detail differences that must yet be resolved. This resolution will require great consideration to fairly weigh the requirements for simplicity and flexibility with the desire for uniformity and technical correctness. This is the ongoing challenge of standardization.

REFERENCES

1) R. R. Fergusson, M. Larose, J. G. Nault, Digest Supplement, Symposium on Optical Fiber Measurements, Boulder, CO, USA, 1982.

2) CCITT Contribution No. 289, April 1984, (to be published as amended version of Recommendation G.651 - Characteristics of 50/125μm Multimode Graded Index Optical Fibre Cables, 1st Quarter 1985).

3) CCITT Temporary Document 46-E, May 1984, to be published as Recommendation G.652 - Characteristics of a Single Mode Fibre Cable, 1st Quarter 1985).

4) Electronic Industries Association, 2001 Eye Street N.W., Washington, DC, 20006. Refer to RS-455 - series documents.

5) International Electrotechnical Commission Technical Committee No. 46; Subcommittee 46E: Fibre Optics Draft for the second issue of Publication XXX, Optical Fibres, Chapters I and II. (Yellow Book), and Supplement A to Publication XXX (Grey Book).

OPTICAL FIBER SENSORS

A. Dandridge, J. H. Cole and G. H. Sigel, Jr.
Naval Research Laboratory
Washington, DC 20375

Recently, many types of sensor using optical fiber, either as the transduction element or as a communication link to an optical sensor, have been developed. These devices range from simple on/off types of device to highly sensitive interferometric designs. The wide range of these devices means there is no one type of fiber to fill the requirements of fiber sensors. In this paper, we will describe the various types of fiber optic sensor, however, the emphasis will be on the properties of the fiber used in the sensor, rather than the source, demodulation or systems aspects. Typically, the more complex interferometric sensor designs have the most stringent requirement in terms of the fiber properties. In this case, both optical and mechanical properties of the composite fiber structure (i.e., fiber and jacket) are important in determining the operation of this type of device. Another approach -- the microbend sensor also requires particular mechanical and optical properties to function in an optimum manner. Finally, the use and application of polarization preserving fiber in interferometric sensors will be briefly discussed.

The wide range and diversity of optical fiber sensors make them difficult to categorize, however, shown in Figure 1, five broad categories are identified. The first four types of device measure intensity changes induced by the parameter to be sensed. In types A and B, the light leaves the fiber, interacts with a sensor element (typically bulk optics) before being collected by the return fiber. In types C and D, the light that is sensed typically remains in the fiber, but either optical or mechanical perturbations couple light out of the fiber core, thus allowing measurement of the phenomena causing the perturbation. Typically, these first four types of sensor use multimode fiber

rather than single mode. In the fifth type of the device, the light remains in the fiber coil, but a perturbation to the fibers environment causes an optical phase shift within the fiber; this then is referenced to another fiber unexposed to the perturbation -- using interferometry, a very accurate measurement of the phase shift may be made. This type of device usually employs single mode optical fiber.

Examples of these different sensor types are shown in figures 2 a,b,c,d and e. As already indicated types A and B require fiber similar to that required in communications, obviously loss (bend and microbend) should be minimized, however, no unique fiber characteristics are required. In type C, where the element performing the sensing is short, typically the refractive index of the fiber (possibly declad) is the important parameter.

Many different variants of the extended intensity fiber sensor (type D) have been demonstrated. With radiation sensors, the increased fiber loss with radiation may be optimized with specific fiber materials. Some temperature sensing configurations also require fibers doped with specific materials. All intensity devices require certain optical power levels which are determined by core size and numerical aperture, etc. The microbend sensor, for example, requires additional mechanical and optical properties of the sensing fiber. A small fiber diameter and a large optimum microbend periodicity (see figure 3) increase the fiber compliance and therefore improve sensor response within the limits set by optical constraints. A soft buffer layer tends to reduce microbend sensitivity by reducing the coupling of the mechanical deformer to the glass fiber. A low index, soft coating relative to the cladding results in guided cladding mode which can recouple into the core, thus reducing the sensor response. Therefore, a thin, hard, higher index coating directly on the glass fiber is optimum for the microbend sensor.

The interferometric sensor has been used in many sensor configuration (see

figure 2e). We will describe two types of sensor -- acoustic and magnetic. Figure 4 depicts a typical single mode optical fiber construction for interferometric acoustic sensors. Although the outer hard coating (E) performs the major role in acoustic sensitivity, the fiber composite must be designed to provide unique characteristics for acoustic sensor applications. Typically for a given sensor application, one wishes to package the optical fiber in as small a volume as practical. This requirement results in a minimum bend specification substantially lower than for typical telecommunication applications. The refractive index of the core (A) and cladding (B) and core size must be optimized to minimize the excess bend loss in the fiber. The overall diameter of the glass layers, core (A), cladding (B) and substrate (C) must be reduced from the 125 μm telecommunications standard to about 70-80 μm to reduce the bending stress. The smaller diameter fiber also reduces loading effects. The soft coating (D) is utilized to reduce microbending and local stresses on the glass; however, to minimize the fiber volume, this layer should be relatively thin ~ 50 μm. Finally, a number of hard coatings can be utilized. Figure 5 shows the normalized acoustic phase sensitivity $\Delta\phi/\phi\Delta P$ plotted as a function of total fiber diameter. Due to the dependence of the acoustic sensitivity on both the Young's and bulk moduli, different coatings are optimum for different fiber diameters. Metal coatings may be employed to reduce acoustic sensitivity. Magnetic sensors use similar technology, but the fibers may be bonded directly onto metallic glass strips or coated with magnetostrictive materials.

Finally, specific sensors (e.g., the fiber gyro) and certain configurations require polarization preserving fiber. Many design characteristics are retained, however, all the components (pigtailed lasers, couplers, modulators and sensor elements) need to be fabricated from polarization preserving fibers.

Types of Fiber-Optic Sensor

Fig. 1

eg switch, keyboard, proximity, security, viscometer

VISCOMETER

measurement up to 40,000 psi

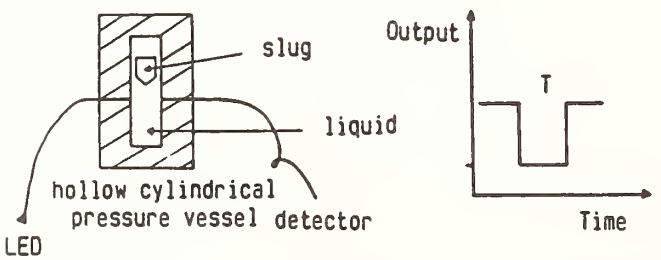

viscosity proportional to T

Fig. 2a

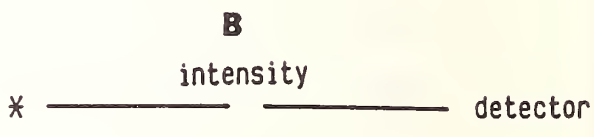

eg acoustic, temperature, current, security, pressure, fluorimeters

PHOTOELASTIC
FIBER-OPTIC HYDROPHONE

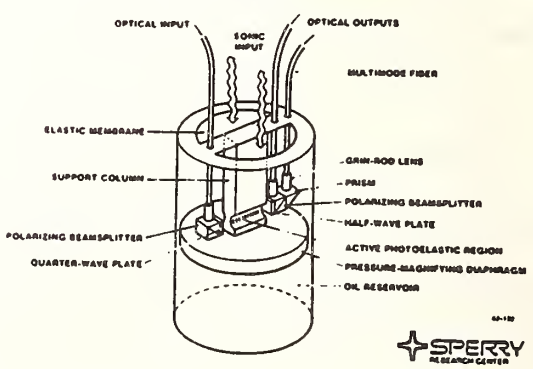

Fig. 2b

C

intensity

* ——————∿—————— detector

eg temperature, refractive index, liquid level

REFRACTIVE INDEX

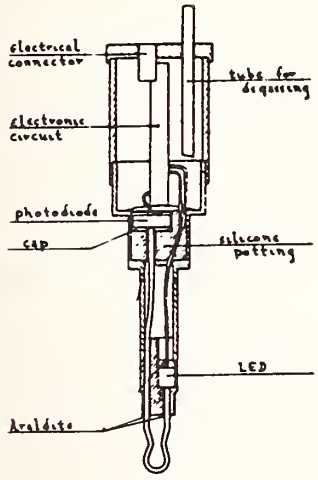

Harmer

Fig. 2c

D

intensity

* ——————o—————— detector

eg temperature, radiation, acoustics, turbidity (oil)

MICROBEND

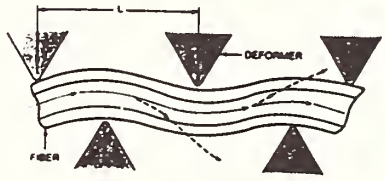

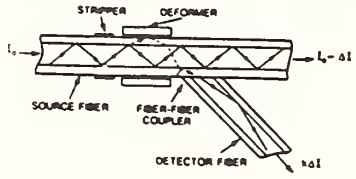

Davis

Fig. 2d

E

phase

* ——————o—————— detector

eg pressure, acoustic, ultrasonic, acceleration

magnetic, rotation, temperature, microwave, current

INTERFEROMETRY: 1) Mach Zehnder
2) Michelson
3) Sagnac

1) and 2) act as an extremely sensitive strain gauge, capable of measuring length changes of 10^{-14}m, ie for 100m sensor 1 part in 10^{16}

Features: sensitivity, linearity, versatility
common technology base

Fig. 2e

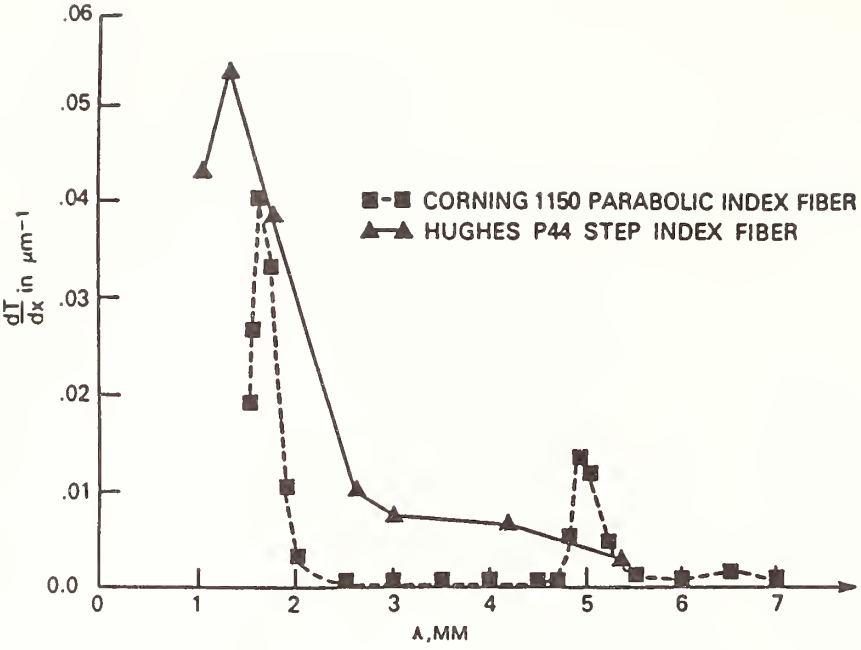

Fig. 3

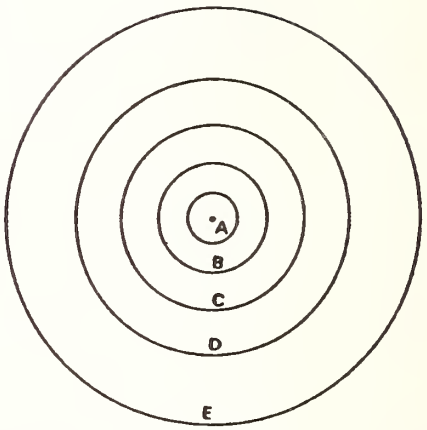

Fig. 4. A typical single-mode ITT fiber: core (*A*), cladding (*B*), substrate (*C*), soft coating (*D*), and hard coating (*E*).

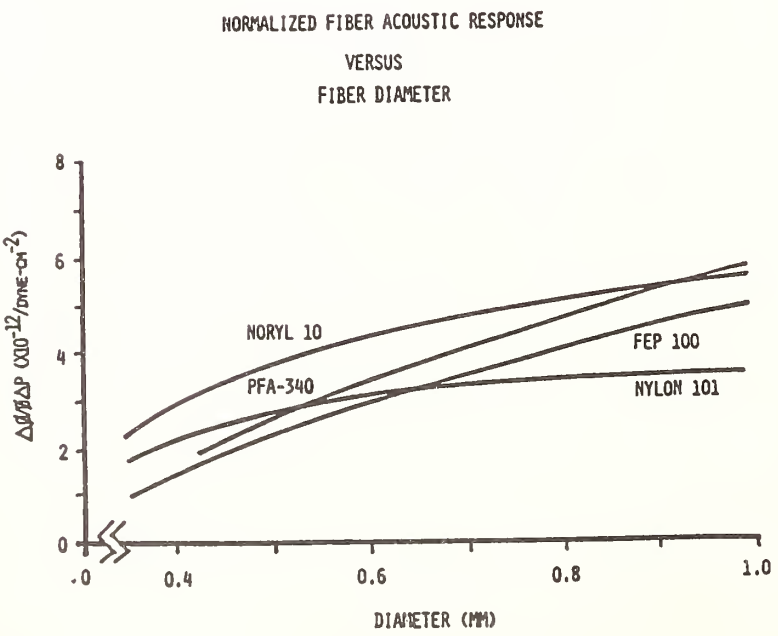

Fig. 5

THE PHASE VELOCITY AND LOSS COEFFICIENT OF OPTICAL FIBERS VIEWED AS STIFF STRINGS

Frank W. Cuomo

Department of Physics, University of Rhode Island, Kingston, R.I. 02881
and
Naval Underwater Systems Center, Newport, R.I. 02841

ABSTRACT

The standing wave method has been widely used in the determination of the damping properties of viscoelastic solids in the 100-10,000 Hz range and loss coefficients have been obtained either by the experimental observation of the decay modulus or the half-power bandwidth of each resonant peak. This paper investigates by this method the behavior of optical fibers to mechanical vibrations. It is found that for plastic clad fibers the phase velocities are largely dependent on the tension and mass density while for other fibers tested the system behaves as a stiff string whereby the modulus of elasticity takes on a more pronounced role. Experimental data are presented to illustrate the differences in loss factors and phase velocities for several optical fiber configurations.

INTRODUCTION

The recent analysis of multilayer optical fibers, identifying the coating properties which optimize the fiber acoustic sensitivity, has shown that pressure sensitivity is strongly influenced by the elastic coefficients of the fiber coatings. The measurement of the elastic moduli of some fiber coatings has provided the necessary relationship between the core strains and the properties of the fiber layers necessary to the calculation of the sensitivity.[1] Optical fiber research in underwater communication has also been extensive and it has been found that the elastic and damping properties of optical waveguides,

with or without ruggedization, are very useful in system characterization. In this paper the measurement of these properties is obtained by resonance methods utilizing three types of optical fibers. Since a string under tension can also have stiffness, such as the case for ruggedized fibers, the approach used considers both parameters by treating the problem of a stiff string, as described by Morse and Ingard.[2] This method is found advantageous in the experimental determination of the phase velocities, damping factors and elastic moduli of the optical fibers under test.

DATA ANALYSIS

Utilizing the mathematical treatment given in reference 2 resonance modes in optical fiber samples were generated by driving the samples transversely. The samples were fixed at both ends at 9.5", using several known tensions, and the resonant peaks were determined. In addition, the half-power bandwidth points were obtained to establish the loss coefficient, tan D, at each resonance mode. Since the expressions developed for a stiff string contain both the tension, T, and the modulus of elasticity, Q, it is possible to obtain the modulus, if the tension is known, by curve fitting. This method was effectively used to determine the extent of stiffness for each sample. Three multimode optical fiber samples are discussed in this paper, namely, one hytrel-buffered, one plastic-clad and a third one hytrel-buffered and ruggedized with S-glass epoxy. Figures 1, 2 and 3 illustrate some of the results of this investigation. Figure 1 shows the frequency dependence of the loss tangent and Figure 2 shows the same dependence of the phase velocity. Figure 3 provides for the hytrel-buffered fiber the wavenumbers indicative of the expected elastic moduli based on theoretical predictions.

CONCLUSIONS

The following conclusions have been derived from this study:

A. RUGGEDIZED

1. Damping independent of frequency & tension
2. Moduli independent of tension
3. Phase velocity dependent on stiffness

B. HYTREL-CLAD

1. Damping dependent on frequency
2. Moduli dependent on tension
3. Phase velocity dependent on tension & stiffness

C. PLASTIC-CLAD

1. Damping dependent on frequency & tension
2. No moduli at higher tensions
3. Phase velocity dependent on tension

REFERENCES

1. Lagakos, N., Schnaus, E.U., Cole, J.H., Jarzynski, J., and Bucaro, J.A., "Optimizing Fiber Coatings for Interferometric Acoustic Sensors," IEEE Journal of Quantum Electronics, Vol. QE-18, No. 4, pp. 683-689, April 1982.
2. Morse, P.M., and Ingard, K.U., "Theoretical Acoustics," McGraw-Hill Book Co., pp. 187-191, 1968.

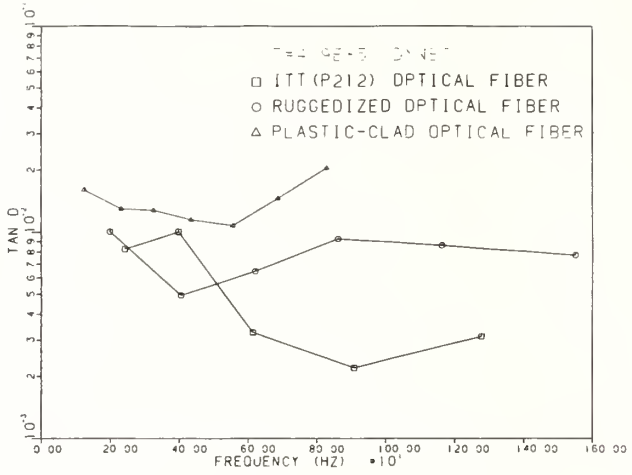

DAMPING FACTORS OF OPTICAL FIBERS

FIGURE 1

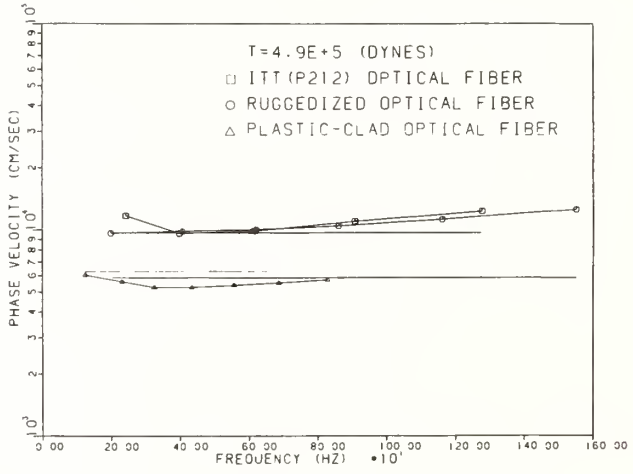

PHASE VELOCITY OF OPTICAL FIBERS

FIGURE 2

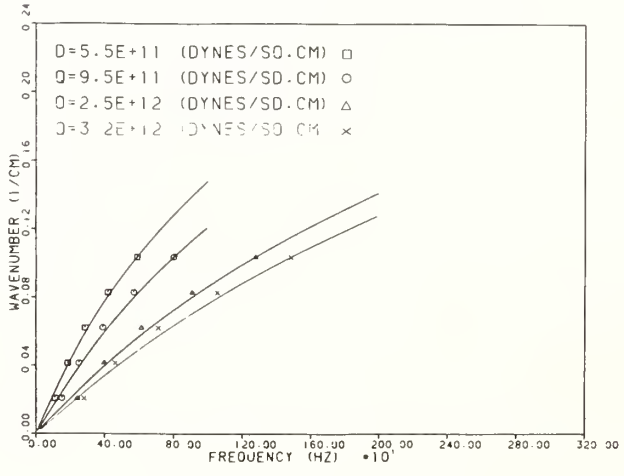

ITT (P212) OPTICAL FIBER

FIGURE 3

POLARIZATION SHUTTLE PULSE TECHNIQUE

C. S. Brown and F. T. Stone
AT&T Bell Laboratories
Norcross, Georgia 30071

INTRODUCTION

A single-mode fiber is in reality a two-mode fiber. If the fiber is azimuthally symmetric, the two-modes have the same group velocity. Under more realistic conditions, geometrical, material, and stress irregularities cause the two modes to travel at different speeds. This results in both pulse spreading, a potential bandwidth-limiting factor for wideband systems,[1] and fluctuations of the state of polarization, which limit the operation of coherent systems.[2] To satisfy the many applications of single-mode fibers, both high-and low-birefringence fibers are being developed, and the need for practical and repeatable measurement techniques to characterize the polarization properties of such fibers is increasing.

Several birefringence-measurement techniques are currently in use; however, only a few can measure low birefringence.[3] The most popular, the cut-back method,[4] is destructive[5] and exhibits poor repeatability.[6] In this paper we report on a new technique, the polarization shuttle pulse (PSP) method, for measuring birefringence and related polarization effects in low birefringence (i.e., $\delta\beta$ = 3.6°/m to 360°/m) single-mode fibers of short lengths (20 to 100 cm).

BIREFRINGENCE MEASUREMENT USING THE CUT-BACK TECHNIQUE

The phase delay induced by birefringence at an arbitrary position z along the fiber is given by $\delta\phi(z) = \delta\beta z$ where $\delta\beta = \beta_x - \beta_y$ is the difference between the propagation constants of the two polarizations. A closely related quantity is the beat length defined by $L_b = 2\pi/\delta\beta$. When $\delta\beta = \beta x - \beta y \neq 0$, the birefringence induces a phase delay causing the state of polarization to evolve cyclically along the fiber, with L_b the length of one cycle. Hence there is a $2\pi n$ (n an integer) ambiguity in determining $\delta\phi$.

Each birefringence-measurement technique accounts for that $2n\pi$ ambiguity in different ways. The cut-back method eliminates it by determining the phase delay for two different lengths. The difference between the two lengths, however, must be less than the beat length of the fiber. Unfortunately, the beat length is not known a priori, so much trial and error is necessary. Also, the cut-back procedure itself disturbs the birefringent state of a low-birefrigence fiber, causing poor repeatability.

To determine the repeatability of the cut-back method, we measured the phase delay on uncabled and cabled single-mode fibers

under three different conditions, which simulate the errors expected from different aspects of the cut-back procedure: (A) the fiber configuration and the fiber output position relative to the detector were held constant, (B) the angle of the fiber output position relative to the detector was rotated through 90°, while everything else was held constant, and (C) the fiber layout was randomly varied, while everything else was held constant. The standard deviations shown in Table I give an idea of the errors involved in the various aspects of the cut-back procedure.

Note that the standard deviation of a cabled fiber is much less than that of the uncabled fiber. The large increases in the standard deviation come primarily from changes in the fiber layout, i.e., condition (C). Fiber rotation, i.e., condition (B), does not effect the repeatability as much since the low twist rates involved induce little phase delay. Because the cut-back method inadvertently involves both conditions (B) and (C), it contains the errors associated with those measurement variations. For uncabled fibers, the standard deviation is almost 2π, suggesting difficulty in removing the $2n\pi$ ambiguity.

POLARIZATION SHUTTLE PULSE (PSP) TECHNIQUE

The precision of measurements on low-birefringence fibers can be improved by nondestructively measuring the length dependence of phase delay on a single short length (<1 meter) of cabled fiber, thereby eliminating variations in fiber layout and position. To do that, we evaluated a polarization shuttle pulse technique. The PSP technique is a modification of the method used to measure pulse spreading in multimode optical fibers.[7] To measure polarization properties, a linear polarizer, a Soleil-Babinet Compensator (SBC), and a linear analyzer are added to the conventional shuttle-pulse arrangement. The measurement set-up is shown in Figure 1.

Output from a 1.329 μm laser diode was coupled into 7m of polarization maintaining fiber. The light was then collimated and passed through a linear polarizer. A stable polarized output was always observed. The shuttle-pulse arrangement consisted of two 80% reflecting mirrors and two precision fiber holders designed to keep the short straight section of cabled fiber (≈ 25 cm) perpendicular to the mirrors. The output pulses were collimated, passed through the SBC and the linear analyzer, and focused onto a PIN diode. The electrical signals were then amplified and read off a sampling scope. In this way the phase delays for the initial pulse and the subsequent shuttles were determined. Because the initial pulse corresponds to a fiber length L and subsequent shuttle pulses correspond to lengths of 3L, 5L, etc., the phase delay as a function of length is determined nondestructively.

Several data points representing an average of 100 readings were taken about the nulls of the initial pulse and the first and second shuttles. As the intensity as a function of the retardation introduced by the SBC is sinusoidal, the data about the nulls was fitted to a parabola and the minima found that way.

PSP data is shown in Figure 2. The mean of the difference in phase delay between the shuttles was $\delta\phi = 19.6 \pm 2.2$ deg. for a length $2L = 52.2$ cm. The birefringence was therefore $\delta\beta = 37.5 \pm 4.2$ deg/m. The beat length corresponding to this birefringence was $L_b = 9.5 \pm 1.1$ m.

SUMMARY

Because the PSP method does not require moving the fiber, errors created by twists and rearrangements (cases B and C in Table II) are avoided. Repeatedly measuring several other fibers using the PSP method resulted in standard errors similar to those of the fiber reported in Table II. In all cases, the repeatability was far better than that of the cut-back method, because only the errors in repeatedly measuring phase delay (with all other conditions held constant) are involved. Therefore, the PSP method gives significantly improved precision in the measurement of short lengths of low-birefrigence fibers.

1. D. Marcuse and C. Lin, "Low Dispersion Single-Mode Fiber Transmission - The Question of Practical Versus Theoretical Maximum Transmission Bandwidth," IEEE J. Quantum Electronics QE-17, 869, (1981).

2. T. Okoshi, "Heterodyne and Coherent Optical Fiber Communications: Recent Progress," IEEE Trans. Microwave Theory Tech. MTT-30, 1138, (1982).

3. F. M. Sears, "Review of Polarization Measurement Techniques," to be published.

4. S. R. Norman, D. N. Payne, and M. J. Adams, "Fabrication of Single-Mode Fibers Exhibiting Extremely Low Polarization Birefringence," Electron. Lett. 15, 309, (1979).

5. K. Kikuchi and T. O. Okoshi, "Wavelength-Sweeping Technique for Measuring the Beat Length of Linearly Birefringent Optical Fibers," Optics Lett. 8, 122, (1983).

6. W. K. Burns, R. P. Moeller, and C. L. Chen, "Depolarization in a Single-Mode Optical Fiber," J. Lightwave Tech. LT-1, 44, (1983).

7. L. G. Cohen, "Shuttle Pulse Measurements of Pulse Spreading in an Optical Fiber," Applied Optics 14, 1351, (1975).

Table I: Std. Dev. of the Birefringence for A) Fiber Untouched, B) Fiber Rotated, and C) Fiber Layout Varied

	A	B	C
Coated (≈ 6m)	± 17°/m	± 19°/m	± 330°/m
Cabled (≈ 3m)	± 10°/m	± 19°/m	± 71°/m

Table II: Std. Dev. of the Birefringence for the PSP Method

	A*	B	C
Cabled ≈ 28 cm)	± 4.2°/m	Absent in PSP Method	Absent in PSP Method

*The improvement over the cut-back method is due in part to the parabolic fit. The use of the fit could reduce the cut-back error A comparably. However, the larger errors B and C would remain.

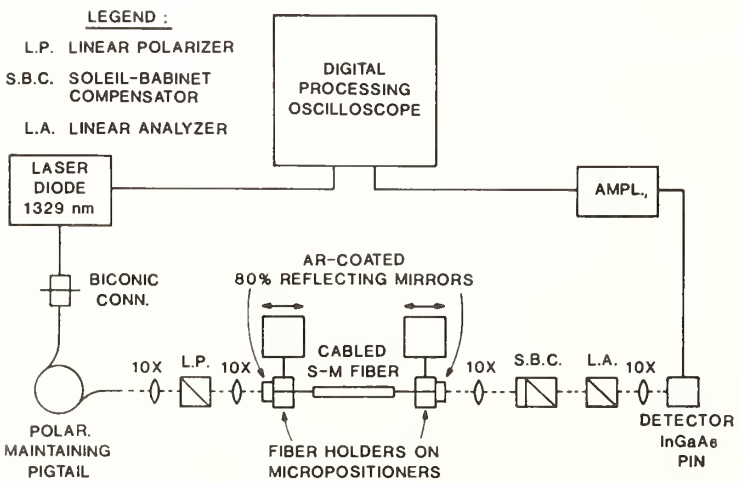

FIGURE 1. POLARIZATION SHUTTLE PULSE MEASUREMENT SET-UP

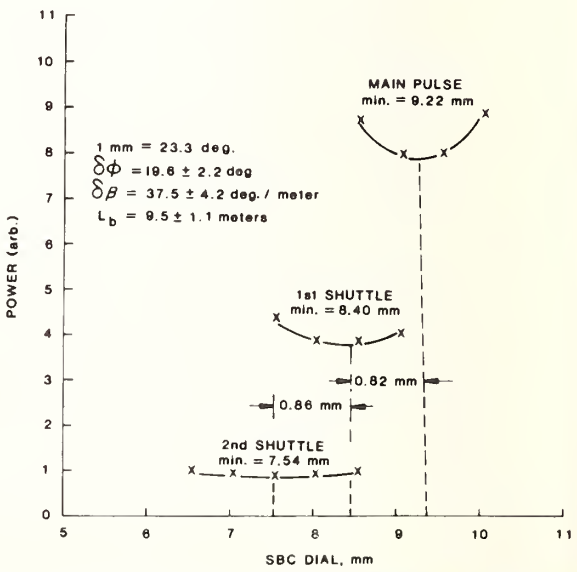

FIGURE 2. MINIMUM PHASE ANGLE OF MAIN PULSE AND FIRST AN SECOND SHUTTLES FOR 26 cm OF CABLED FIBER. TH MINIMA ARE READ FROM THE PARABOLIC FITS.

A NEW TECHNIQUE FOR THE MEASUREMENT OF AXIAL-STRESS IN OPTICAL-FIBRE PREFORMS

M.P. Varnham, S.B. Poole and D.N. Payne
Department of Electronics, The University, Southampton, UK.

The ability to measure the axial stress in optical-fibre preforms is essential for the development of highly-birefringent[1] and other specialist fibres, in which high levels of thermal stress are deliberately introduced to modify the fibre propagation characteristics. Conversely, it has been found that the loss of telecommunications-grade fibre can be reduced by minimising the stresses within the core[2]. To date, axial stress profiles have been measured by the rather cumbersome method of reconstruction from the retardation profiles measured transversely across the preform[3,4,5]. However, this technique has not seen widespread routine use, presumably because the results rarely justify the complexity of the measurement. In this paper we present a new method for measuring the axial stress profile which should see widespread adoption as a result of its simplicity and convenience. The method has the advantage that it uses the same hardware and software that are commonly used in transverse refractive-index profiling [6,7,8] and it is therefore readily incorporated into existing equipment. The technique can also in principle be applied to two-dimensional stress profiling of asymmetric preforms. In addition, the work provides a new insight into how thermal stresses affect fibre refractive-index profiling techniques.

Transverse refractive-index profiling of both symmetric and asymmetric preforms is based on the measurement, either directly or indirectly, of the optical path-length difference $\eta(\rho,\theta)$ between a ray passing through the preform and an equivalent ray in the index-matching fluid[6]. (Here ρ is the ray offset and θ is the azimuth of the ray - see Figure 1). The axial stress $\sigma_z(r,\theta)$ in the preform causes $\eta(\rho,\theta)$ to be dependent upon the polarisation orientation of the incident light. Hence a retardation,

$$R(\rho,\theta) = \eta_z(\rho,\theta) - \eta_\theta(\rho,\theta) \qquad (1)$$

exists across the preform. Here η_z, η_θ are the optical path-length differences seen by light polarised axially and transversely to the preform axis respectively. Reconstruction of the refractive-index profile from the η_z and η_θ data will yield two different effective refractive-index profiles, $n'_z(r,\psi)$ and $n'_\theta(r,\psi)$ respectively. The difference between these profiles can be shown by the application of elementary elastic theory to be:

$$n'_z(r,\psi) - n'_\theta(r,\psi) = -C\,\sigma_z(r,\psi) \qquad (2)$$

where the stress-optic coefficient $C = -3.5 \times 10^{-5}$ mm^2/kg for high silica glasses. Thus the difference between the refractive index profiles seen transversely by z-polarised and θ-polarised light gives the axial stress profile directly.

The above therefore suggests a remarkably easy method for measuring the axial stress profile $\sigma_z(r,\psi)$ in axi-symmetric and non axi-symmetric optical fibre preforms. Using existing transverse refractive-index profiling techniques, we simply measure $n'_z(r,\psi)$ and $n'_\theta(r,\psi)$ with light polarised axially and then transversely to the preform axis, followed by calculation of $\sigma_z(r,\psi)$ from equation (2). Fig. 2 illustrates the two profiles $n'_z(r,\psi)$ and $n'_\theta(r,\psi)$ measured by the standard spatial-filtering technique[6] with the sole addition of a polariser. In this case, the preform is circularly symmetric and consists of a silica substrate, a phosphorus/fluorine-doped outer matched cladding, a depressed boron-doped inner cladding and a germania-doped core. The axial-stress profile reconstructed from these measurements, Figure 3, reveals that the depressed boron-doped inner cladding supports 15 kg/mm^2 of axial tensile stress, whereas the levels of tensile stress in the core are somewhat lower at 5 kg/mm^2. As expected, the outer matched cladding and substrate exhibit a lower compressive stress of 2 kg/mm^2.

The existence of stress-induced multivalued refractive-index profiles in the preform which depend on the polarisation of the measurement light source obviously affects conventional transverse

refractive-index profiling measurements. A related topic has been addressed by Scherer[9], who showed that thermal stresses cannot be neglected in the design of graded-index fibres. We note that the effective refractive-index profile measured with unpolarised light is the average of the effective profiles, $(n'_z + n'_\theta)/2$. Again, elasticity theory reveals that this is equal to $(n_x + n_y)/2$, where n_x and n_y are the real real refractive indices seen by light polarised in the x and y directions respectively (see Figure 1). Fortunately, therefore, the transverse refractive-index profiling techniques yield the average profile seen by unpolarised light travelling down the fibre. This is an important result, since it quantifies for the first time how thermal stresses affect the transverse profiling methods.

The axial stress measurement is currently being applied to non axi-symmetric profiles (e.g. Bow-Tie preforms[1]). Data concerning resolution, accuracy and repeatability will be presented at the Conference.

Acknowledgements

The measurements described in this paper were made on the York Technology P101 Preform Profiler. We would like to thank York Technology for their co-operation. The preforms were supplied by R.D. Birch and E.J. Tarbox.

References

1. R.D. Birch et al, Electron. Lett. 24, 1036, 1982.

2. B. Ainslie et al., in Proc. 9th ECOC, Geneva, 1983.

3. P.L. Chu et al, Appl. Opt., 18, 707, 1982.

4. R.B. Calligaro et al, Electron. Lett. 18, 474, 1982.

5. N. Shibata et al, Appl. Opt., 3507- , 1982.

6. P.L. Francois et al,IEEE J. Quant. Electron., 18, 524, 1982.

7. P.L. Chu, Electron. Lett., 15, 295, 1979.

8. D. Marcuse et al, Appl. Optics, 18, 14, 1979.

9. G.W. Scherer et al, Appl. Optics, 19, 2000, 1980.

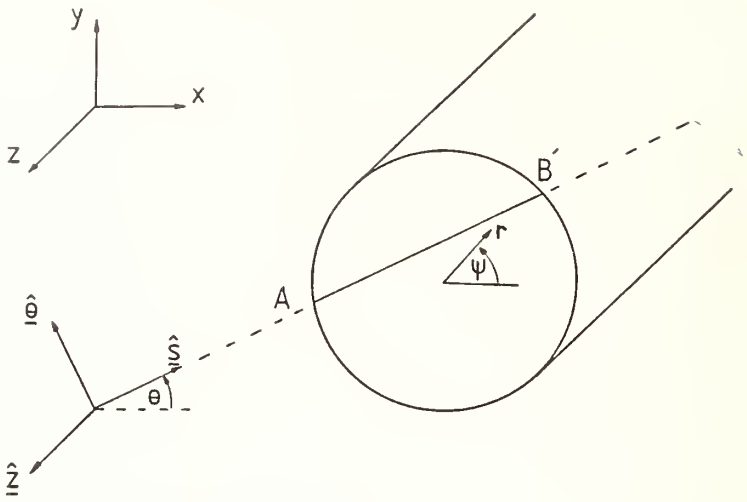

Fig. 1: Co-ordinate system

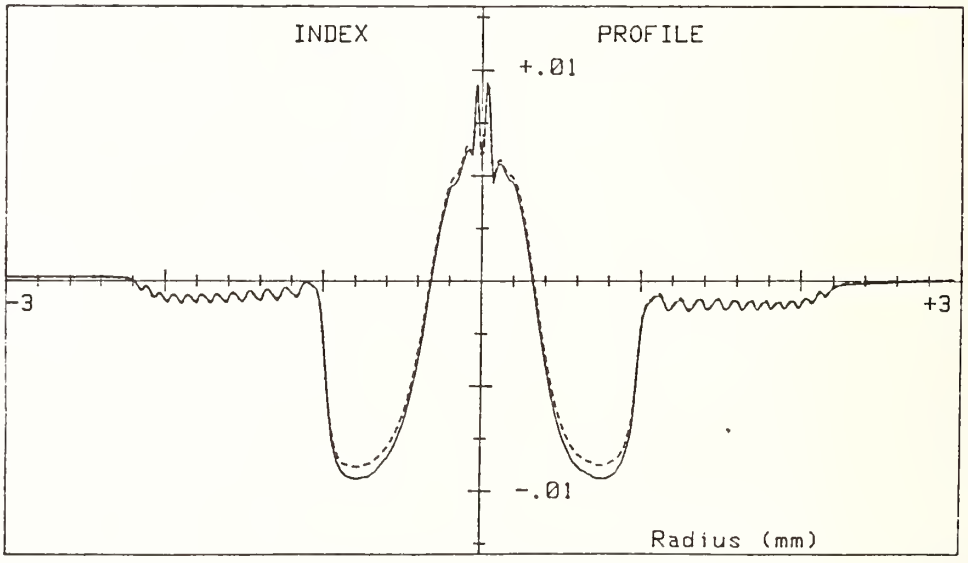

Fig. 2: Refractive index profiles measured for light polarised axially (dashed) and transversely (solid line) to the preform.

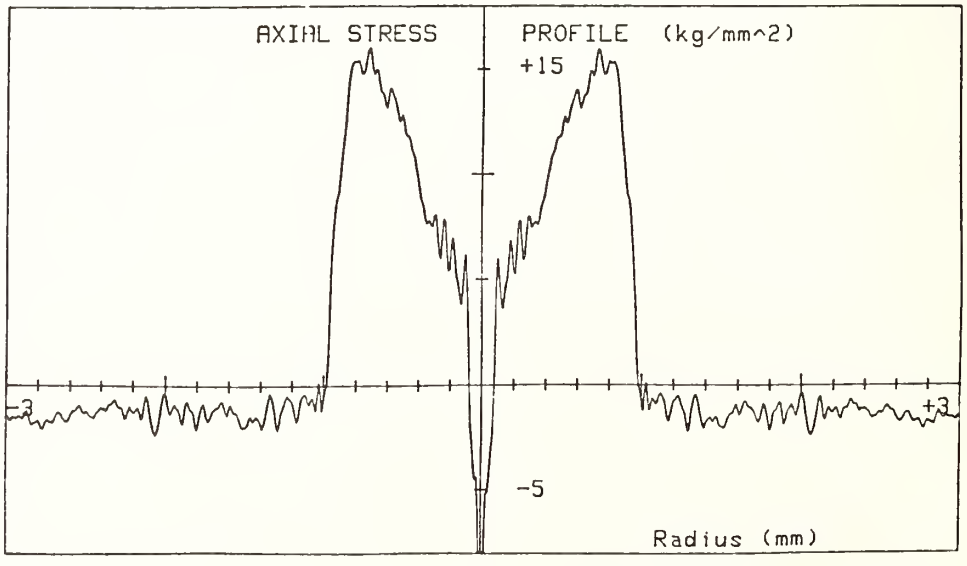

Fig. 3: Axial stress profile calculated from Fig. 2.

MULTIMODE FIBER MEASUREMENTS - PRESENT AND FUTURE

A. H. Cherin
AT&T Bell Laboratories
2000 Northeast Expressway
Norcross, Georgia 30071

I. INTRODUCTION

Multimode graded-index fibers are commonly used as the transmission medium in the intracity trunking and loop feeder distribution portions of modern telecommunication systems. It also appears likely that multimode fibers will be used, for the foreseeable future, in local area networks that offer a wide variety of integrated services. Because multimode fibers are used for both short and long distance applications, a number of different measurement methods have been developed to describe their transmission characteristics. This paper reviews some of the standardized multimode measurement methods and highlights current areas of concern related to the measurement of bandwidth, numerical aperture, core diameter and attenuation. In addition a performance related specification parameter known as the "intrinsic quality factor" (IQF) will be briefly discussed.

II. BANDWIDTH MEASUREMENT

The pulse broadening and in turn the bandwidth observed in multimode fibers is dependent upon the fiber's differential mode delay, attenuation and mode mixing characteristics. The measured value obtained for bandwidth is a function of the launching conditions and spectral width of the measurement source. Figure 1 illustrates how varying the launching condition of the source with a mode scrambler followed by a variety of mode filters affects the measured bandwidth of a multimode fiber. Although it is widely understood that a controlled launching condition will improve the precision of bandwidth measurements, the choice of the particular launching condition that gives the best prediction of the bandwidth of concatenated sections is unclear. The problem of

choosing the optimum launching condition is exacerbated by profile compensation effects in adjacent cable sections and imprecise knowledge of the length scaling coefficients of the fibers. The Electronic Industries Association (EIA) recommends overfilling the core and numerical aperture of a factory length of test fiber by placing a mode scrambler between the source and the fiber.[1] Study group XV of the CCITT recommends that bandwidth measurements be made with the same "equilibrium mode distribution" (EMD) that is used for attenuation measurements. The EMD launching condition can be approximated with a mode filter following the scrambler. Additional reduction in the measurement variation of factory bandwidth measurements can be achieved by using the 3 dB bandwidth from a Gaussian fit to the fiber transfer function instead of the transfer function itself.[2] The measurement of fiber bandwidth in the field is complicated by interconnection frames in the transmission path that contain connectors and splices. Interconnection devices can decrease the precision of a bandwidth measurement by disturbing an EMD (underfilled) launching condition if it is present at the input end of the interconnection frame. The most precise field measurements can be obtained by using a mode scrambler to produce the EIA recommended overfilled launching conditions.

III. NUMERICAL APERTURE

The numerical aperture (NA) of a graded index multimode fiber is an important parameter that is a direct measure of a fiber's light gathering efficiency and sensitivity to microbending loss. Two standardized measurement methods are commonly used to obtain a fiber's numerical aperture. In the first method the NA is calculated from a measured value of delta, the fractional difference between the peak refractive index of the core (n_1) and that of the cladding (n_2). Delta is obtained along with the fiber's core diameter from its refractive index profile. The relationship between a fiber's maximum theoretical numerical aperture and delta is given by:[3]

$$NA = \sqrt{n_1^2 - n_2^2} \cong n_1 \sqrt{2\Delta}$$

The numerical aperture can also be obtained directly from a fiber's far-field radiation pattern, since it is the sine of the maximum half-angle (in air) of the guided radiation cone. That is, the relationship between NA and the maximum half-angle, θ_a, is:

$$NA = \sin \theta_a$$

Since the EIA defines a fiber's NA between points 5% above the baseline in the far-field pattern and the CCITT defines the NA from a fiber's index profile, values for NA obtained from the different definitions will not be the same. In order to resolve these differences, a number of multimode graded-index fibers were measured using both the refractive index profile and far-field meaurement methods. A relationship was then developed between the 5% definition for NA obtained from the far-field measurements and the NA obtained from the profile measurements. This relationship requires multiplying the 5% far-field NA by 1.094 to yield a value that is equal to the maximum theoretical NA obtained from profile measurements.

IV. CORE DIAMETER

The core diameter of the multimode graded-index fiber is defined by the CCITT and the EIA, from the refractive index profile, as that diameter passing through the core center and intersecting the index profile (shown in Figure 2) at the points n_3, where $n_3 = n_2 + k(n_1 - n_2)$. The EIA has defined the value of $k = 0.025$ to minimize the differences between the refractive index profile and transmitted near-field measurement methods for obtaining core diameter.[4,5] Unfortunately the CCITT has used the value of $k = 0.05$ in their definition of core diameter. A simple change in the value of k by CCITT would result in a universal definition of core diameter that would allow the most commonly used measurement techniques to be in agreement.

V. ATTENUATION MEASUREMENTS

For long distance telecommunications applications, the attenuation of a length of fiber should be measured in such a way that the losses can be added linearly to enable the prediction of the total attenuation of concatenated links. EMD launching conditions that restrict power from being launched into higher order lossy modes, yield linearly additive attenuation values. The EIA attenuation test procedure[6] recommends two methods (the mode filter and 70/70 beam optics launch) to restrict the launched optical power. Interlaboratory measurement comparisons have shown no significant difference between the two methods and a mean standard deviation of 0.23 dB between the participants in the interlaboratory comparison.[1]

The characterization of fibers for short distance applications poses a number of difficult problems that are currently under study. A typical application, such as a wide band premise network, is connector intensive and uses light emitting diodes as the optical source. It is likely that the LED source and lossy connectors will excite high order lossy modes that will produce significant transient losses in the fiber. The excitation of high order lossy modes can produce losses that are 1-2 dB greater than fiber losses measured under steady state conditions.[7] The accurate characterization and optimum utilization of short distance systems will require the development of techniques for determining the transient losses in these systems.

VI. INTRINSIC QUALITY FACTOR (IQF)

An essential part of the fiber standardization process is the characterization of transmission parameters that optimize the economic specification of fiber tolerances and satisfy system performance requirements. An intrinsic quality factor (IQF) has been developed to efficiently allow the tolerancing of fiber parameters that effect splice loss.[8] Measurements of the delta (or NA), core diameter, core/clad eccentricity and core ovality of

a production fiber are used as input to a computer program containing an experimentally verified splice loss model. The computer program calculates the fiber's IQF. The IQF is a figure of merit that is a measure of the fiber's average bidirectional splice loss relative to a nominal fiber of the same type. By setting a tolerance on the IQF, system performance levels can be guaranteed without negatively effecting product yield. If each individual parameter were toleranced independently, unnecessarily tight tolerances would result that could reduce production yield.

REFERENCES

1. D. L. Franzen, G. W. Day, and R. L. Gallawa, "Standardizing Test Conditions for Characterizing Fibers," Laser Focus, 8/81.
2. F. T. Stone, "Problems in Bandwidth Measurment and a Suggested Solution," Journal of Lightwave Technology, Vol. LT-1, No. 1, 3/83.
3. D. Marcuse, "Principles of Optical Fiber Measurement," Academic Press, 1981.
4. A. H. Cherin, P. J. Rich and S. C. Mettler, "Measurement of the Core Diameter of Multimode Graded-Index Fibers: A Comparison of Transmitted Near-Field and Index Profiling Techniques," Journal of Lightwave Technology, Vol. LT-1, No. 2, 6/83.
5. E. M. Kim and D. L. Franzen, "Measurement of the Core Diameter of Graded-Index Optical Fibers: An Interlaboratory Comparison," Applied Optics, Vol. 21, No. 19, 10/82.
6. EIA Document RS-455-46, "Spectral Attenuation Measurement for Long-Length, Graded-Index Optical Fibers."
7. A. H. Cherin, E. D. Head, C. R. Lovelace and W. B. Gardner, "Selection of Mandrel Wrap Mode Filters for Optical Fiber Loss Measurements," Fiber and Integrated Optics, Vol. 4, No. 1, 1982.
8. D. W. Peckham, S. C. Mettler, and R. B. Kummer, "A Systematic Approch to Specifying Multimode Fiber Manufacturing Tolerances," NBS Symposium on Optical Fiber Measurements, 10/84.

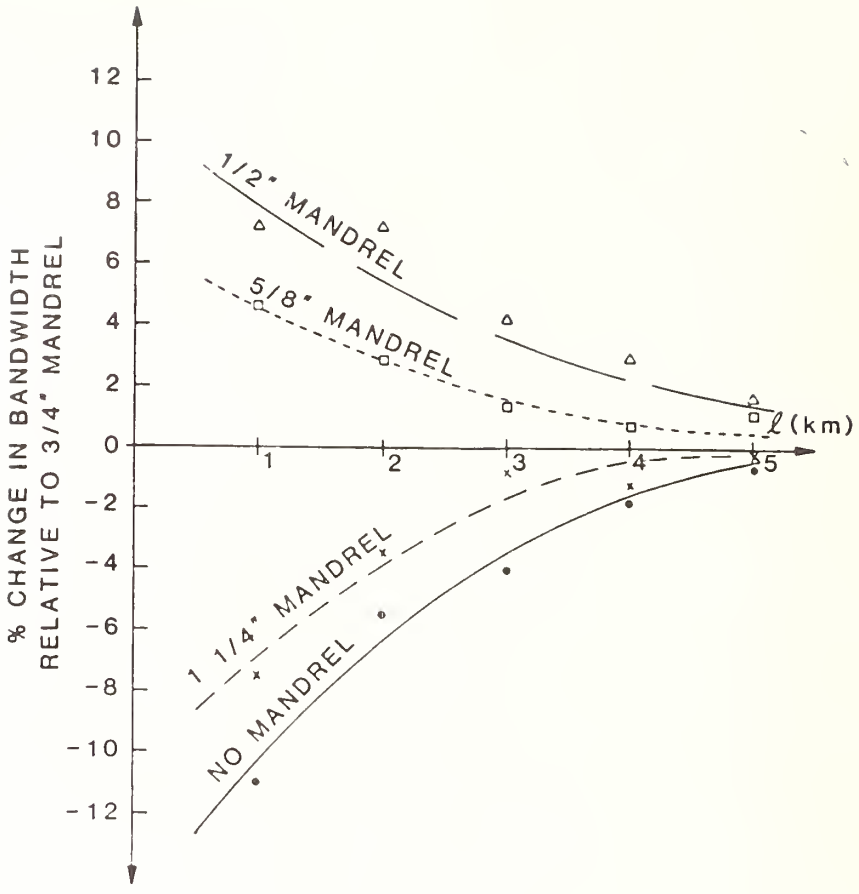

FIGURE 1

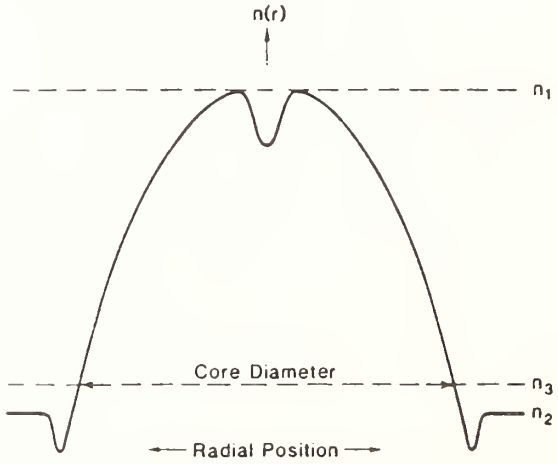

Near-parabolic refractive-index profile used for defining core diameter.

FIGURE 2

"A SYSTEMATIC APPROACH TO SPECIFYING MULTIMODE FIBER MANUFACTURING TOLERANCES"

D. W. Peckham, S. C. Mettler, and R. B. Kummer
AT&T Bell Laboratories
2000 Northeast Expressway
Norcross, Georgia 30071

INTRODUCTION

Modern low loss multimode fibers operating in the long wavelength windows are re-emphasizing the need for low loss fiber splicing. Moreover, advances in fiber joining technology increase the importance of minimizing the effects of fiber parameter variations on splice loss, making the selection of fiber manufacturing tolerances more important.

The fiber intrinsic parameters which have the greatest influence on splice loss are core radius (a), delta (Δ) (or numerical aperture), core eccentricity, and ovality. The traditional approach to setting manufacturing tolerances on these parameters is to consider the effect on splice loss of each parameter independently. This approach, however, does not take into account the compensating or compounding effect of simultaneous parameter deviations. For example, a fiber with a $+\delta a$ (i.e., a positive core radius deviation from the nominal) and a $-\delta\Delta$ will have a lower splice loss (when spliced to a nominal fiber) than a fiber with the equivalent magnitude deviations, but with both deviations of the same sign (i.e., $+\delta a, +\delta\Delta$ or $-\delta a, -\delta\Delta$). Since the effect of the combined parameter deviations is

not determined, the individual parameter tolerances are typically specified assumming the worst case combination of parameter deviations even though the probability of occurrence may be small.

An appealing alternate approach to fiber intrinsic parameter specification is to use a fiber intrinsic quality factor (IQF) specification. The IQF is a measure of the fiber parameter deviations weighted with respect to splice loss. With this approach, for example, a fiber with a large deviation of one parameter is acceptable only if the other three parameters are near nominal or if they produce an effect on splice loss that compensates for the large deviation. Thus, less stringent requirements on individual fiber parameters are needed to maintain the same mean splice loss performance as with the traditional approach (i.e., higher product yield). Alternatively, improved system splice loss can be realized while maintaining the same yield.

INTRINSIC QUALITY FACTOR

The IQF is the average bidirectional splice loss (the average splice loss occurring when light is propagated in each direction through the splice) when the fiber is spliced to a nominal fiber with no extrinsic misalignment. For example, a 54 μm core radius, 1.25% Δ fiber (with no eccentricity or ovality) when spliced to a nominal (50 μm,

1.3% Δ) fiber produces a 0.02 dB loss when light is launched into the splice from the nominal fiber, and 0.11 dB loss in the other direction, and has an IQF of 0.065 dB ((0.02 + 0.11)/2). The IQF can be measured or it can be calculated using factory measurement data as input to a splice loss model. Although other models could be used, the results presented in this paper were obtained using the empirical Gaussian splice loss model.[1]

RESULTS

Table I compares the mean and maximum IQF, and the "production yields" (normalized to the conventional approach yield) of the two specification approaches when applied to a fiber data base randomly generated using typical fiber parameter statistics. The example of the "conventional" approach limits the parameter deviations so that, when taken individually, they result in an average bidirectional splice loss (ABSL) of 0.1 dB or less. The "IQF" approach, with an IQF limit of 0.14 dB, maintains the same mean splice loss performance of the fibers (0.09 dB), but significantly decreases the worst case splice loss (0.15 dB versus 0.56 dB), while also increasing the normalized product yield (1.00 versus 1.11) when compared to the "conventional" approach. Alternatively, improved splice loss could be realized while maintaining similar yield.

SUMMARY

A systematic approach to fiber parameter specification which includes the effects on splice loss of parameter deviations has been presented. An example has been presented which illustrates the possible improvements in splice loss performance and yield obtainable with this approach.

REFERENCES

1. S. C. Mettler, "A General Characterization of Splice Loss for Multimode Optical Fibers," BSTJ, Vol. 58, No. 10, December 1979 and references cited therein.

TABLE I

	Conventional Approach (ABSL ≤ 0.10 dB)	Recommended Approach (w/IQF)
Δ:	1.3 ± 0.17%	1.3 ± 0.29%
a:	25 ± 2.3 (μm)	25 ± 3.4 (μm)
ecc:	≤ 2.4 (μm)	≤ 3.0 (μm)
Ovality	≤ 19.6%	≤ 24.3%
IQF	-	≤ 0.14
Max. Loss (ABSL)	0.56 dB	0.14 dB
Mean Loss (ABSL)	0.09 dB	0.09 dB
Normalized Yield	1.00	1.11

BANDWIDTH OPTIMISATION OF A MULTIMODE FIBRE INSTALLATION

S.C. Hampson

BICC Telecommunication Cables Limited, Prescot, England.

ABSTRACT

The Autocorrelation Function (ACF) Effective Bandwidth (Ref.1) was used to predict the concatenated frequency transmission response of a multimode fibre installation. The -3dB (Optical) bandwidth for each route fibre was then measured and the figure compared with that which had been previously predicted. A programme of cross-jointing was then devised in order to achieve the optimum transmission response for the installation. A specific objective of gaining a -3dB (Optical) bandwidth figure greater than 140 MHz for all route fibres was also set and achieved.

BACKGROUND

The installation in question runs from a local telephone exchange to a repeater station, a distance of 22.8km. This incorporates two intermediate regenerator stations thus dividing the route into 3 sub-sections of lengths 7.8km, 7.8km and 7.3km respectively. Due to difficulties experienced during cable laying, several short cable lengths were installed, see Fig 1 for a schematic of the route.

The cable system consists of eight loosely tubed fibres jointed by the fusion arc technique. The overall joint enclosure is sealed by the injection weld method.

The grade for the individual fibre was a -3dB (Optical) nominal minimum modal bandwidth of 800 MHz-km and a nominal maximum attenuation of 1.2dB/km was utilised.

SYSTEM PERFORMANCE

The cables were manufactured at the BICC cabling plant, Manchester. The Autocorrelation Function Effective Bandwidth for each of the individual fibres was derived by applying the formula :

$$BW(ACF) = 0.3\ BW(-3dB) + 0.454T^{-1}$$

where BW(-3dB) is the measured fibre bandwidth and T is the half-time to the 5% height of the autocorrelation function of the impulse response. This calculation does not require a separate measurement other than the routine factory measurement of frequency response, since the ACF is obtained from this by computation. The measurement data for the individual fibres used for the section between the two regenerators are given in Table 1.

To predict the route fibre frequency responses the ACF Effective Bandwidth figure was substituted into the formulae:

$$Bw\ (Corrected) = \left(\frac{Original\ Length}{Installed\ Length}\right)^{0.75} \times BW(ACF)$$

and

$$BW\ (Section)^{-1/\gamma} = \sum_{i=0}^{i=n} BW\ (Corrected)_i^{-1/\gamma}$$

For the 3 sections was assumed to be 0.78, while a value of 0.75 was applied for fibre sub-division.

The frequency transmission responses were then obtained for the twenty-four route fibres. The recorded bandwidths respresent the -3dB (Optical) point on the frequency response. These results show an agreement to the figure which had been previously predicted. The two sets of data are given in Table 2.

CROSS JOINTING PROGRAMME

To achieve the optimum transmission performance for the installation, a computer programme was used to calculate the frequency response of various crossed-fibre combinations.

It was established that a total number of 18 cross splices would be required at 6 joint locations. Bandwidth measurements were taken after each splice had been made. This figure was then compared to the value which had been previously predicted for that combination of fibres. On no occasion did the cross-jointing programme require modification on account of the measured figure showing a large variance from the value predicted.

The final figures achieved after the programme had been completed are given in Table 3 along with the predicted value.

CONCLUSION

The Autocorrelation Function Effective Bandwidth, proved to be a very useful tool when predicting the frequency transmission response of concatenated fibres. The actual spread between measured values was decreased and the objective of a -3dB (Optical) bandwdith figure of greater than 140 MHz was achieved for all 24 routes fibres.

The criterion established for performance prediction was very successful, and showed that when using the ACF Effective Bandwidth to optimise system fibres a concatenation constant lower than 0.78 could be used in future. This is thought to be due to the fact that the ACF Effective Bandwidth as currently defined does tend to give a pessimistic figure.

BICC now design all their multimode optical fibre systems on the basis of the ACF and have been extremely successful in predicting the frequency transmission responses for these installations.

REFERENCES

1. Determine the Concatenated Dispersion of Multimode Fibres, R.W. Blackmore and N.G. Batty - Symposium in Optical Fibre Measurements, Boulder, 1982.

FIG. 1. SCHEMATIC OF CABLE INSTALATION

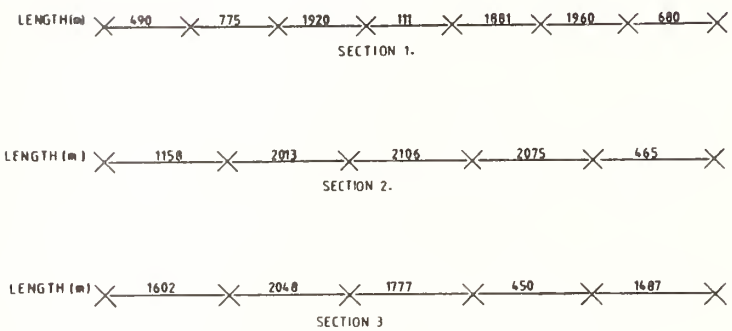

FIBRE NUMBER		1	2	3	4	5	6	7	8
CABLE POSITION	MEASUREMENT								
1	BW (-3dB)	811	890	910	847	947	967	861	890
	BW (ACF)	645	-1GHz	998	-1GHz	934	926	760	-1GHz
2	BW (-3dB)	981	987	804	800	920	923	924	809
	BW (ACF)	510	938	803	962	967	-1GHz	-1GHz	-1GHz
3	BW (-3dB)	846	850	853	893	818	829	835	869
	BW (ACF)	532	-1GHz	513	>1GHz	953	550	668	-1GHz
4	BW (-3dB)	861	833	819	989	978	907	905	817
	BW (ACF)	837	612	608	-1GHz	866	-1GHz	997	760
5	BW (-3dB)	811	890	910	847	947	967	861	890
	BW (ACF)	645	-1GHz	998	-1GHz	933	926	760	-1GHz

TABLE 1. INDIVIDUAL BANDWIDTH DATA – FIBRES FORMING SECTION 2.
(VALUES IN MHz-km)

	ROUTE FIBRE	1	2	3	4	5	6	7	8
SECTION 1	PREDICTED VALUE	196	171	128	163	120	160	131	155
	MEASURED VALUE	165	141	111	157	130	166	131	132
SECTION 2	PREDICTED VALUE	98	167	118	271	184	171	243	227
	MEASURED VALUE	101	156	111	190	156	139	139	247
SECTION 3	PREDICTED VALUE	131	216	166	159	186	122	177	171
	MEASURED VALUE	112	186	163	155	271	123	127	155

TABLE 2 MEASURED/PREDICTED FIGURES FOR STRAIGHT JOINTED SECTIONS

	ROUTE FIBRE	1	2	3	4	5	6	7	8
SECTION 1	PREDICTED VALUE	152	153	160	158	160	151	148	146
	MEASURED VALUE	175	167	165	150	202	152	152	259
SECTION 2	PREDICTED VALUE	146	152	153	140	151	146	149	162
	MEASURED VALUE	180	176	149	176	149	167	200	185
SECTION 3	PREDICTED VALUE	143	140	163	155	154	140	140	155
	MEASURED VALUE	174	232	190	210	174	163	177	196

TABLE 3. FINAL MEASURED / PREDICTED FIGURES FOR CROSS JOINTED SECTIONS

AUTOMATED DIFFERENTIAL FIBER STRAIN MEASUREMENT SYSTEM FOR SINGLE AND MULTIMODE FIBER

K. H. Hafemeister
T. A. Clarke
E. J. Buonopane

Siecor Corporation

Hickory, N.C.

Introduction:

Many optical fiber cable designs exist today which incorporate free space around the fiber to meet the tensile or temperature operating windows (example: loose tube, slotted core). This free space allows the fibers to remain strain-free while the cable itself is under tensile or temperature stress. Only after a certain load will the fibers use up all the free space available to them and begin to see the effects of the cable loading forces. The amount of load that the cable can withstand without imparting stress to the fiber is calculated by certain design parameters. This paper describes a fiber strain measurement system that can, as one option, measure the load level at which the fibers in the cable first see strain, thus ensuring the parameters of the cable design are met. This system also determines the amount of strain seen on a fiber at any stress situation and can evaluate the amount of residual strain cabled fibers see after tensile load is released.

Theory:

A tensile load placed on an optical fiber will cause the fiber to elongate. The nature of glass dictates that this elongation, or strain, is linear until the fiber breaking point is reached. The fiber strain measurement system measures this elongation by launching light pulses into the fiber and measuring the time delay that occurs as the pulses travel through the elongating section. This time delay is then converted into a value of present fiber strain. /1/

The time delay is expressed as

(1) $$\Delta t = \frac{L}{c}\Delta n + \frac{n}{c}\Delta L + \frac{\Delta n \Delta L}{c}$$

where
- L = length under load
- ΔL = change in length (elongation)
- c = speed of light in vacuum
- n = group refractive index
- Δn = change in refractive index due to strain

Assuming $\frac{\Delta n \Delta L}{c}$ is negligible, the fiber strain ε_F can then be expressed as

$$(2) \qquad \varepsilon_F = \frac{\Delta L}{L} = \frac{c}{nL} \cdot \Delta t - \frac{\Delta n}{n}$$

The refractive index change with strain is given as

$$(3) \qquad \frac{\Delta n}{n} = k \frac{c}{nL} \Delta t$$

where k is a fiber related proportionality factor. /2/

Substituting (3) into (2) gives

$$(4) \qquad \varepsilon_F = \frac{\Delta L}{L} = \frac{c}{nL} (1 - k) \Delta t$$

Technique:

To measure fiber strain, the cable sample under test is first fixed on a long length tensile tester, which can load a section of the cable up to 126 meters long with a stress varying from 0 (neglecting the weight of the suspended sample) up to 36 KN. The ends of the cable are brought to the measurement system and prepared. One fiber end is placed in a bare fiber adapter and coupled to a connectorized 50 μm core fiber pigtail mounted on a laser diode. The other end of the fiber is coupled into a silicon PIN diode using a SELFOC lens.

Laser	846 nm	FWHM	50 ps
Laser	1200 nm	FWHM	200 ps
Receiver	PIN Diode	FWHM	250 ps
Jitter	50 ps		
Resolution	10 ps	= 0.002% ε_F	
Accuracy		±0.002% ε_F	

The laser reference trigger signal is sent through a delay time generator, which compensates the sample length to adjust the position of the signal. The signal then travels through a trigger recognizer and into a digital oscilloscope.

The received signal from the PIN diode is sent through a sampling head into the oscilloscope. The oscilloscope averages the signal and smooths the curve to reduce the error in calculating delay time.

Actually measuring the delay time between the reference and the test pulse can be accomplished several ways. The method used in this system

has the Tektronix 7854 oscilloscope find both FWHM (half power level) points for the reference pulse and average them using $t_{ref} = (t_1 + t_2)/2$ (see Fig. 2 below). As load is applied to the cable, the position of the pulse is intermittently sampled. The same procedure is used to calculate an average $t_{test} = (t_3 + t_4)/2$. The delay time Δt is calculated in the computer using the formula $\Delta t = t_{test} - t_{ref}$.

Special Considerations:

This technique takes into account the differential refractive index response of the fiber under test. Using the technique may cause inaccuracies due to the material dispersion through the strained fiber section. The procedure outlined previously has been shown to be accurate with most pulse shapes, and also compensates for attenuation and distortion of the pulse shape that may occur during testing.

Output:

Fig. 3 shows a typical result generated by the computer and graphed using an X-Y Plotter. Cable strain, measured using a strain gauge attached to the cable and interfaced with the computer using an IEEE bus, is plotted along with the fiber strain, versus tensile force. The program also gives the strain at maximum force and after the load is released, as well as printing specific test criteria information directly on the results graph. The format of the graph enhances cable design analysis in that the onset of fiber strain, the fiber strain seen at specific load levels and the residual strain are all easily read from the graph or printed separately on the output page.

K for a Single Mode Fiber:

A test was set up to determine the correction factor k due to refractive index change for a single mode fiber. This test used a tight buffered cable with one single mode fiber central to the cable, ensuring that any strain applied to the cable is mechanically coupled to the fiber. The cable was loaded to 350 N and the cable strain measured using a strain gauge attached to the cable. The fiber strain was measured at both 846 and 1200 nm. Comparing the difference between the measured fiber strain and the measured cable strain gave a correction factor at both wavelengths of k=-0.20 for the single mode fiber tested.

Summary:

The fiber strain system described provides an easy, accurate method of characterizing cables with respect to their design parameters.
The computer driven system is easily used in a quality control environment, where cable designs can be type tested to ensure product specifications are met. The system can be used with multimode and single mode systems, once cable related proportionality constants have been determined.

/1/ Philen, D.L., Patel, P.D.
Measurements of strain in optical fiber cables using a commercial distance meter
ECOC 82 communication AV II-3

/2/ Sutor, Norbert.
Testing the Mechanical and Thermal Characteristics of Optical Cables.
Siemens Telcom Report 6 (1983), pp. 183-187.

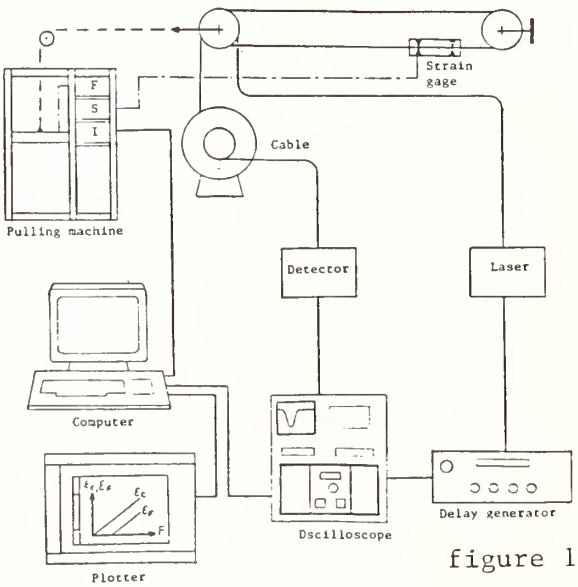

figure 1

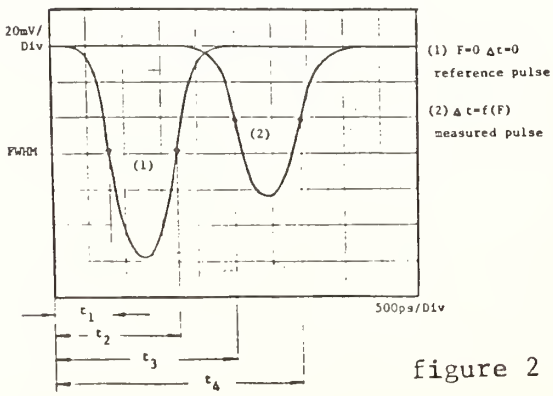

figure 2

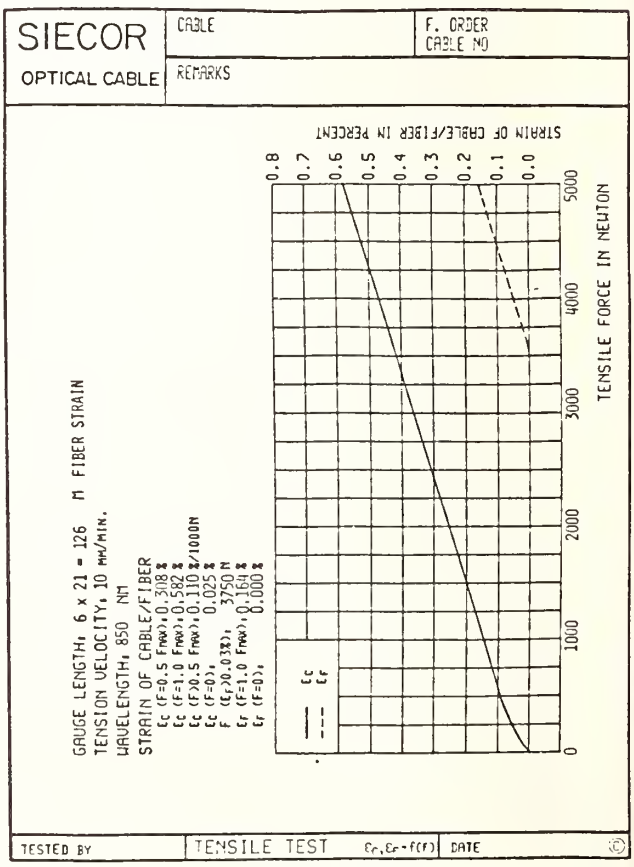

figure 3

The distribution of H_2 gas along an inland optical fibre cable

S Hornung, S A Cassidy, M H Reeve B.T.R.L. Martlesham Heath, Ipswich, Suffolk, UK

1. Introduction. Recently a good deal of interest has concentrated on the effects of H_2 on the optical attenuation of fibre (1). The work has mainly focused on the response of fibre to relatively high levels of H_2, often at elevated temperatures. Little has been reported of actual levels of H_2 in cables in operational environments.

In this paper we report the field measurement of levels of H_2 inside an optical fibre cable and it's distribution along the cable length. The cable chosen was a BICC "Jubilee" type, linking Guildford to Aldershot. It was selected because it contains high phosphorus doped multimode fibre, which is particularly sensitive to H_2 (2). We also report two follow-up experiments, which together with a simple model go some way in explaining the nature of the experimental results.

2.1 Field measurement. H_2 was detected by a portable "Exhaled H_2 Monitor" (made for the medical profession), which is in essence a fuel cell.

20cc samples of gas were drawn off at a series of joint housings along the cable route via Schroeder valves (part of the cables pressurisation arrangement) and introduced into the instrument. The instrument was re-calibrated at each measurement point. The results are plotted in Figs. 1 to 3. The pressurisation path of Guildford to Aldershot was interrupted on either side of a midpoint regenerator AP1. This resulted in two independently pressurised systems, Guildford-AP1 and Aldershot-AP1. The distribution of H_2 in these sections is similar, starting at 0 at the exchange (high pressure) end, and rising to a maximum value at the dead end (AP1). The peak value recorded anywhere was 394ppm. Measurements on the adjoining Aldershot-Camberley cable also fit this pattern.

We propose the following model. H_2 is continuously generated along the cable length at a constant rate of R cc/sec/cm of cable, and diffuses through the cable walls at the rate C*W cc/sec/cm of cable. Here C is the partial pressure of H_2, and W is an effective diffusion constant. H_2 is also swept along the cable by a flow of gas C*F. The flow F is a constant in a particular part of a cable and is assumed to be caused by some leakage further down the cable. In the two cable sections described above, a main leak is assumed to be situated at a single point along the length. Two values of F are then used, a higher one up to the leak and a very small one beyond it. By equalising the H_2 generation and dissipation rates we can derive the concentration of H_2 along cable length x, as :

$$C = \frac{R}{W}\left[1 - \left(1 - \frac{W}{R}C_o\right)\exp-\left(\frac{Wx}{FV_o}\right)\right] \qquad (1)$$

C_o is the initial partial pressure of H_2 and V_o is cable volume per unit length. Figs. 1 to 3 also show simple fits to the experimental data points using the above equation. The calculated values of R, W and F are given in table 1.

2.2 Diffusion measurements. To convert the fitted values of R, W and F in arbitrary units into real numbers given in table 1, more measurements were needed. W was measured directly. Nitrogen containing a known percentage of H_2 was passed along two short (0.1m) and two long (2.5m) cable samples, each surrounded by a sealed copper tube. The level of H_2 in the copper tubes was monitored as function of time (Fig. 4), giving $W=3.7*10^{-8}$ cc/sec/atm/cm of cable at 20 ^{o}C. Doubling the samples and using different lengths allowed the elimination of end effects and greatly reduced the possibility of a freak defect in the construction.

The nature of the cable construction is that the most significant route for H_2 to escape is along the aluminium barrier overlap. (Fig.5) The diffusion through aluminium is much slower. The aluminium barrier is polyethylene coated and the heat of the final polyethylene layer coating seals the overlap producing a 6mm deep and 40µm high polyethylene channel. The diffusion rate under these conditions would be about $6.1*10^{-10}$ cc/sec/atm/cm of cable. The much larger experimental value implies that the overlap region is not perfectly sealed.

2.3 Equilibrium level test. The level of H_2 was measured in a spare cable length. As the cable had never been pressurised, this then gave a result of H_2 level in the absence of flow. The cable was connected at one end to a supply of compressed N_2 and at the other to the H_2 detector. The level of H_2 in the spare cable was found to be uniformly 364ppm, dropping to zero at the cable ends due to diffusion. Using the constants R, W, V_o and C_0, the build up of H_2 can be expressed as:

$$C = \frac{R}{W}\left[1 - \left(1 - \frac{W}{R}C_o\right)\exp-\left(\frac{Wt}{V_o}\right)\right] \qquad (2)$$

The spare cable is 2years 5months old ($7.62*10^{7}$ sec), $C=3.64*10^{-4}$ atm, $C_0=0$. Using the experimentally measured $W=3.7*10^{-8}$ cc/sec/atm/cm of cable, we calculate that $R=1.5*10^{-11}$ cc/sec/cm of cable. Finally the experimentally measured $R=1.5*10^{-11}$ cc/sec/cm of cable and $W=1.58*10^{-8}$ cc/sec/atm/cm of cable (corrected for field temperature of 5 ^{o}C),(4,5) are substituted into equation 1. giving the values of F in the various cable sections. In this calculation we note that the partial pressure of H_2 is $1.6/10^{6}$ times the concentration measured in ppm due to the cable's pressurisation to 1.6atm. It is assumed that the H_2 generation rate is the same in the field and in the spare cable.

3. Discussion. Taking into account the exponential nature of H_2 build up, the equilibrium level in this type of cable will be 400ppm (at 1.6 atmospheres). The increase in attenuation of phosphor-doped multimode fibre at this level of H_2 is very much subject to the nature of extrapolations from experiments spanning a few months to 30 years. For low phosphorus doped fibre up to approximately 0.06dB/km at 1.3μm can be expected (3).

It is apparent that the quality of the Aluminium water barrier (APL) seal is important. Fig.6 shows a comparison of H_2 build up for the measured value of W, for the value of W in the case of a perfectly made APL seal and in the case of a completely sealed up cable. If the water barrier was perfectly sealed then the level of H_2 after 2.5 years would be a factor of 3 higher. A poorer water barrier is therefore an advantage in this respect, but must be balanced against the risk of moisture ingress.

The presence of air flow in the cables clearly reduces the average H_2 level to well below 400ppm. A certain level of flow could therefore be engineered into any system, which could also sweep out any moisture.

Much work still needs to be done to identify the sources of H_2 generation. In the simple model described in this paper the H_2 generation rate was assumed to be constant. It is not clear whether H_2 in inland cables is generated by corrosion/polymer degradation process, or whether H_2 is released from material where it was trapped. These H_2 producing processes may have quite different profiles with time, which would make extrapolations to system lifetime difficult.

4. References

1.Increased Attenuation of Optical Fibres Caused by Diffusion of Hydrogen. K J Beales et. al. 9th. ECOC Geneva October 1983.

2.Optical Loss Increase of Phosphor-doped Silica Fibre at High Temperature in the Long Wavelength Region. N Uesugi et. al. Appl. Phys. Lett. 43(4) 15 August 1983.

3.Hydrogen Effects in Installed Cables and Under Accelerated Conditions. J S Stannard-Powell et. al. IEE Colloquium, June 11-12 1984 London.

4.Polythene. A Renfrew and P Morgan, 2nd Edition, 1960.

5.Polymer Handbook. J Bandrup and E H Immergut, (Editors) 1966.

Table 1.	Guildford-AP1.	Aldershot-AP1.	Aldershot-Camberley
R cc/s/cm of cable	$1.5 * 10^{-11}$	$1.5 * 10^{-11}$	$1.5 * 10^{-11}$
W cc/s/cm of cable ($5^{o}C$)	$1.58 * 10^{-8}$	$1.58 * 10^{-8}$	$1.58 * 10^{-8}$
F_1 cc/s	$8.2 * 10^{-2}$	$6.5 * 10^{-2}$	$4.9 * 10^{-2}$
F_2 cc/s	$0.03 * 10^{-2}$	$1.6 * 10^{-2}$	-

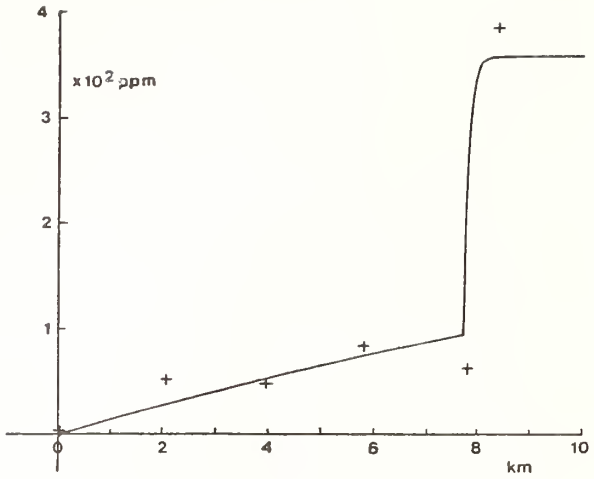

Fig.1 H_2 in Guildford-AP1 section.

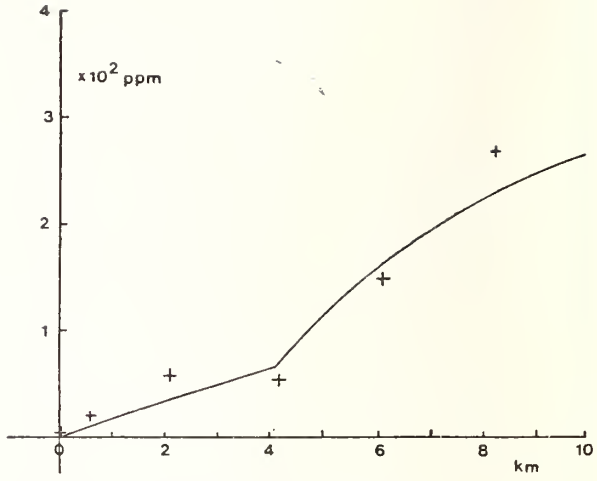

Fig.2 H_2 in Aldershot-AP1 section.

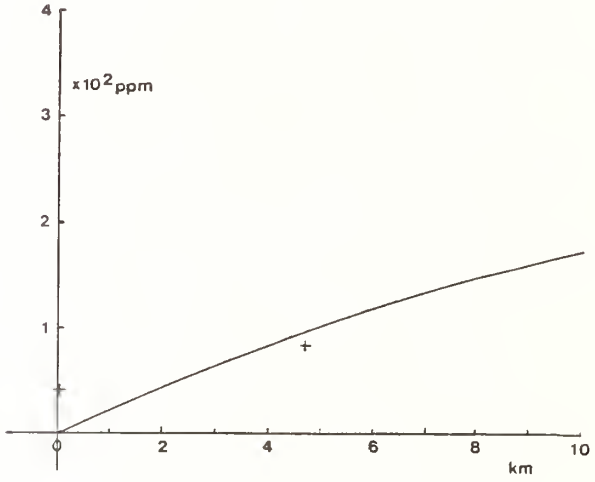

Fig.3 H_2 in Aldershot-Camberley section.

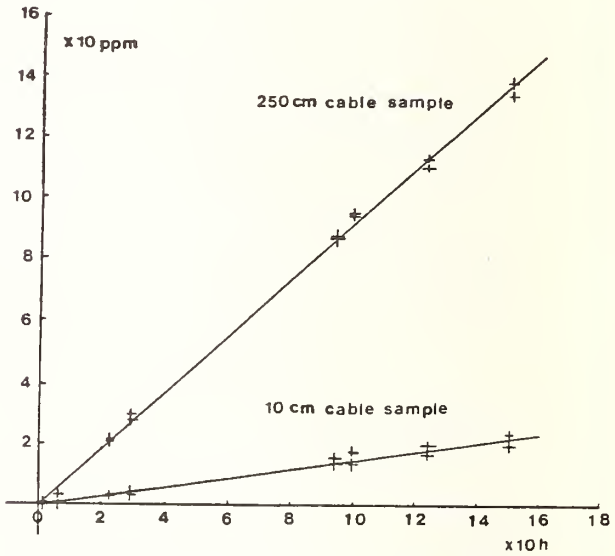

Fig.4 H_2 diffusion from cable samples.

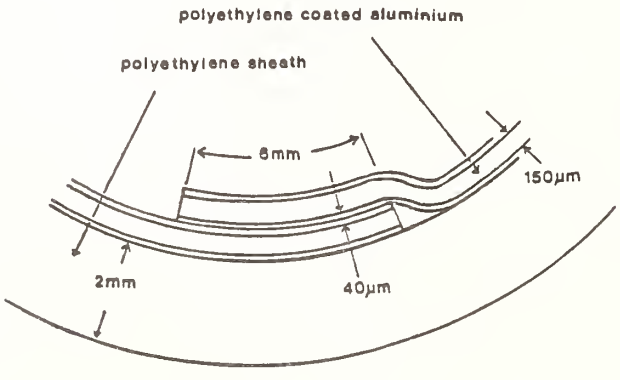

Fig.5 Water barrier overlap.

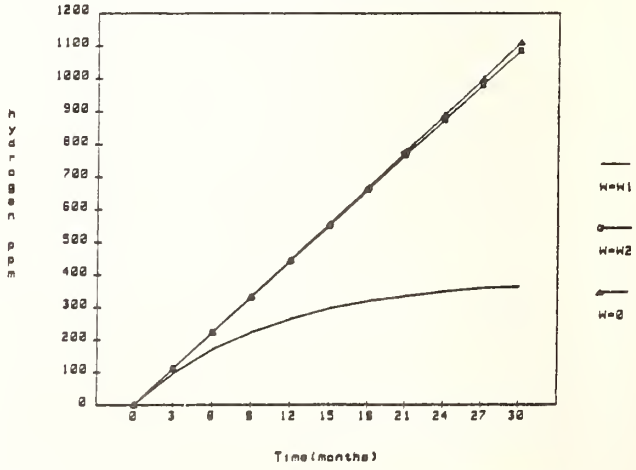

Fig.6 H_2 vs. time $W_1=1.6*10^{-8}$cc/s/cm/atm, $W_2=6.1*10^{-10}$cc/s/cm/atm.

ADVANCES IN OPTICAL TIME-DOMAIN REFLECTOMETRY

A.H. Hartog,
York Technology Ltd., Avenger Close, Chandler's Ford, SO5 3DQ, UK.

1. Introduction

In recent years, optical time-domain reflectometry (OTDR)[1] has progressed from a laboratory experiment to a technique in everyday use by manufacturers and users of optical fibres. The principal attraction of the technique is its ability to give, non destructively, a good indication of the fibre-loss uniformity and therefore to reveal any localised defects in the fibre. It has also been employed as a means of measuring accurately fibre[2] and splice losses[3], and of studying the longitudinal variation of fibre parameters[4,5].

Briefly, OTDR involves the launching of a short pulse of light into the fibre. As the pulse travels along the fibre, its energy is lost in part to Rayleigh scattering. Some of the scattered light is recaptured in the backward direction and guided towards the launching end where it may be detected. The signal obtained takes the form:

$$P_s(t) = P_o W \eta(z) \exp\left[-\int_0^z 2\alpha(z)dz\right] \qquad (1)$$

where the time and position variables t and z are related by $z = v_g t/2$ (v_g is the group velocity). $P_o W$ represents the forward pulse energy, $\alpha(z)$ the local attenuation and $\eta(z)$ the backscatter factor. $\eta(z)$depends on the fibre waveguide and scattering properties and varies from typically 300 W/J for multimode fibres[6] at 850nm to 10 W/J for single-mode fibres at 1300nm[7,8].

It is clear from (1) that a backscatter signal will not in general give the local fibre attenuation directly since any longitudinal change in the rate-of-decay of $P_s(z)$ could be caused equally by variations of $\eta(z)$ or of $\alpha(z)$. Nevertheless, the mere presence of a non-uniformity normally provides most of the information required and if the measurement is repeated from the opposite fibre end, the effects may be separated unambiguously[4,5]. This paper will review the development of OTDR with particular emphasis on long range single-mode measurements at 1300nm and beyond.

2. Performance Criteria in OTDR

Dynamic range is the single most important criterion of the performance of an OTDR. It is a measure of the fibre loss through which the backscatter signal may be measured to a given accuracy and is expressed in "dB one-way". Although definitions abound, that preferred by the author, particularly for long wavelength systems, is the range at which the signal from Rayleigh scattering becomes equal to the r.m.s. noise.

The spatial resolution of an OTDR depends on the ability of the instrument to respond to an abrupt change of backscatter signal along the fibre and is determined by the convolution of the probe pulse with the impulse response of the optical receiver and data-acquisition equipment. At high resolution, the probe pulse energy is reduced and the noise-equivalent power of the receiver is increased; both effects lead to a reduction in the signal-to-noise ratio. A strong trade-off thus exists between the dynamic range and the spatial resolution of the measurement, and equipment specifications must be considered with this point in mind. More-

over, resolutions quoted in fact frequently refer to the sample separation of the data acquisition electronics rather than to the system analogue risetime.

In addition, the design of an OTDR is influenced by the requirement for portability and ruggedness which usually dictates fairly simple optical designs,the use of injection lasers and precludes any significant cooling of the detector. The wavelength of the probe pulse must be close to the fibre operating wavelength if valid attenuation measurements are to be obtained and to avoid spurious wavelength dependent effects such as the second-mode cut-off loss peak or the microbending edge in single-mode fibres.

As a point of reference, commercially available OTDRs at 850nm typically use a semiconductor laser source, a silicon avalanche photodiode detector (APD) and an all-fibre directional coupler. Typically the dynamic range is 25dB one-way for a resolution of 10m.

3. Operation at Long Wavelength and with Single-Mode Fibres

Pulsed sources for OTDR at 1300nm are not so readily available as at 850nm; their output power is lower and their reliability and temperature stability are worse. Moreover, the silicon APD, an almost ideal detector, does not respond at 1300nm and no other material has shown a similar performance. Germanium APD's are particularly at a disadvantage because, in the bandwidths of interest, their leakage current severely limits the receiver sensitivity. Presently none of the commercially-available APD's can compete at 1300nm with PIN diodes, although some of the laboratory quaternary devices would provide a small improvement in

receiver sensitivity.

Additional difficulties are encountered in the design of single-mode reflectometers. For example, the power available from single transverse-mode injection lasers is low and efficient launching into single-mode fibres is difficult owing to the ellipticity and astigmatism of the laser output. Moreover, the backscatter factor is lower in these fibres than in multimode fibres at the same wavelength. The design of single-mode OTDR's must also avoid any polarisation sensitivity in the return optical path, which would lead to an unwanted modulation of the backscatter signal in accordance with the local fibre birefringence.

4. Long-Range Single Mode OTDR at 1300nm

Much work has been devoted recently to the development of OTDR systems for testing single-mode communications at 1300nm and beyond. In this application, the minimum requirement is to detect a break within a repeater span (25dB of fibre loss at 140 Mb/s). A spatial resolution of 100m is usually adopted which is sufficient to determine with certainty the fibre section at fault. There is an overwhelming need for the equipment to be portable and rugged which precludes, for example, the use of high power lasers and cryogenic detectors. In practice, only low-noise analogue direct detection and heterodyne detections are serious contenders.

In the first approach[9,10], a PIN photodiode operated at room temperature is used together with an ultra-low-noise FET-input preamplifier; the receiver sensitivity reported is 30pW before averaging. Multichannel digital averaging allows a further improvement in sensitivity to 30fW in a measurement time of 20 min.

With a semiconductor laser, a dynamic range of 30dB one-way has been obtained, the highest value reported to date. The sensitivity of this receiver matches that of a photon counting receiver using a Ge APD at 77K[11].

In heterodyne detection[12,13], the probe pulse and hence the backscattered power is frequency-shifted with an acousto-optic deflector (AOD) and mixed on the photodiode with an unshifted portion of the source power, which is used as a local oscillator. A backscatter signal is obtained at the intermediate frequency (IF), equal to the frequency shift of the AOD. The detected signal is proportional to the product of the backscatter and local oscillator (LO) electric fields. With sufficient LO power, the signal at the IF can be made large compared with the receiver noise. A coherent backscatter receiver can in principle be two orders of magnitude more sensitive than a direct detection front-end. However, this scheme requires the use of extremely narrow linewidth sources (i.e. a spectral width of the order of the IF bandwidth). Apart from the practicalities of producing a 1MHz linewidth portable laser, the output power of such sources is usually substantially lower than that available from unstabilised lasers. This offsets at least in part the sensitivity advantages of the coherent detection scheme and the best results published to date[13] have failed to match the dynamic range performance of direct detection, although a receiver sensitivity better by a factor of 4 has been demonstrated. Coherent detection suffers from its intrinsic sensitivity to the state-of-polarisation of the back-scatter signal and to the speckle-like noise associated with the

use of a highly monochromatic source[14].

5. Conclusions

Research into both coherent and direct-detection long-range OTDR systems is active and it is clear that further improvements will be achieved; these will result in part from the availability of better devices namely, higher power, narrower linewidth lasers for coherent detection and low-leakage current APD's for direct detection. Progress is rapid in both of these areas and it is not yet clear which approach will prove to be the most effective in practical instruments.

Finally the use of OTDR has spread into new areas and recently it has been applied to the development of distributed sensors, an area which shows considerable scope for innovation in optical time domain reflectometry.

The author would like to thank M.P. Gold for helpful discussions.

References

1. M.K. Barnoski and S.M. Jensen, Appl. Opt., 1976, 15, pp. 2112-2115.
2. B. Costa, et al., Electron. Lett., 1980, 16, pp. 352-353.
3. M.P. Gold, et al., Electron. Lett., 1984, 20, pp. 338-340.
4. P. DiVita and U. Rossi, Opt. & Quant. Electron., 1980, 11, pp. 17-22.
5. M.P. Gold and A.H. Hartog, Electron. Lett., 1982, 18, pp. 489-490.
6. A.R. Mickelson and M. Eriksrud, Appl. Opt., 1982, 21, pp. 1898-1909.
7. E. Brinkmeyer, Electron. Lett.,
8. A.H. Hartog and M.P. Gold, J. Lightwave Technol., 1983, LT2, pp. 76-82.
9. M.P. Gold and A.H. Hartog, Electron. Lett., 1984, 20, pp. 285-287.
10. M.P. Gold, submitted to J. Lightwave Technol.
11. P. Healey, Electron. Lett., 1981, 17, pp. 751-752.
12. P. Healey and D.J. Malyon, Electron. Lett., 1982, 18, pp. 862-863.
13. S. Wright, et al., Proc. 9th ECOC, Geneva, 1983, pp. 177-180.
14. W. Eickhoff and R. Ulrich, Tech. Digest 3rd IOOC, San Francisco, 1981, pp. 76-78.

1.3 μm PORTABLE REFLECTOMETER FOR THE FIELD TEST OF SINGLE-MODE FIBER CABLES

-°-

J.J. BERNARD, E. DEPRESLES, L. JEUNHOMME, J.L. MONCELET

LABORATOIRES DE MARCOUSSIS, CGE RESEARCH CENTER
91460 MARCOUSSIS - FRANCE

M. CARRATT

C.L.T.O - COMPAGNIE LYONNAISE DE TRANSMISSIONS OPTIQUES
35, rue Jean-Jaurès - B. P. 20
95871 BEZONS CEDEX - FRANCE

INTRODUCTION

The growth of single-mode optical fiber transmission systems at 1.3 μm requires test instruments for field use, specially designed for attenuation measurements, splices control, detection and localization of possible breaks.
We describe in this paper a new portable optical time-domain reflectometer using the correlation technique [1], designed for the field test of single-mode fiber cables.
This device, presently beeing developped,shows a 15 dB one-way dynamic range together with a 10 m ultimate spatial resolution.

PRINCIPLE

The instrument consists of a pseudo- random 2^{15} -1 bits NRZ sequence generator, wich modulates a GaInAsP/InP buried-heterostructure single-mode laser (see figure 1). The optical power is injected into the test fiber through a single-mode fiber splitter and a pigtail fiber.

The backscattered light is then detected by an avalanche photodiode and the electrical signal is multiplied by the shifted emitted sequence after amplification. The RC integrator provides an analog signal, the amplitude of wich is proportional to the optical power backscattered from the analyzed point in the fiber. The time delay between the emitted and the shifted sequences corresponds to the two-way propagation time up to this analyzed point.
The time delay is controlled by a minicomputer, connected to the correlator output through an analog-to-IEEE 488 interface.
By varying the time delay, we can obtain the whole backscattering curve of the fiber.
Two kinds of measurements are possible : first the test of a complete long length fiber (20 km or more) with a 250 m spatial resolution, second a more accurate analysis in a specified window with a high spatial resolution (up to 10 m), for any abscissa.
Presently, the attenuation measurement sensitivity is 0.2 dB. It can be improved by decreasing the source and reception noises.

EXPERIMENTAL RESULTS

As an illustration, figure 2 shows the test result of a 17 km-long single mode fiber, the end of wich was immersed in an index-matching liquid, in order to avoid any optical reflection that could trouble the reception operation.
An averaging number of 16, together with a 40 m spatial resolution, gives a 13 dB one-way dynamic range. A more than 15 dB one-way dynamic range has been attained by improving the averaging number up to 128, with a measurement time close to 20 mn.

CONCLUSION

This correlation optical time-domain reflectometer, through its high performance, its large variety of software and its very easy implementation is particularly well suited to the needs of single-mode fiber systems users.

ACKNOWLEDGEMENTS

The authors would like to thank then colleagues of CGE Research Center for there help with many aspects of this work, and G. Le Blevennec of CLTO for his technical support.

REFERENCE

[1] P. Healey "Pulse compression coding in optical time domain reflectometry". 7th ECOC, Copenhaguen, 8-11 Sept. 1981.

FIGURE 1 - SCHEMATIC DIAGRAM OF THE CORRELATION REFLECTOMETER

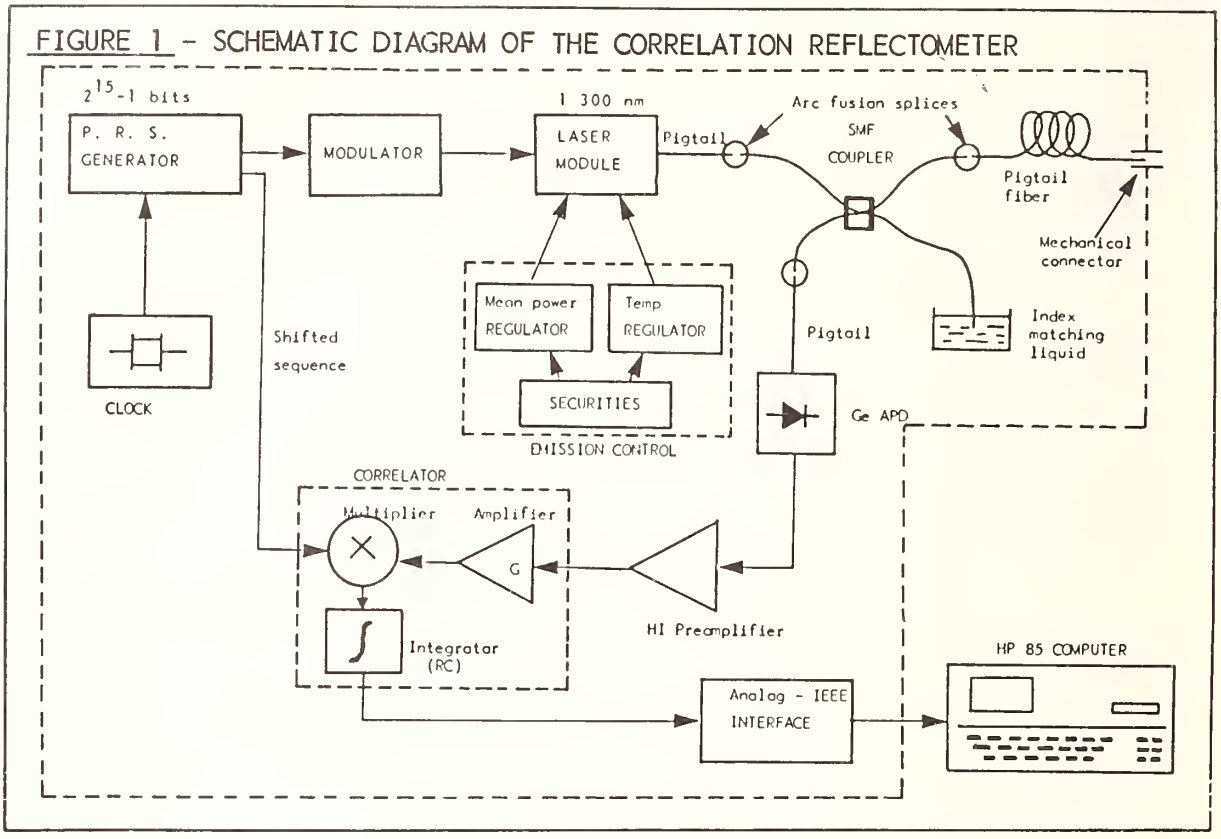

FIGURE 2 - ANALYSIS OF A 17 KM LONG SINGLE-MODE FIBER

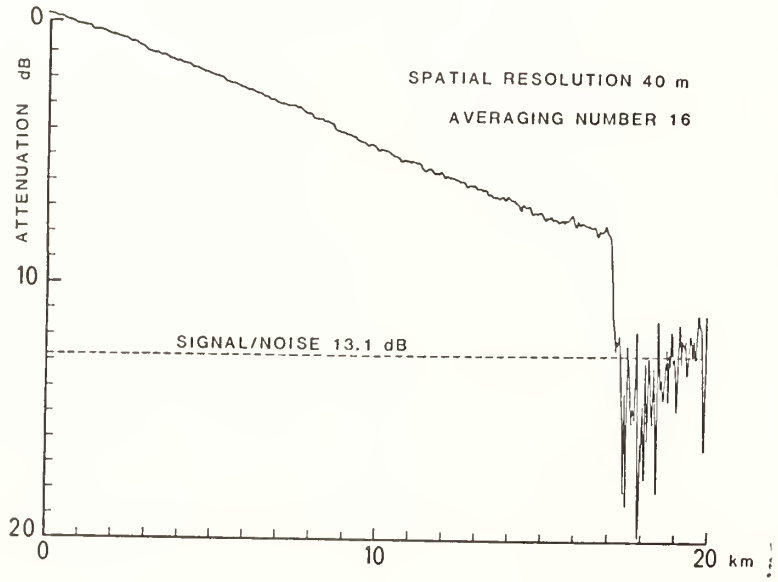

FIGURE 3 : PHOTOGRAPH OF THE REFLECTOME

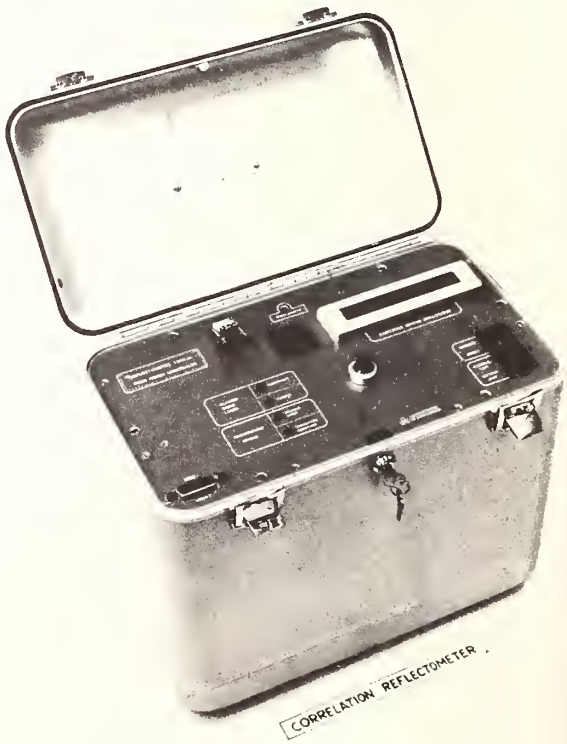

LONG-TERM HIGH-STABLE OPTICAL FIBER LOSS MEASURING EQUIPMENT

Y. Namihira
KDD R&D Labs
1-23, Nakameguro 2-Chome
Meguro-ku, Tokyo, Japan

H. Wakabayashi
KDD Head Office
3-2, Nishishinjuku 2-Chome
Shinjuku-ku, Tokyo, Japan

H. Yamamoto S. Adachi
Ando Electric Co., Ltd.
19-7 Kamata 4-Chome, Ota-ku, Tokyo, Japan

1. INTRODUCTION

Optical fiber submarine cable systems are promising for international transmission lines because of the possibility of a more economical high-capacity digital lines compared with the conventional submarine systems.(1)(2)(3) Optical fiber submarine cable development requires the precise evaluation of cable transmission characteristics over a long period under various environmental conditions such as tensile force, water pressure and ambient temperature. For this reason, cable testing facility which can simulate the ocean bottom conditions are used to evaluate the effects of external conditions on loss. Physical limitations on the cable testing facility, however, limit the cable length to no more than 100 to 200 meters, and, with lengths of cable in this order, a loss measurement resolution of 0.001 dB is required.(4) The authors have developed a technique making use of an LED light source and a high-stability constant-temperature box capable of control to within 0.1°C to perform measurements with a dynamic range of approximately 10 dB, a resolution of 0.001 dB and a stability of ±0.001 dB over a 5-hour-period.(5)

This paper describes a comparison measuring method which enables the measurement of very small variations in optical fiber loss, a capability not available with previously used direct measuring method.

2. OUTLINE OF THE MEASURING SYSTEM

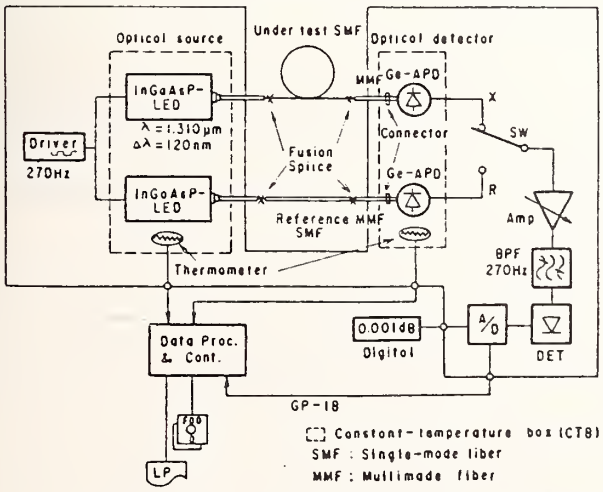

Fig 1 Block diagram of measuring system for minute variations of optical-fiber loss

Fig. 1 shows the block diagram of the measuring system. To obtain better temperature stability than that of a laser diode, an LED (double-hetero structure InGaAsP/InP) is used as the light source. In the conventional comparison measuring method, a light from one optical source is divided into two signals using a fiber divider, one for the

reference fiber (R-side) and the other for the fiber under measurement (X-side). However using present techniques, there are some problems in the stability of temperature characteristics of the fiber divider. Accordingly, in this paper, as the comparison measuring method, we use the two LED optical sources with the almost same characteristics.

On the light-receiving end, no-bias 100 μm diameter Ge-APDs are used as optical detectors to achieve high-stability and a high signal-to-noise ratio.

The optical outputs from the reference fiber (approx. 5 m in length) and the fiber under measurement are opto-electrically converted by the Ge-APDs individually and then the signals are processed. The LEDs are modulated at 270 Hz (i.e., a non-integer multiple of commercial power line frequency of 50 or 60 Hz) and the receiving circuitry consists of an amplifier, narrow-band bandpass filter and detector circuit. The A-D converted X-side and R-side optical powers are calculated internally, and the difference between these two values (X-R) is displayed in four digits with a resolution of 0.001 dB.

Some of the data including the optical fiber loss variations are entered into the controller and stored onto floppy disk as well as being printed to a plotter. To be able to accommodate power failures occurring during long-term measurements, an auto-start function is designed into the system.

3. ADVANTAGES OF THE COMPARISON MEASURING METHOD

In the long-term measurement of minute optical fiber cable loss variations with high accuracy and stability, the following are some causes of systematic variations.

a. LED Output level variation caused by ambient temperature variations.
b. LED Output level variation caused by drive current variations.
c. Receiving level variation caused by wavelength variations.
d. Ge-APD Sensitivity variation caused by ambient temperature variations.
e. Variations in the receiving circuitry (amplifier circuit, bandpass filter and detector) caused by ambient temperature variations.
f. Signal-to-noise ratio.

Both the LED and Ge-APD are enclosed in a constant-temperature box, making the expected stability 0.003 dB at room temperature, based on the previous system results. In addition, since this system uses the comparison method, as long as the channel-to-channel tracking of the variations between the two LEDs is approximately 80%, a stability of 0.001 dB is easily achievable. Variations with respect to drive current and wavelength are made negligible by enclosing both the devices and drive power supply in a constant-temperature box. Also, since the receiving system amplifier, bandpass filter and detector are commonly used in the measurement of the R and X side signals, long-term variations are cancelled. The system noise level is approximately -80 dBm, so that

with a signal level of -45 dBm, a signal-to-noise ratio of 35 dB is achieved. Although this is equivalent to 0.003 dB in level variation, averaging can be expected to improve the signal-to-noise ratio.

The internal temperatures of the constant-temperature boxes used to house the sending and receiving sections are A-D converted individually and this data is sent to the controller, at which software making use of this temperature data compensates for overall temperature stability.

4. EQUIPMENT STABILITY

Table 1 shows the design goals and actually achieved performance. Fig. 2 shows the results of a 100-hour stability test on the system performed at room temperature. Fig. 2(a) and 2(c) show the (X-R) and (R) stability respectively, while Fig. 2(b) and 2(d) show the temperature variations of the light source side and receiving side constant-temperature boxes, from which it can be seen that both have stability of approximately ±0.2°C. Fig. 2(e) indicates room temperature variations.

By having the controller perform averaging of measured data, a resolution of 0.001 dB or better is achieved.

Table 1. Design goal and actual value of measuring system

	Design goal	Actual value
Optical source	LED	InGaAsP-LED
Wavelength	1.30 ± 0.03 (μm)	1.310 (μm)
Dynamic range	≥10 dB	≃12.0 dB
Measurig system stability	≤ ±0.003 dB/year	± 0.001/100H
	≤ ±0.001 dB/year (Target value)	
Resolution	0.001 dB	0.001 dB
LED output power	≥ -45 dBm	X; -38.6 dBm
	≥ -40 dBm (Target value)	R; -37.7 dBm
Optical detector	Ge-APD	Ge-APD
Temperature stability of CTB*	≤ ± 0.2°C/year	≤ ±0.2°C/100H
Test Fiber	SMF (≃9/125 μm)	SMF
Ambient Temperature	23±5°C	23±5°C

* CTB : constant-temperature box

5. CONCLUSION

The comparison measuring method in place of the previously used direct measuring method shows good results in performing measurement of minute variations in optical fiber characteristics with both high accuracy and high resolution. The system described is suitable for use in the development of optical submarine fiber cable systems. The system configuration is shown in Fig. 3.

6. ACKNOWLEDGEMENT

The authors wish to thank Dr. H. Kaji, Dr. C. Ota, Y. Iwamoto and M. Nunokawa in KDD Labs., and Y. Niiro and H. Yamamoto in KDD Head Office for their discussions and encouragement, and T. Ueno and K. Inoue in Ando Electric Co., Ltd., for their helpful assistance and cooperations.

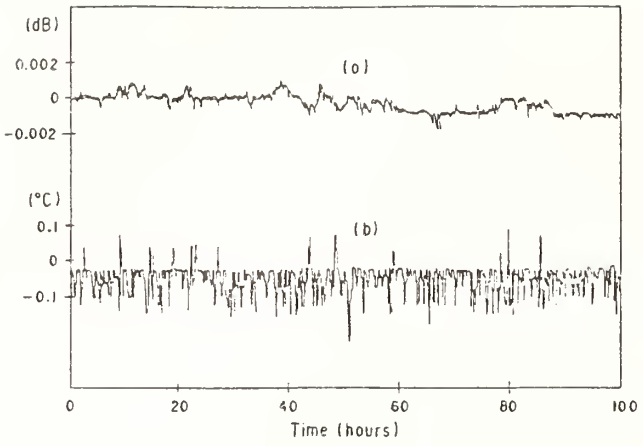

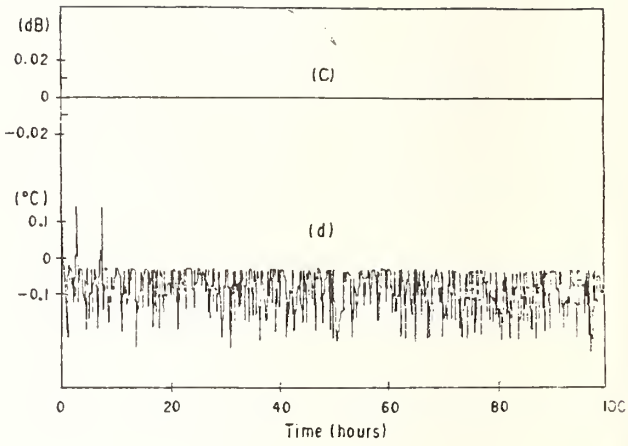

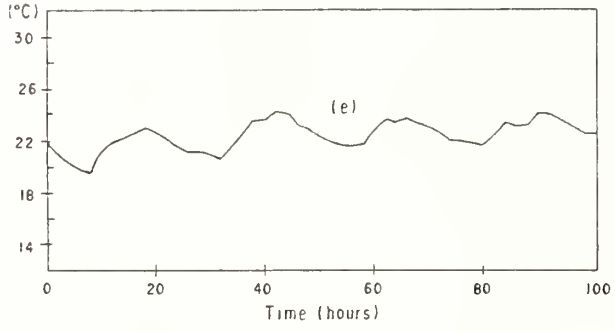

Fig 2 Meosuring system stobility

(a) (X-R) stability

(b) temperature variations of the light source side CTB

(c) (R) stability

(d) temperature variations of the recieving side CTB

(e) room temperature variations

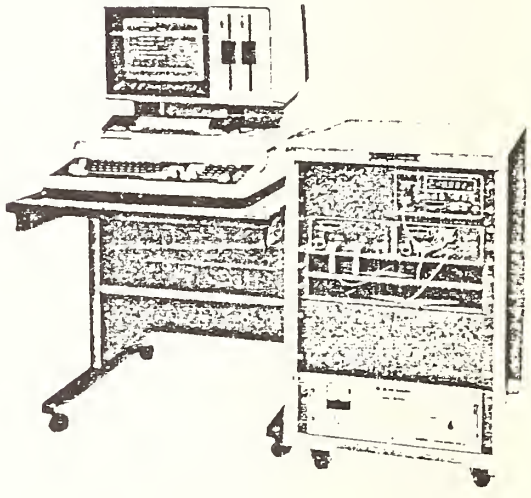

Fig 3 System configuration

References

1. Runge P.K., Trishita P.R. "The SL Undersea Lightguide System" IEEE, vol. SAC-1, No3, April, pp.459-466, 1983.
2. Niiro Y. "Optical Fiber Submarine Cable System Development at KDD" ibid., pp.467-478, 1983.
3. Amano K., Niiro Y., Furusawa K., Nunokawa M., and Wakabayashi H. "50 km, Two Repeaters Sea Trial of Optical-Fiber Submarine Cable System", Electron Lett, vol. 18 No.22, pp.952-953, 1982.
4. Furusawa K., Nunokawa M., Ejiri Y., and Yamamoto H. "Longlength Tension and High Water-Pressure Test Facilities for Optical Fiber Submarine Cables" Technical Report of IECE Japan, cs-83-150, pp.61-68,1983.
5. Namihira Y., Wakabayashi H., and Yamamoto H. "High-Stability Measuring Equipment for Very Small Variations of Optical-Fiber Loss", Electron Lett, vol.18, No.3, pp.124-126, 1982.

Accurate Determination Of Optical Fibre Length From Measurements In The Frequency Domain

D. L. Walters
Standard Telecommunication Laboratories Limited,
London Road, Harlow, Essex, UK.

INTRODUCTION

The precise measurement of the length of an optical fibre at various stages of processing, cabling, handling and installation yields important information which can be used to help to predict the long-term mechanical and optical performance of the finished cable.

The large-scale routine manufacturing of a wide variety of optical cables which is now taking place made desirable the development of equipment which could be used regularly to evaluate fibre strain in factory and laboratory environments, and in the field. This paper describes the operation and application of such a measurement system.

The following capabilities were required:

a) A dynamic range capable of measuring lengths up to 50 km of single mode fibre.
b) An optical length resolution of 10 ppm or 10 mm, whichever is the larger.
c) An accuracy of 200 ppm or 20 mm, whichever is the larger.
d) The ability to measure the length when only one fibre end is available, with minimal equipment modification.
e) The capability to measure either absolute optical length or length change during monitoring, with minimal equipment modification.
f) The equipment must be capable of being used by relatively unskilled factory personnel.

Although a number of measurement systems have in the past been used to make accurate measurements of optical length (refs. 1-4), no existing system satisfied all of the above requirements.

EQUIPMENT

Figure 1 is a block diagram of the measurement system. The combination of the dynamic range requirement and factory safety considerations necessitated that the source be a low-power 1300 nm laser with a single-mode fibre tail. The laser is modulated with a radio-frequency sine wave and the vector voltmeter measures the phase difference between the signal applied to the laser and the signal received at the output of the PINFET detector.

Figure 1 shows the situation in which the equipment has access to both ends of the fibre. In this case coupling to the fibre is achieved with a micro-manipulator assembly at the launch end and an elastomeric splice at the detector. Coupling loss is much less than 1 dB. If access to only one fibre end is possible during measurement, the inaccessible end is prevously chemically silvered and the signal is launched and received via a single-mode y-coupler, the connection to the fibre under test being again via an elastomeric splice.

MEASUREMENT METHOD

For an rf signal with modulation frequency f, the phase change ϕ across a length ℓ of fibre with effective refractive index N, is:

$$\phi = 360\ \ell Nf/C \qquad (C = 3 \times 10^{8}\ ms^{-1})$$

The length can therefore be found from the gradient of the phase/frequency characteristic, assuming the refractive index. Since the refractive index itself varies with temperature and strain, it is useful to define the concept of optical length i.e. N ÷ an assumed refractive index (1.453). In order to obtain this optical length with 10 ppm resolution a phase change of at least 5×10^{4} degrees must be observed. As with any phase-measuring instrument, the vector voltmeter measures a phase difference between -180^{o} and $+180^{o}$, any multiples of 360^{o} being ignored. To allow for this, the system controller varies the modulation frequency by a small amount at first, and then by increasingly larger amounts obtaining at each stage a more accurate figure for the optical length while ensuring that at no time is the frequency change sufficiently large to "miss" a 360^{o} phase shift. Once the operator has aligned the system optically, the

measurement sequence is completely automatic. Total measurement time is about two minutes, and at the end of the measurement sequence the controller prints the optical length, together with the estimate of its standard error calculated from a least squares fit.

The physical length of the fibre can be deduced from the optical length, provided that the effective refractive index of the fibre at 1300 nm is known. In practice it is the proportional change in physical length i.e. the strain, which is normally required. To know this it is not necessary to know the exact refractive index, but merely how it varies with temperature and strain.

It can be shown that:

$$\Delta\ell = \frac{\Delta L - \ell\Delta T(\sigma\alpha + \beta)}{\sigma}$$

Where $\Delta\ell$ = change in physical length, ΔL = change in optical length, L = optical length, ℓ = datum physical length, ΔT = Temperature change, α = physical length temperature coefficient, β = refractive index temperature coefficient, $\sigma = 1 + \frac{\ell}{N}\frac{\partial N}{\partial \ell}$

The refractive index strain coefficient $^{\ell}/_{N}.\ ^{\partial N}/_{\partial \ell}$ can be measured for a particular fibre by measuring fibre extension under load v. phase change. This parameter is linear up to at least 2% strain, and has been found in practice to vary very little from fibre to fibre.

If it is required to measure length change while monitoring at a constant frequency, the same equipment can be used with different software. In this case the length change $\Delta\ell$ which produces a phase change $\Delta\phi$ at constant frequency is:

$$\Delta\ell = \frac{\Delta\phi C}{720\ fN\sigma}$$

EQUIPMENT PERFORMANCE AND APPLICATIONS

The measurement system meets all the specified requirements and sets of this equipment are currently being used successfully in both laboratory and factory environments.

A typical application is shown in Fig. 2, which shows the temperature coefficient of the length of a fibre coated with a tight jacket of a high temperature polymer. Other phenomena investigated have included the long-term relaxation of compression produced by nylon coating, and fibre strain relief in a number of different cable designs. These results will be presented and discussed at the Symposium.

REFERENCES

1 A.H. HARTOG et al: Variation Of Pulse Delay With Stress And Temperature In Jacketed And Unjacketed Optical Fibres, Optical and Quantum Electronics 11 (1979), 265-273

2 R. KASHYAP and M.H. REEVE: Single-Ended Fibre Strain And Length Measurement In Frequency Domain, I.E.E. Electronics Letters, (1980), Vol. 16, No. 18, pp.689

3 D.L. PHILEN and P.D. PATEL: Measurement Of Strain In Optical Fibre Cables Using A Commercial Distance Meter, 8th E.C.O.C., Cannes, (1982), Paper A VII

4 S. HORNUNG and M.A. REEVE: Measurements Of Strain In Cabled Monomode Fibre, N.B.S. Symposium On Optical Fibre Measurements, (1982)

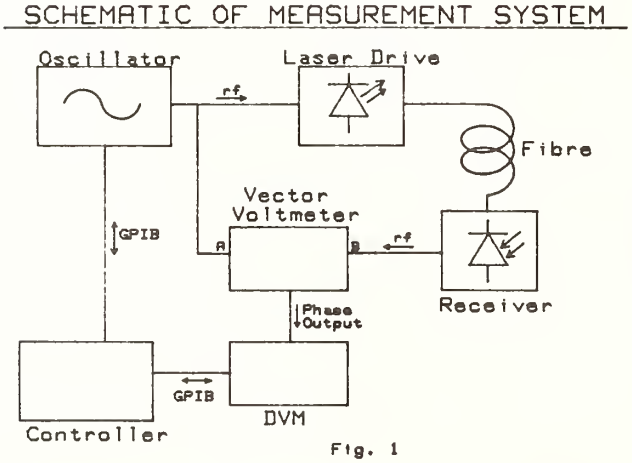

Fig. 1

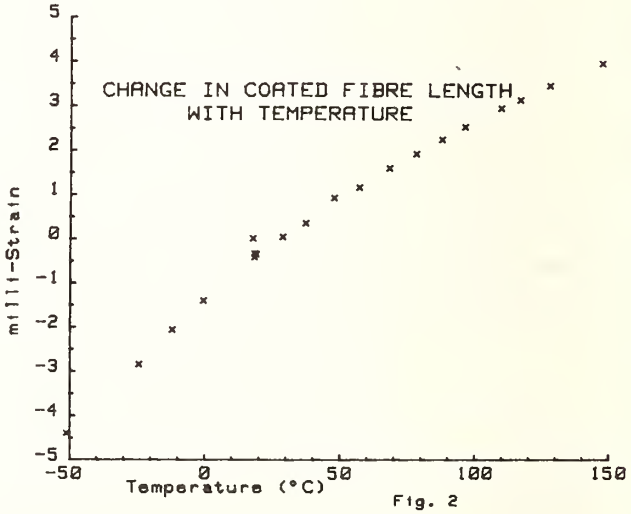

Fig. 2

ELIMINATION OF THE INFLUENCE OF Q-SWITCHED-MODE-LOCKED LASER JITTER IN SAMPLED TIME-DOMAIN MEASUREMENTS

E.J.R. Hubach, A.B. Sharma*, S.J. Halme
Helsinki University of Technology, Communications laboratory,
Otakaari 5A, SF-02150 ESPOO 15, Finland

*Tampere University of Technology, Laboratory of Electronics,
Box 527, SF-33101 TAMPERE 10, Finland

Introduction

A tuneable short-pulse source that is being widely used for fiber measurements is the Q-switched mode-locked Nd-YAG laser in conjunction with a "Raman fiber" /1/. The usual method of detection is a fast diode coupled to a sampling oscilloscope. A major concern with such a set-up is the existence of timing jitter which tends to be about 50 ps, and which is usually associated with jitter in the Q-switch and mode-lock pulse trains.

We have found that the sub-harmonic content of synchronizing signals is the main source of error, and that the "jitter" is mostly a systematic effect that can be virtually eliminated. Here we show that through a proper choice of the fixed ratio between the Q-switch and mode-lock frequencies, timing jitter can be effectively eliminated. For our system, the total system jitter is 5 ps (RMS), which is less than the specified value for our sampling oscilloscope.

The problem of sub-harmonics

In the visual inspection of normal oscilloscope traces and due to sample filtering, the influence of sub-harmonics is to produce a jittery trace, so that a systematic effect appears to be random jitter (Figure 1). However, the effect can be isolated by photography under slow sweep, in which case multiple repetitive pulses can be easily identified (Figure 2).

The required frequency-stability for mode-locked laser operation necessitates the use of overtone quartz-crystals to generate the driving signal (of frequency f_m) for the acousto-optic loss-modulator in the laser cavity and the digital delay generator reference clock. A third overtone crystal leads to sub-harmonic components of $1/3\ f_m$ and $2/3\ f_m$ due to non-linearity of the crystal characteristic. Calculations and measurements both confirm systematic timing errors of about 100 ps (peak) with sub-harmonic levels around -35 dB in relation to the level of f_m. Figure 3 shows the spectral content of the mode-lock signal. Simple electrical filtering is not effective as the optical devices of the laser cavity are part of the process.

The oscilloscope trigger is derived from the mode-lock signal. A comparator detects a preset level-crossing and a trigger is generated at every upgoing edge of the mode-lock signal f_m. The lower level sub-harmonics add to the mode-lock reference amplitude so that the trigger level will be reached slightly sooner or later than with a spectrally clean reference (Figure 4). Therefore, a periodic timing offset will be generated.

For an example case with one $1/3\ f_m$ sub-harmonic of amplitude A1 (like in Figure 4), the worst case time deviation T_{lw} will be:

$$T_{lw} = T_m * \arcsin (A1/A3) / 2\pi \qquad (1)$$

where A1 is the amplitude of the sub-harmonic, A3 the amplitude of the mode-lock frequency f_m and $T_m = 1/f_m$. The worst case situation occurs when the sub-harmonic amplitude is maximal at a trigger level crossing. Whether the worst case deviation is reached, depends on the relative phase of the spectral components. The phase relation is determined by the circuit configuration. But as the apparent jitter is determined by the limits of largest positive and negative time-offset of three triggering moments, the (fixed) relative phase plays a minor role. If, for example, the positive time deviation is moved from worst case to a smaller offset, one of the negative offsets will grow accordingly.

With third-order overtone crystals every third trigger-pulse will have the same systematic offset. Because of the sampling of different pulses to make up a complete picture, a multiple pulse will be displayed if samples are related to triggers with differing offset.

Solution to the problem and results

The cure lies in relating correctly the timing sequences in the measurement system. The key point is to relate the oscilloscope trigger to pulses with identical systematic timing offset. The Q-switch is intermittently opened to allow the generation of high-power optical pulses. One of the pulses in the Q-switched row is chosen for display and thus sampled with the rate of the Q-switch frequency. A digital counter string is used to generate the Q-switch repetition rate from the mode-lock synchronizing signal. If the division ratio of the counter is chosen to be an integer multiple of 3 then the Q-switch is opened at a moment related to a particular timing offset and the scope trigger will be generated accordingly.

With this technique the systematic timing error was completely eliminated for a single-pulse display and our total random error is now 5 ps RMS (Figure 5). The necessary circuitry was incorporated in a specially designed delay generator based on Advanced Schottky TTL. Pulse displays have been taken from different measurements during system development. In Figure 5 the detector is slightly overdriven to minimize the influence of other sources of error.

Conclusion

In this paper, we draw attention to the influence of the sub-harmonic content of crystal oscillators upon the "jitter" performance of an important source for fiber measurements. We show that the effect is predominantly systematic and can be easily eliminated by judicial choice of the division ratio between mode-lock and Q-switch frequencies. The validity of our arguments is apparent from the jitter value of 5 ps RMS in our system, in contrast to our previous effective value of 100 ps.

References

/1/. Cohen L.G., Chinlon Lin, Pulse delay measurements in the zero material dispersion wavelength region for optical fibers, Applied Optics 16, 3136 (1977)

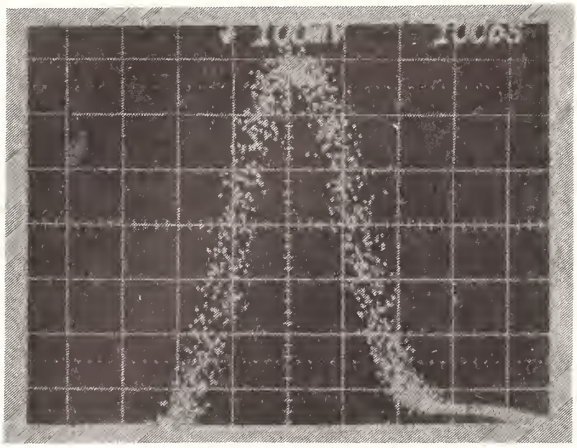

Figure 1. Typical Nd-YAG pulse display on sampling oscilloscope. Presence of maximum noise amplitude at steepest edges of the pulse reveals time-jitter origin of noise.

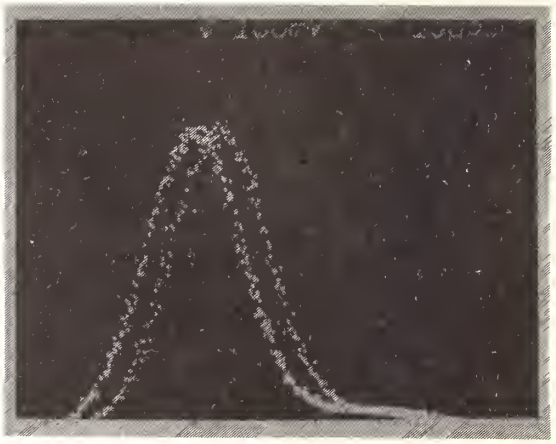

Figure 2. Display of laser output showing multiple pulses. Depending on the relative phase of the sub-harmonics, three separate pulses can be distinguished.

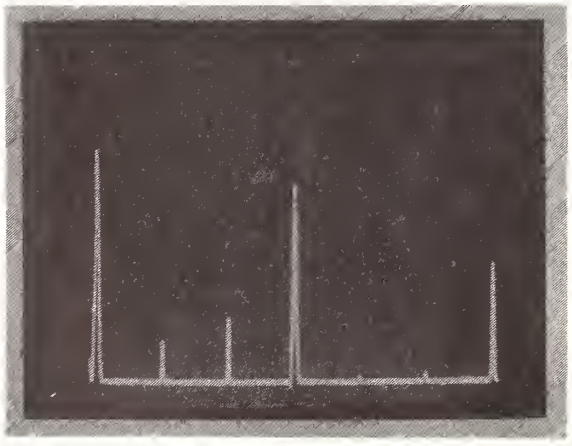

Figure 3. Spectral content of the mode-lock reference signal. The central peak is the f_m component. Scale 0 - 100 MHz horizontal; vertically 10 dB / div.

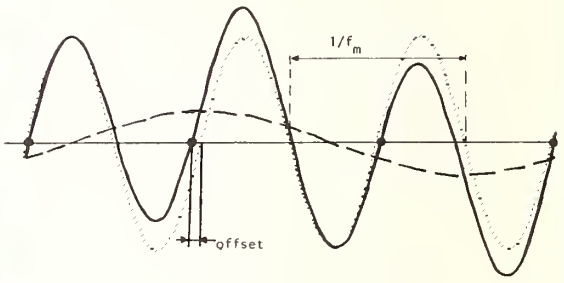

Figure 4. Timing offset shown for an arbitrarily phased subharmonic at one third of the mode-lock frequency. Trigger level crossings are marked with a black dot.

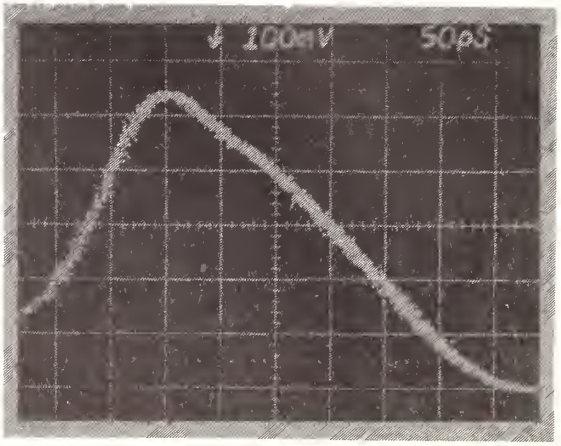

Figure 5. Laser output after applying proper division ratio. Detector is slightly overdriven. Sample filtering is normal.

ACCURATE SPECIFICATION OF SINGLE-MODE DISPERSION MEASUREMENTS

Felix P. Kapron and Tom C. Olson

ITT Electro-Optical Products Division
7635 Plantation Road, N.W.
Roanoke, Virginia 24019-0065

INTRODUCTION

Fiber chromatic dispersion is usually specified in terms of a maximum absolute value over a particular wavelength range. However, a maximum ±3.5 ps/km-nm between 1280 and 1340 nm, for example, is a worst-case estimate that ignores the better fiber performance attainable over much of the wavelength window. High bitrate single-mode systems will require a more flexible and precise specification, such as proposed in this paper, that does not stress manufacturing measurement time or yield.

DELAY AND DISPERSION FORMULAS

We first rewrite, in a uniform notation, expressions for the group delay per unit length $\tau(\lambda)$ that have been used in the literature. One containing λ^2 and λ^{-2} terms[1] becomes

$$\tau_1(\lambda) = \tau_o + \frac{S_o}{8}\left(\lambda - \frac{\lambda_o^2}{\lambda}\right)^2 \qquad (1)$$

where τ_o is the minimum delay at the zero-dispersion wavelength λ_o. The dispersion $D(\lambda) = d\tau/d\lambda$ is then

$$D_1(\lambda) = \frac{S_o}{4}\left(\lambda - \frac{\lambda_o^4}{\lambda^3}\right) \qquad (2)$$

where S_o is the value of the dispersion-slope $S(\lambda) = dD/d\lambda$ at λ_o.

Another expression [2], in which dispersion is proportional to $(\lambda - \lambda_o)/\lambda^2$, we rewrite as

$$\tau_2(\lambda) = \tau_o + S_o \lambda_o^2 \left(\frac{\lambda_o - \lambda}{\lambda} + \ln \frac{\lambda}{\lambda_o} \right) \tag{3}$$

$$D_2(\lambda) = S_o \left(\frac{\lambda_o}{\lambda}\right)^2 (\lambda - \lambda_o) \tag{4}$$

Finally, a Taylor-expansion [3] may be written

$$\tau_3(\lambda) = \tau_o + \frac{S_o}{2} (\lambda - \lambda_o)^2 - \frac{C_o}{6} (\lambda - \lambda_o)^3 \tag{5}$$

$$D_3(\lambda) = S_o (\lambda - \lambda_o) - \frac{C_o}{2} (\lambda - \lambda_o)^2 \tag{6}$$

where C_o is the dispersion-curvature $C(\lambda) = -dD/d\lambda$ at λ_o.

EXPERIMENTAL FITS

Spectral group delay measurements were made on 15 similar single-mode fibers, using the common Raman fiber pulsed laser technique [1]. Figure 1 is a typical best-fit to the group delay expression τ_3 with the associated dispersion curve D_3. For all fibers, the table gives the mean best-fit parameters to the group delay expressions:

Fit Equation	τ_1	τ_2	τ_3
Zero-Dispersion Wavelength (λ_o, nm)	1311	1308	1314
Dispersion-Slope x 10^3 (S_o, ps/km-nm^2)	86.7	88.5	87.2
Dispersion-Curvature x 10^6 (C_o, ps/km-nm^3)	-	-	141
Closeness of Fit (standard deviation, ps/km)	11.2	17.4	8.5

Note that the zero-dispersion wavelength λ_o and the dispersion-slope S_o both depend upon the fit used. Although τ_3 gives the best fit, it requires at least four measurement wavelengths, compared to three for τ_1 and τ_2.

Figure 2 shows the deviations of dispersions D_1 and D_2 from the preferred D_3 for one fiber. Although the discrepancy is as large as 1 ps/km-nm at 1550 nm, all fits agree within 0.3 ps/km-nm between 1200 and 1480 nm for this fiber. In fact, within ±30 nm of λ_o, the linear approximation to all expressions

$$D_4(\lambda) \simeq (\lambda - \lambda_o)\, S_o \tag{7}$$

is within 4% of the more accurate fits D_1 and D_3.

CONCLUSIONS

Chromatic dispersion measurement results can be more accurately described in terms of two parameters: zero-dispersion wavelength λ_o and dispersion-slope S_o at that wavelength. Fitting data to τ_3 is especially accurate for obtaining these, but even the simpler forms (τ_3 with $C_o = 0$, or τ_2) are sufficient within 30 nm of λ_o. This specification also has the advantage that throughout this window, FWHM pulse broadening T over fiber length L may be very accurately written[4] in terms of the source FWHM linewidth $\Delta\lambda$ centered at wavelength λ_s:

$$T = S_o\, L\, \Delta\lambda \left[(\lambda_s - \lambda_o)^2 + (0.3\ \Delta\lambda)^2\right]^{1/2} \tag{8}$$

REFERENCES

[1] Love, W. F.: 'Bandwidth spectral characterization of GeO_2-P_2O_5-SiO_2 multimode optical waveguides', 6th ECOC, York, 1980, pp 113-116.

[2] Gloge, D., Ogawa, K., and Cohen, L. G.: 'Baseband characteristics of long-wavelength LED systems', Electron. Lett., 1980, 16, (10), pp 366-367.

[3] Pearson, A. D., Lazay, P. D., and Reed, W. A.: 'Bandwidth optimization of depressed index single-mode fibre by means of a parametric study', 8th ECOC, Cannes, 1982, pp 93-97.

[4] Kapron, F. P.: 'Dispersion-slope parameter for monomode fiber bandwidth', OFC 1984, New Orleans, pp 90-92.

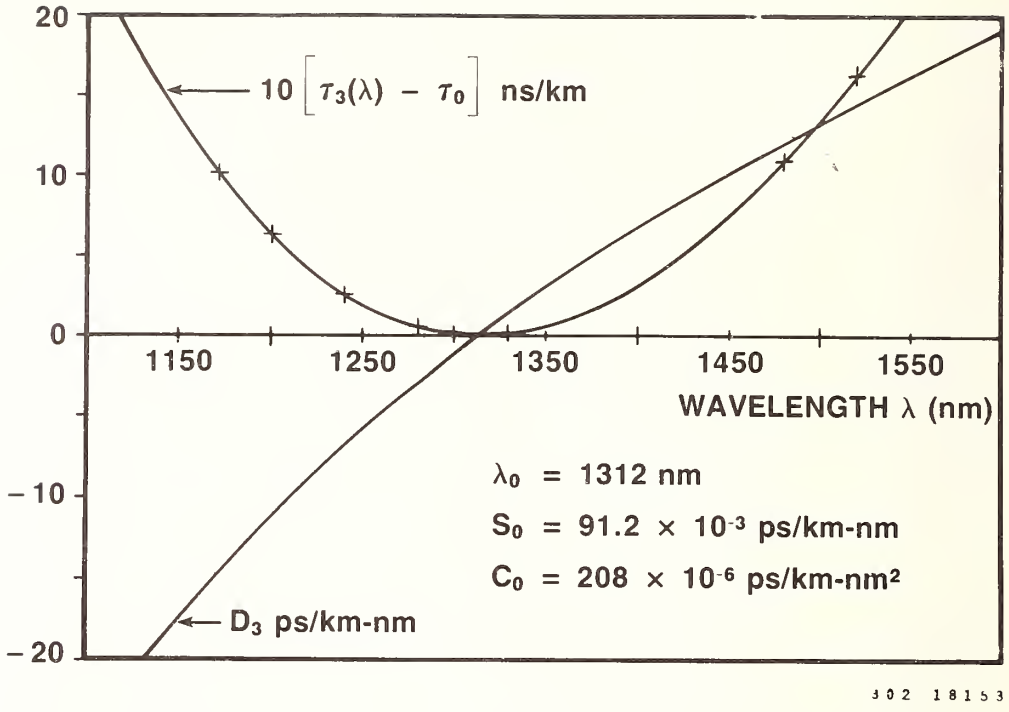

Figure 1. Spectral Group Delay Data Fit to Equation (5) and Derived Single-Mode Fiber Dispersion of Equation (6).

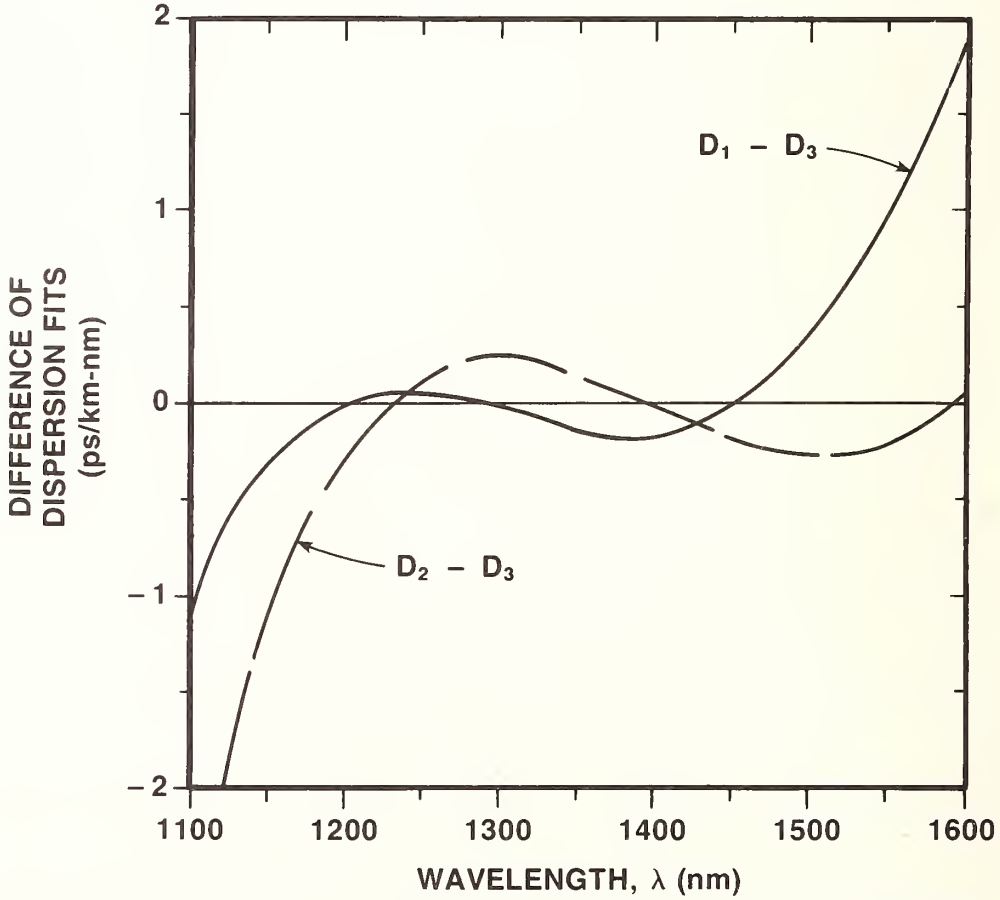

Figure 2. Difference of the Dispersions of Equations (2) and (4) from the Best-Fit (6) of Figure 1.

Multiple-Wavelength System for Characterizing Dispersion in Single-Mode Optical Fibers

Robert A. Modavis and Walter F. Love

Corning Glass Works
Research and Development Division
Corning, New York 14831

Introduction

It is important to be able to characterize chromatic dispersion in single-mode fibers for purposes of quality control and process feedback. The measurement system should be simple to use and maintain, yet contain sufficient accuracy and precision to satisfy transmission system design considerations. This paper discusses such a system which utilizes a 5-wavelength method and compares the measurement results with those obtained using a fiber Raman laser.[1,2] Algorithms have been developed which extend the capability from step-index profile fiber designs previously considered[3] to newer and more complex designs[4,5] which shift and flatten the chromatic dispersion.

Experimental

Five semiconductor lasers operating in the short-pulse mode and long-wavelength range of interest are used. Three lasers operating near 1300 nm, viz., 1190, 1270, 1330 nm and two near 1500 nm, viz., 1490 and 1560 nm were chosen to optimize characterization of both present and future fiber designs. These are pigtailed to step-index profile single-mode fibers whose output ends are positioned in a multi-element connector. The position of the first pigtail is adjusted manually while the remaining ones are positioned under computer control to image the light into the test fiber as can be seen in Fig. 1. A 1/4-meter monochromator (λ-meter) is used to monitor the center wavelength of the semiconductor lasers. The output light from the test fiber is collected and imaged onto a germanium avalanche photodiode. High-speed amplifiers and a sampling oscilloscope are used to process the signal. Typical pulse widths are ~200 psec (detector-limited) and the time jitter is ~20 psec.

Time delay measurements are made as a function of wavelength $\tau(\lambda)$ to within an arbitrary additive constant. The dispersion is obtained as $D = \frac{d\tau}{d\lambda}$.

Results

This measurement system has been calibrated against our fiber Raman laser system[2] and a set of comparison measurements have been made. Figure 2 shows the chromatic dispersion obtained from the two systems where a worst case is displayed for ease of viewing. For five comparison measurements all values of the zero dispersion wavelength, λ_o, agreed to within 1 nm for nominal 1300 nm-design fibers. The 3-parameter polynomial approximation to the Sellmeier function is used to curve-fit the time delay data, viz., $\tau = a + b\lambda^2 + c\lambda^{-2}$, where λ is wavelength.

For nominal 1550 nm dispersion shifted fibers, an empirical 3-parameter algorithm has been developed which fits the fiber Raman system data (~10 points) to within ~20 psec/km. The time delay data and least-squares fit are shown in Fig. 3 for both systems. Agreement to within 0.25 psec $nm^{-1}km^{-1}$ is obtained at 1550 nm.

Segmented-core fibers[4,5] which have a flattened dispersion over the range 1300-1550 nm have also been measured. The 4-parameter algorithm used to fit the time delay data is given by, $\tau = a_o + a_1(\lambda-b) + a_3(\lambda-b)^3$, where b is the inflection point. A nonlinear least squares analysis has been developed and is used to fit the data. Figure 4 shows the results for both measurement systems where the quality of the fit is ~20 psec/km. Typically, agreement is 0.35 psec $nm^{-1}km^{-1}$ for dispersion over the 1300 to 1600 nm range.

Summary

We have developed a 5-wavelength method for measuring dispersion in single-mode fibers. Comparisons with a fiber Raman system have yielded excellent agreement and are summarized in Table 1. Time delay curve-fitting algorithms with a minimum number of parameters have also been obtained and these allow the extension of the measurement system capability to dispersion shifted and flattened fibers.

Acknowledgements

We wish to thank Mr. T. A. Cook, Mr. D. Smith, and Mr. J. Dunning for technical assistance and Dr. W. Kane and Dr. D. B. Keck for discussions.

References

1. L. G. Cohen, P. Kaiser, and C. Lin, Proc. IEEE 68, 1203 (1980).
2. W. F. Love, in digest of 6th European Conference on Optical Communication, York, UK, 1980, p. 113.

3. C. Lin, A. R. Tynes, A. Tomita, P. L. Liu and D. L. Philen, Bell System Technical Journal 62, 457 (1983).
4. V. A. Bhagavatula, M. S. Spotz, W. F. Love and D. B. Keck, Electronics Letters 19, 317 (1983).
5. L. G. Cohen, W. L. Mammel, and S. J. Jang, Electronics Letters 18, 1023 (1982).

Table I

Fiber Type	Comparison Accuracy (psec $nm^{-1}km^{-1}$)	Precision (psec $nm^{-1}km^{-1}$)
unshifted (1300 nm)	0.10	0.04
shifted (1550 nm)	0.25	0.06
flattened (1300-1600 nm)	0.35	0.09

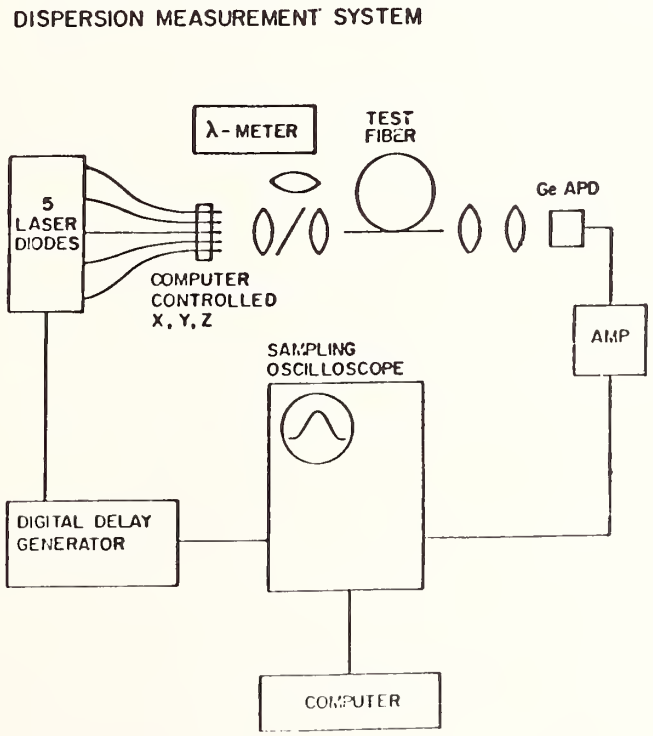

Fig. 1 Five-Laser Dispersion Measurement System

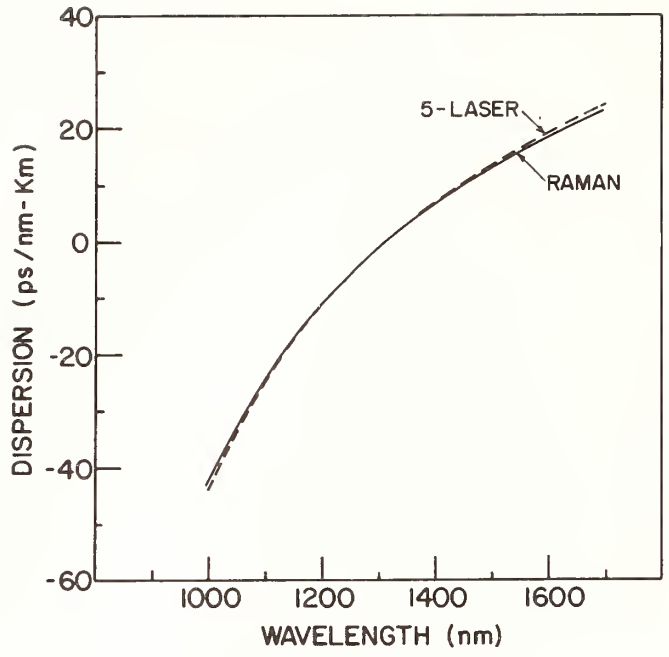

Fig. 2 Comparison of dispersion for unshifted (1300 nm) type fiber using 5-laser and Raman systems.

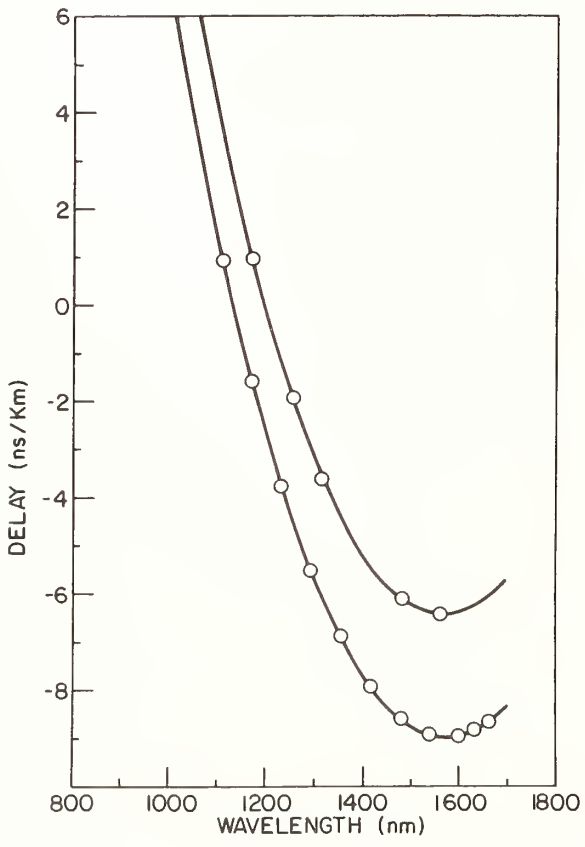

Fig. 3 Delay time versus wavelength for shifted (1550 nm) type fiber. An offset was introduced between the 5-laser and Raman measurements.

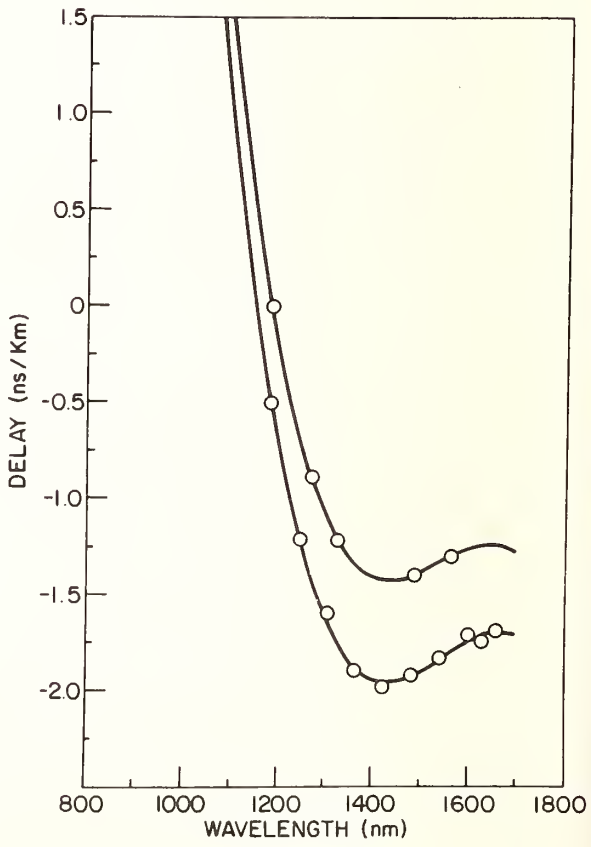

Fig. 4 Delay time versus wavelength for dispersion-flattened fiber using 5-laser and Raman results.

HIGH ACCURATE AUTOMATIC MEASUREMENT EQUIPMENT FOR CHROMATIC DISPERSION MAKING USE OF THE PHASE-SHIFT TECHNIQUE WITH LDs

K.TATEKURA, H.NISHIKAWA, M.FUJISE, AND H.WAKABAYASHI
KOKUSAI DENSHIN DENWA CO., LTD. (KDD)
NISHISHINJUKU 2-CHOME, SHINJUKU-KU, TOKYO 160, JAPAN

1.INTRODUCTION In the long haul optical fiber submarine cable system, the accurate knowledge of chromatic dispersion in single-mode fibers is necessary because the mode partition noise[1] can be the dominant limitation on a system error rate as well as transmission loss.

Many techniques for the chromatic dispersion measurement have been developed;[2-4] most of them could be hardly adapted to industrial stage or in the field environment because of complex set-ups and/or delicate operation. In this paper, a high accurate measurement equipment, that makes use of sinusoidally modulated LDs, is demonstrated. It is likely to match all the requirements in respect to the repeatability and absolute accuracy of measurement, the dynamic range, and the easiness in operation.

2.SET-UP AND PRINCIPLE The scheme of the measuring set-up is shown in Fig.1, and Fig.2 is the front view of the equipment whose size is about 1570(H)x540(W)x710(D) mm. The phase-shift is adopted technique[5] because the accuracy is very high and the set-up is simple. There are equipped seven LDs having different wavelengths from 1200nm to 1330nm in the present system. Each LD is sinusoidally modulated (30MHz- 800MHz), and the output signal are devided into the main and reference signals. Part of the reference signal is used to measure characteristics of each LD. The main and reference signals through O/Es are once converted into IF signals

(455kHz), and filtered by a narrow bandpass filer in order to improve SN ratio. Any wavelength is sequentially selected by the 7x1 single-mode optical switch shown in Fig.1. The phase delay difference between the signal through the test fiber and the reference signal is measured by the phase detector.

Utilizing the measurement data, the delay time against the wavelength is expressed by a polinominal approximation (Fig.3) with the aid of the root mean square technique. Finally, the chromatic dispersion (Fig.4) is calculated by differentiation of the above approximation.

3.PERFORMANCE Figs.5 and 6 show the measurement results successively carried out every one hour. In the repeatability tests, accuracy was very good, and the variation of the zero-dispersion wavelength was within ±0.5 nm, and that of slope in the dispersion curve was within ±0.01ps/km nm^2. Absolute accuracy has been tested as well by comparison with the results obtained on the same fibers by the fiber Raman technique[2]. Table 1 allows the comparison of the zero-dispersion wavelengths obtained by the fiber Raman and present techniques. Both results are in good agreement.

The present measuring equipment has the dynamic range more than 30 dB, which is corresponding to the possible measurement fiber-length of more than 50 km. The large dynamic range is the most excellent feature in LDs as the light sources. The sources are thermally controlled so as to work at constant wavelength within the surrounding temperature of 5°C-35°C. In the present system, all the dispersion measurement processes are automatically controlled by a personal computer, and it takes about three minutes to measure one fiber sample.

4.CONCLUSIONS The high accurate automatic equipment for the chromatic

dispersion of single-mode fibers has been successfully demonstrated. The repeatability and absolute accuracy of measurement as well as the dynamic range meet all the practical requirements. Moreover, the easy operation and the short measurement time are very attractive for the measurements at field or factories.

ACKNOWLEDGMENTS: The autors wish to express their thanks to Mr. Y.Ishikawa, Dr. H.Kaji, Mr. Y.Niiro, and Mr. Y.Iwamoto for their encouragement. They also wish to thank Ando Electric Co., LTD. for manufacturing the equipment.

REFERENCES

1 K.OGAWA; IEEE J. Quantum Electron., vol.QE-18, no.5, May 1982.

2 K.KITAYAMA et. al.; APPLIED OPTICS, vol.20, no.14, July 1981.

3 C.LIN et. al.; Proc. OFC'82, Phoenix, AZ, Apr. 1982.

4 B.COSTA et. al.; Electron. Lett., vol.19, no.25/26, Dec. 1983.

5 M.TATEDA et. al.; APPLIED OPTICS, vol.19, no.5, Mar. 1980.

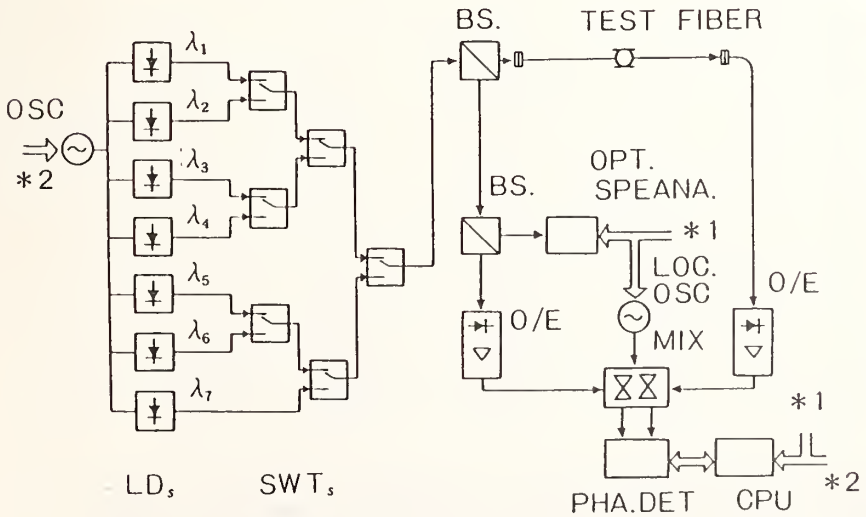

Fig.1 Scheme of the measureing set-up

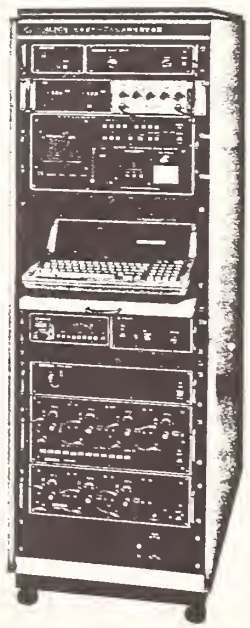

Fig.2

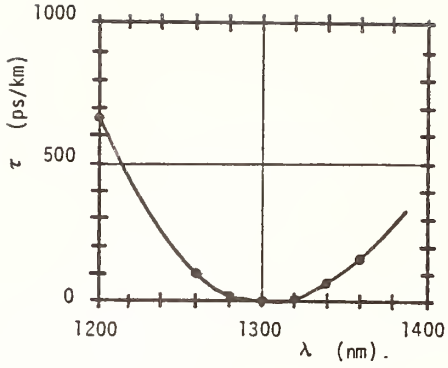

Fig.3
Delay time curve
•denotes the measured points.

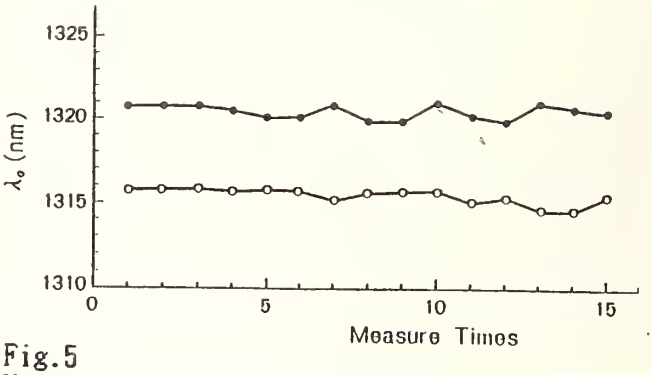

Fig.5
Variation of the zero-dispersion wavelengths in the repeatability test, where two typical fibers (~6Km) were measured.

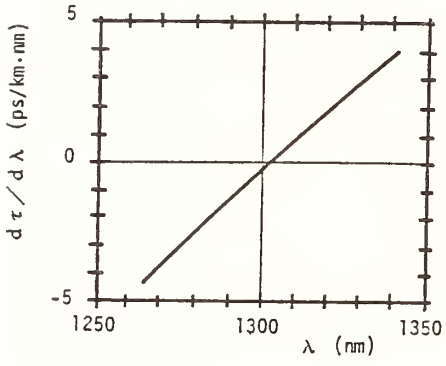

Fig.4
Calculated dispersion curve

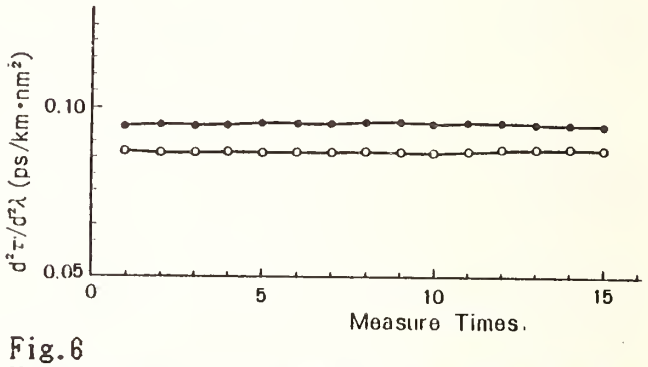

Fig.6
Variation of the slope of dispersion curves in the same test as Fig.5.

Table 1 Comparison of the zero-dispersion wavelengths

FIBER NO.	$2w_0$ (μm)	Δ (%)	λ_0 (nm)	λ^*_0 (nm)	$\delta\lambda$ (nm)
F 1	9.7	0.33	1331	1331	0
F 2	9.7	0.30	1334	1336	-2
F 3	9.9	0.33	1332	1336	-4
F 4	9.5	0.30	1321	1322	-1
F 5	9.4	0.30	1331	1331	0
F 6	10.3	0.29	1330	1330	0
F 7	11.9	0.28	1292	1290	2
F 8	11.7	0.29	1296	1296	0
F 9	10.0	0.30	1305	1306	-1
F 10	10.9	0.33	1302	1304	-2

$2w_0$: the mode field diameter, Δ : the index difference ,
λ_0 : the zero-dispersion wavelength by the fiber Raman technique,
λ^*_0 : the zero-dispersion wavelength by the phase shift technique,
$\delta\lambda$: $\lambda_0 - \lambda^*_0$, lengths of test fibers were around 8Km.

PRECISION INTERFEROMETRIC MEASUREMENT OF DISPERSION IN SHORT SINGLE MODE FIBERS

M. J. Saunders
W. B. Gardner
AT&T Bell Laboratories
2000 Northeast Expressway
Norcross, Georgia 30071

Disadvantages of the conventional pulse delay method[1] for measuring single mode fiber dispersion are the high cost of the equipment, the requirement for long (~ km) lengths of fiber, and the eye hazard due to the high laser power levels.

To overcome these disadvantages, interferometric methods for measuring dispersion in fibers using both the Michelson[2] and Mach-Zehnder[3-6] arrangements have been devised. We have used a 100 watt quartz halogen source, a monochromator, and a Mach-Zehnder interferometer with a motor-driven delay line to measure dispersion in fibers as short as 8.6 cm. This test set produces high visibility interference fringes at wavelengths up to 1.7 μm without the use of a reference fiber.

A diagram of the apparatus is shown in Figure 1. After alignment is effected with the laser, visible fringes are obtained with the monochromator and microscope. Mirrors C and D are used to make the fringe separation larger than the detector diameter. The monochromator is then tuned to an infrared wavelength and the fringe visibility curve is obtained (Figure 2) by motor-driving the variable delay path. This procedure is repeated at other infrared wavelengths. All of the visibility curves are then repeated with the fiber removed.

If the path difference between the two arms produces a phase difference $\Delta\phi$, the condition for maximum fringe visibility is

$$\frac{d}{d\lambda}(\Delta\phi) = 0 \ . \qquad (1)$$

If the delay path must be adjusted an amount $\Delta\ell$ when the fiber is removed, then condition (1) becomes

$$N(\lambda) = \Delta\ell/\ell + 1 \qquad (2)$$

where $N(\lambda)$ = (LP_{01} group delay per unit length) $\cdot$ c (3)

and ℓ is the length of the fiber.

Figure 2 is a typical set of fringe visibility curves obtained on a 17.5 cm long fiber. Using Eqs. (2) and (3), these data were used to generate the delay curve shown in Figure 3. A Sellmeier fit (the solid line in Figure 3) has its minimum at the zero dispersion wavelength (λ_o). Eight determinations of λ_o were made on an 8.6 cm long fiber and a 17.5 cm long fiber drawn from the same preform. The means were 1470 nm and 1443 nm, respectively, and the σ's are summarized in Table I. The σ's for the delays are deviations from the Sellmeier fit curve.

Table I

Measurement Precision -- Standard Deviations for 8 Measurements per Fiber

	8.6 cm Fiber	17.5 cm Fiber
Zero Dispersion Wavelength	16 nm	5 nm
Group Delay	.025 psec	.019 psec
Group Delay per Unit Length	0.29 ns/km	0.11 ns/km

Because of the short lengths of fiber used, possible errors due to the presence of LP_{11} mode power were also investigated, and will be reported on.

REFERENCES

1. L. G. Cohen and C. Lin, Appl. Opt. 16, 3136 (1977).
2. W. D. Bomberger and J. J. Burke, Symp. on Optical Fiber Measurements, Boulder, October 28-29, 1980, p. 101.
3. H. T. Shang, Electron. Lett. 17, 603 (1981).
4. J. Stone and L. G. Cohen, Electron. Lett. 18, 716 (1982).
5. M. Tateda, N. Shibata and S. Seikai, IEEE J. Quantum Electronics, QE-17, 404 (1981).
6. F. M. Sears, L. G. Cohen, and J. Stone, J. Lightwave Technology LT-2, 181 (1984).

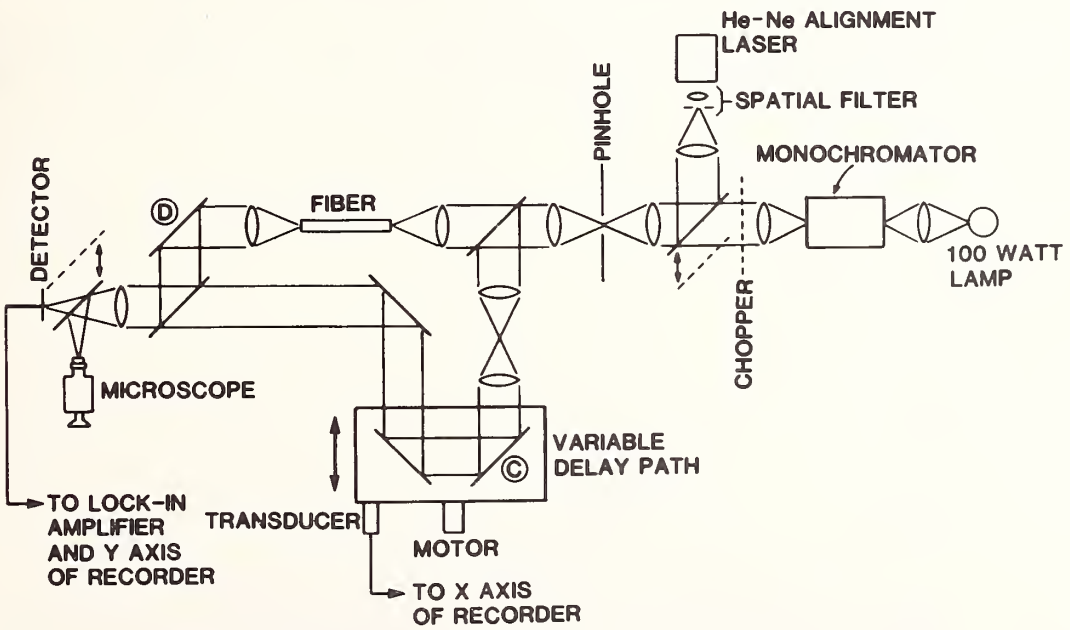

FIGURE 1
SCHEMATIC DIAGRAM OF EQUIPMENT

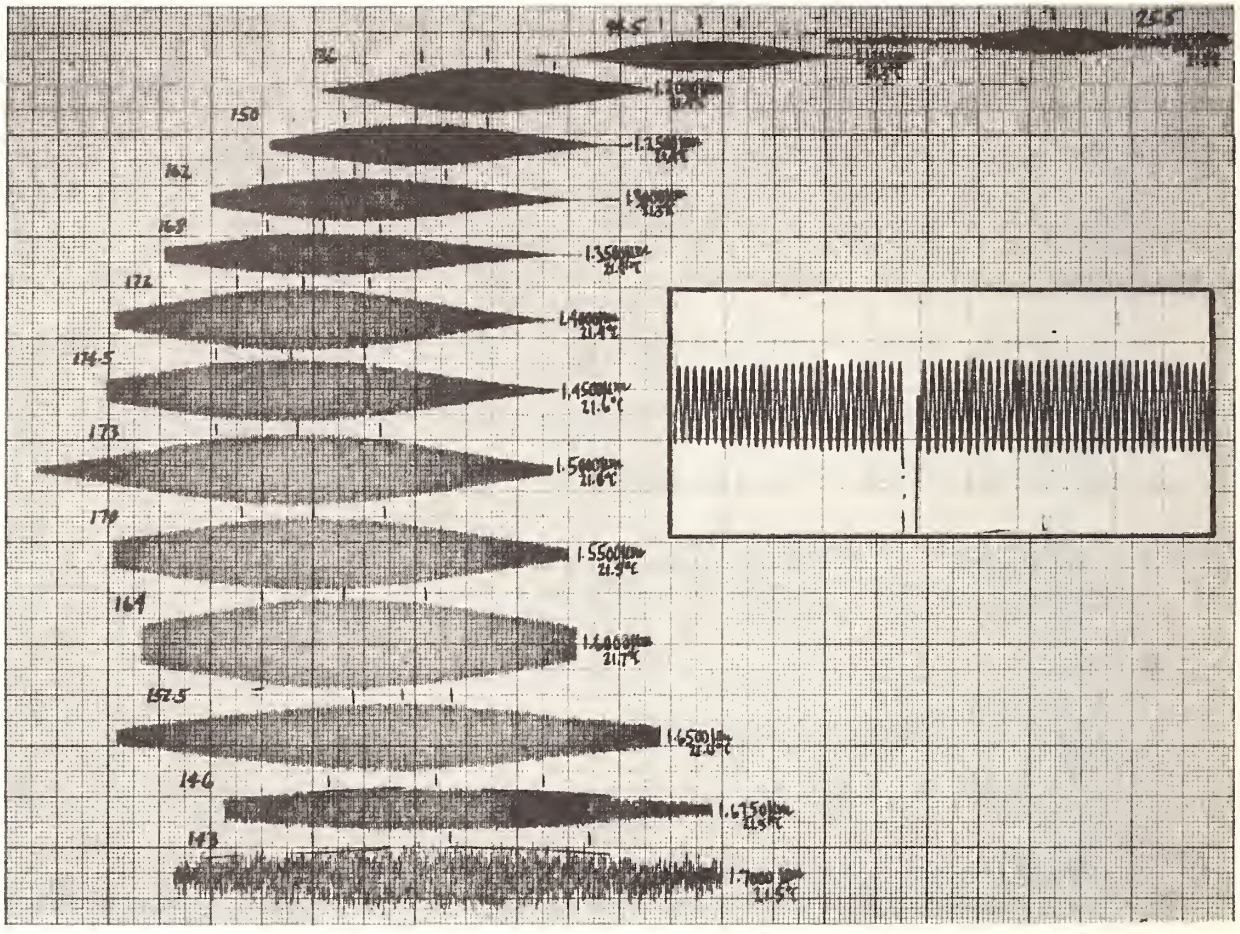

FIGURE 2
VISIBILITY CURVES AT 14 WAVELENGTHS (INSERT SHOWS QUALITY OF FRINGES)

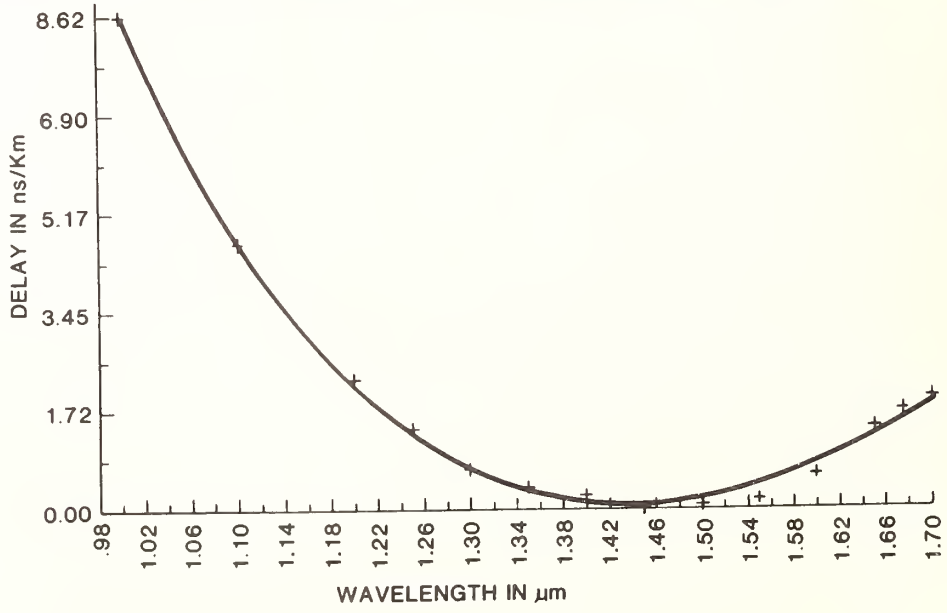

FIGURE 3
GROUP DELAY vs. WAVELENGTH

INTERFEROMETRIC DISPERSION MEASUREMENT IN SINGLE-MODE FIBERS WITH A NUMERICAL METHOD TO EXTRACT THE GROUP DELAYS FROM THE MEASURED VISIBILITY CURVES

L. Oksanen, S. J. Halme

Communications Laboratory
Helsinki University of Technology
SF-02150 ESPOO

Introduction: In research and manufacture it is often desirable to be able to measure dispersion from a short piece, say a few meters, of the fiber. This can be done conveniently with the interferometric group delay measurement method /1/,/2/,/3/ which gives the total dispersion of the fiber. We report on a simple numerical method to extract the group delays from the measured visibility curves. This method eliminates human bias and error inherent in visual inspection of the curves, enhances resolution and facilitates automation of the measurement procedure.

Measurement system: The measurement apparatus is depicted schematically in figure 1. Input light is divided in the first beamsplitter and launched into both arms of the interferometer. The fiber to be measured is inserted into the other arm and the other arm serves as a reference. The relative propagation delay between the arms can be adjusted by the movable corner cube. The light beams from both arms are combined in the second beamsplitter and the resulting interference is detected. Our setup is slightly modified in order to reduce the criticality of the alignment of the interferometer. The light source is a Nd:YAG pumped single-mode Raman fiber and the wavelengths are selected with a monochromator. The length of the fiber is from 3 to 4 meters.

We are interested in the visibility, or the strength, of the interference as a function of the group delay difference between the arms of the interferometer. It is measured by changing the air path length with a motorized manipulator and sampling the receiver output with a digital voltmeter. A typical visibility curve on one wavelength is shown in fig. 2. The noise in the curve is caused by amplitude instability in the Nd:YAG laser, which pumps the Raman fiber. It is rather pronounced because the manipulator sweep is continuous and the reveiver integration time is short compared to the time between the laser pulses. The measured values, typically 256 for one curve, are stored on tape. Notice that the actual path delay difference in our system is four times the distance traveled by the manipulator.

Delay measurement: Because of fiber dispersion the group delay in the fiber changes with wavelength and the visibility curves are obtained at different sweep ranges of the manipulator. The task is to extract the group delays corresponding to the positions of maxima of the curves. If the source spectrum is symmetric this means finding the center of the visibility curve. It can be done approximately by visual inspection of the curves /2/. This, however, may lead to human error or a biased evaluation of the midpoint of the curves. We have developed a simple and accurate numerical method to extract the delays from the corresponding visibility curves.

By using the theory of partial coherence /4/ we can derive the visibility curve for a known source spectrum. We assume that the output spectrum $S(\lambda)$ of the monochromator is Gaussian, equation 1, which is realistic, considering the output spectrum of our monochromator. λ is wavelength, λ_S the center wavelength and $\Delta\lambda$ the 1/e halfwidth of the source spectrum. When $\Delta\lambda << \lambda_S$, the visibility is a Gaussian function of the relative delay $\Delta\tau$, eqn. 2. The 1/e halfwidth T of the visibility curve is given by eqn. 3 where c is the speed of light.

$$S(\lambda) \sim \exp(-(\lambda-\lambda_S)^2/\Delta\lambda^2) \qquad (1)$$

$$V(\Delta\tau) \sim \exp(-\Delta\tau^2/T^2) \qquad (2)$$

$$T = \lambda_S^2/(\pi c \Delta\lambda) \qquad (3)$$

The actual method to find the midpoint of the curve is based on convolution. First we calculate a theoretical visibility curve according to eqn. 2. The result for the wavelength and spectral width of the case of fig. 2 is given in fig. 3a. Notice the different scales of the abscissas. If we now take a convolution of the measured and calculated curves we get a result, the global maximum of which indicates the midpoint of the measured curve /5/. To enhance accuracy we actually use as reference the time derivative of the theoretical curve fig 3b. In this case also the result, depicted in figure 4, is the time derivative of the result of convolving the original curves /5/. Now it is easy to find the zero crossing point of the convolution curve by interpolation and thus to determine the midpoint of the measured curve. The convolution is calculated numerically with the help of a Fast Fourier Transform (FFT) algorithm. To eliminate overlap of the result, a brute force approach is used whereby the calculation for 256 measured points is done for 512 points where the extra points have been filled with zeros. The program to find the midpoint of one curve runs for 3 minutes on a HP-85 microcomputer.

Other reference functions such as sin(x)/x and raised cosine have been tried but the Gaussian one gave the best results. Overall it seems that the effect of the shape of the reference curve isn't very critical, which is a good thing considering the effect the different dispersions of air and fiber and the second order dispersion in the fiber may have on the shape of the measured curve. The optimum spectral width for the calculation of the theoretical curve was found to be 4 nm (1/e fullwidth), which is close to the measured value of the monochromator.

When the Nd:YAG laser is properly tuned the standard deviation in the delay values on one wavelength is under 0.1 ps. This value is better than previously reported and it is achieved with a continous sweep of the motorized manipulator instead of stepping which speeds up the measurement process.

As usual the dispersion is arrived at by least squares fitting a polynomial to the measured delays and differentiating it with respect to wavelength. A typical result of the delay measurement is shown in fig. 5 along with the corresponding dispersion curve. The delay values were measured at 36 different wavelengths. The shorter dispersion curve is the result of an independent measurement (by the interferometric method) made by CNET, France, who also supplied the fiber. The discrepancy between the two curves is probably mainly due to the systematic error in our monochromator. We measured the zero dispersion point as 1383 nm and CNET as 1378 nm. We have repeated the measurement on one fiber 9 times measuring each time the delays on 11 wavelengths (not necessarily the same ones). The standard deviation of the resulting zero dispersion wavelengths was 1.2 nm.

Conclusion: We have presented a simple and accurate numerical method, based on convolution, to extract the group delays from the visibility curves measured in the interferometric dispersion measurement method. It enhances resolution, eliminates operator errors and facilitates automation of the measurement.

Acknowledgments: Financial support from the Finnish Posts and Telecommunications is gratefully acknowledged. We are also grateful to Dr. M. Monerie of CNET for supplying us with the fiber and the results of their dispersion measurement.

References

1. M. Tateda, N. Shibata, S. Seikai:"Interferometric method for chromatic dispersion measurement in a single mode fiber", IEEE Journal of Quantum Electronics, 1981, 17, pp. 404-407

2. L. G. Cohen, J. Stone:"Interferometric measurements of minimum dispersion spectra in short lengths of single-mode fibre", Electron. Lett., 1982, 18, pp. 564-566

3. J. Stone, L. G. Cohen:"Minimum-dispersion spectra of single-mode fibres measured with subpicosecond resolution by white light crosscorrelation", Electron. Lett., 1982, 18, pp. 716-718

4. M. Born, E. Wolf:"Principles of optics", Pergamon Press, 1975

5. A. B. Carlson:"Communication systems", McGraw-Hill Kogakusha Ltd., 1975

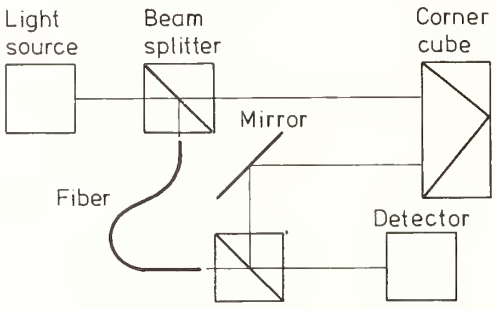

Figure 1.

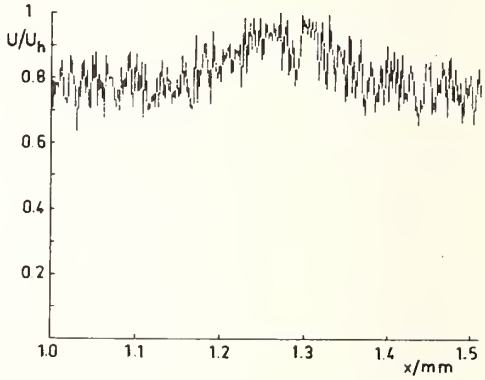

Figure 2.

Figure 3.

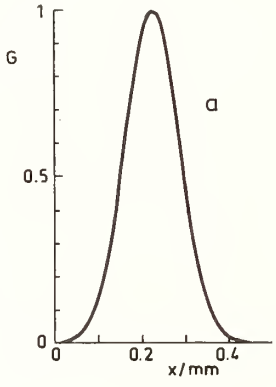

Figure 4.

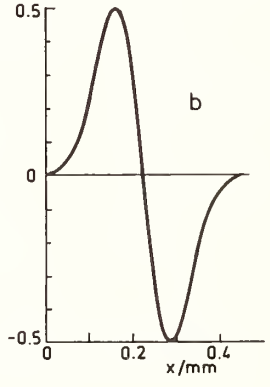

Figure 5.

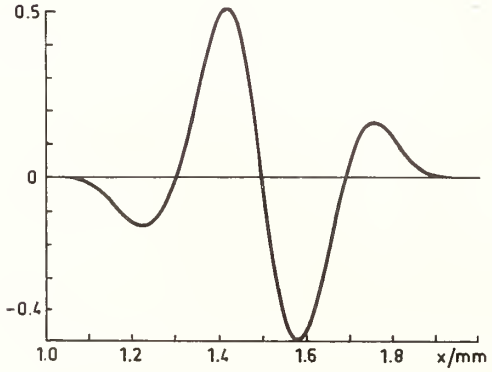

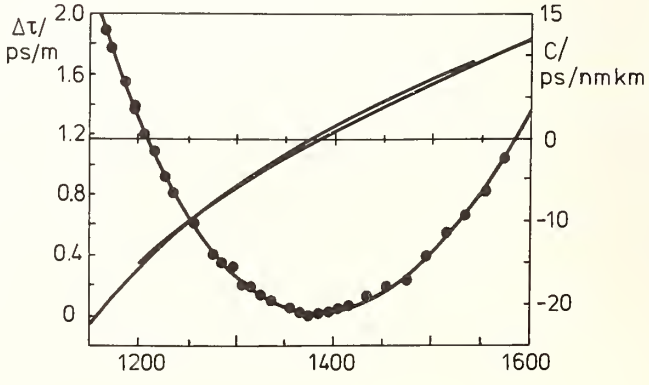

Comparison of chromatic dispersion measurements of single-mode optical fibers by spot-size and pulse delay method

H. Karstensen, L. Wetenkamp
c/o Institut fuer Hochfrequenztechnik, Techn. Univ., P.O. Box 3329
D-3300 Braunschweig ,Germany (Fed. Rep.)

Abstract

The chromatic dispersion of a single-mode fiber can be evaluated with good accuracy compared to a pulse delay measurement by measuring the wavelength dependence of the fundamental mode spot size. With the assumption of simple Gaussian field distributions the spot size is measured using the transverse offset method. For accurate material and profile dispersion data, the refractive index profile of the fiber and also the dopants should be known at least approximately.

Introduction

There is a growing interest in methods for chromatic dispersion measurements which are simple in use but of sufficient accuracy for practice. The most frequently used method is the measurment of the fundamental mode transit time at different wavelengths with a fiber Raman-laser. The dispersion is then given by the derivative of the transit time curve with respect to wavelength. This method has the advantage of high accuracy, but a rather expensive measurement apparatus is required. Recently, interferometric methods have been introduced which, however, either also need a fiber Raman-laser, or, in the case of white light interferometry, reqire extremely high precision adjustments.

As shown by Sansonetti /1/, it is also possible to determine the waveguide dispersion of a single-mode fiber from the spectral behaviour of the fundamental mode spot size. This theory has already been used to evaluate the dispersion of a single-mode fiber with a step-index profile /2/. However, compared to the total chromatic dispersion, in this case the waveguide dispersion was only small, and the final curve showed principally only the material dispersion.

Petermann /3/ extended the theory and took also profile dispersion into consideration. Moreover, his theory is valid for all field functions by defining a spot radius $\bar{w}$ (see eq.(3) of ref./3/), which in the case of Gaussian fields equals the spot radius w_o of $1/e^2$-intensity. With the assumption of linear profile dispersion the chromatic dispersion is given as superposition $\tau' = \tau'_M + \tau'_{WP}$ of material dispersion τ'_M and combined waveguide and profile dispersion τ'_{WP}. The material dispersion is obtained by weighting the dopant dependent material dispersion parameter M with the field intensity, and the expression for τ'_{WP} is given by

$$\tau'_{WP} = \frac{\lambda^{(2-\gamma)}}{2\pi^2 c\gamma} \frac{d}{d\lambda}\left[\frac{\lambda^{\gamma}}{n_1 \cdot \bar{w}^2}\right] \approx -\frac{\lambda}{\pi^2 \cdot c \cdot n_1 \cdot \bar{w}^2}\left[\frac{\lambda}{\gamma \cdot \bar{w}} \frac{d\bar{w}}{d\lambda} - \frac{1}{2}\right] \qquad (1)$$

with λ as wavelength, n_1 as refractive index of the core, and c as velocity of light in free space. The value of γ depends on the profile dispersion parameter P according to $\gamma = 2/(2-P)$.

Throughout this work we used Petermann's relations with the assumption of Gaussian field functions. We made measurements on four different fibers which all have a W-like profile obtained by a GeO_2-doped core with relative refractive-index difference $\Delta^+ = 0.6...0.7$ % and concentric F-doped index depression

around the core with a relative index difference $\Delta^- = -0.3...0.35$ %. Core radii were between 2.5 and 3.0 µm, the outer radii of the index depression ring between 5 and 7 µm. In order to determine τ'_M, we took the material dispersion data of the different fiber regions from literature, and weighted them with measured field distributions. At 1.3 µm wavelength nearly all field intensity is concentrated in the Germania doped fiber core, whereas at 1.8 µm approximately half of the power is guided in the core and the other half in the Fluorine doped ring and the cladding of fused silica. With dispersion data for 6.3 m% GeO_2 -doped silica /4/, for 2.0 m% F-doped silica /5/ and for quenched fused silica /6/, we approximated the material dispersion by the simple relation

$$\tau'_M = \frac{\lambda - 1.3\,\mu m}{\lambda} \cdot 125 \frac{ps}{km \cdot nm} \qquad (2)$$

To determine the profile dispersion we must consider the fact that the total refractive index difference $\Delta_t = \Delta^+ - \Delta^-$ is the essential parameter for the overall dispersion characteristic. With the data for the profile dispersion parameters of GeO_2- and F-doped silica from Adams /7/ we obtain

$$P(\lambda) = \frac{\lambda - 0.83\ \mu m}{6\ \mu m} \qquad (3)$$

as approximation for the wavelength dependent profile dispersion parameter.

Experimental results

The spot size of the fibers was measured with the transverse offset method which has, compared to other methods, the great advantage to detect all power transmitted through the fiber. As a drawback only Gaussian fields can be measured exactly, and it is nearly impossible to evaluate more general mode fields. The effect on our measurements was small: actual fields are very nearly Gaussian in shape and Gaussian approximation was used anyhow.

We made with each fiber four series of measurements within the wavelength region of approximately 1 to 1.8 µm. The spot size was measured in intervals of 50 nm with a repeatability of about ±1 %. Then the w_o-values were averaged and fitted to a polynomial by a least squares method. In Fig. 1 the resulting curves of the spot size w_o versus the wavelength λ are shown for fibers A,B,C and D. From these curves the waveguide dispersion was calculated with the help of eq.(1). In order to show the influence of the profile dispersion, we calculated the dispersion slopes for each fiber, one with P = 0 and the other with the profile dispersion according to eq.(3).

The dispersion characteristics of the fibers A to D, derived in this way, are shown in Figs. 2 to 5. In these Figures, τ'_M is the material dispersion, which is assumed to be the same for all fibers, τ'_1 the total chromatic dispersion including profile dispersion, and τ'_2 the chromatic dispersion without profile dispersion. Moreover, for comparison, the dispersion curve τ'_{PD}, evaluated by pulse delay measurements with a fiber Raman-laser, is shown for every fiber.

Discussion

Firstly, one can see from Figs. 2 to 5 a rather good conformity of the dispersion curves τ'_1 and τ'_2 from the spot size measurements with the dispersion τ'_{PD} from the pulse delay measurement. However, for fibers B and C the curve τ'_1 matches τ'_{PD} more closely, whereas for fibers A and D the curve for τ'_2 follows τ'_{PD} better. To understand this behaviour one has to consider the following: Differences could occur from slight measurement errors in determining $w_o(\lambda)$. Because τ'_{WP} is strongly dependent on $w_o(\lambda)$ itself and on the derivative of w_o with respect to λ, even small errors give rise to great deviations of the

dispersion curve. On the other hand there is a systematic error in our dispersion evaluation, because we approximated the mode field with a Gaussian curve. At shorter wavelengths, the Gaussian approximation holds very well, as shown in Figs. 6 a to h, where the autocorrelation curves of the fundamental mode field, as obtained by the transverse offset method, and the corresponding Gaussian fits of fiber D were plotted. Up to a wavelength of 1.5 µm the mode fields are very nearly Gaussian. At longer wavelengths, however, the mode field has tails, decaying much more slowly than the corresponding Gaussian fit. Therefore the actual spot size $\bar{w}$ is a little wider than the Gaussian spot size w_o. Moreover, the mode power decreases with longer wavelength, because the radiance of a tungsten lamp decreases with wavelength. Thus the measurement error increases, and in the longer wavelength region the measurements are less accurate than at shorter wavelength.

Possibly, the most important reason for the different dispersion characteristics evaluated by the two methods lies in the fact, that the pulse delay measurements are usually made on long length fibers. Thus, this measurement gives a dispersion characteristic averaged over the whole fiber length. On the other hand, in spot size measurements only few meters of fiber are needed, and the evaluated dispersion is valid only for this short piece of fiber. Thus, differences in the dispersion characteristics are inevitable, if the fiber is not completely homogeneous along the length. In addition to this even with ideal fibers differences could result from different curvature. To test the accuracy of this method more thouroughly, one should compare the given results withthe results of a dispersion measurement technique which uses the same short pieces of fiber, e.g. with an interference method.

Acknowledgement

We would like to thank Mrs. Schweitzer for the help in fiber preparation , our collegues of the university of Kaiserslautern, Dr. Klein and Mr. Lieber, for carrying out the pulse delay measurements, and our collegues of the technical university of Braunschweig, especially Mr. Jacob, for helpful discussions.

References

/1/ P.Sansonetti, Modal dispersion in single-mode fibres: simple approximation issued from mode spot size spectral behaviour, Electr. Lett. 18 (1982),647-648

/2/ J.P.Pocholle et al.,Determination of modal dispersion in monomode optical fibres from wavelength dependence of the mode spot size, Electr. Lett. 19 (1983),1093-1094

/3/ K.Petermann, Constraints for fundamental mode spot size for broadband dispersion-compensated single-mode fibres, Electr. Lett. 19 (1983),712-714

/4/ N.Shibata,T.Edahiro, Refractive-Index Dispersion for GeO_2-, P_2O_5- and B_2O_3-Doped Silica Glasses in Optical Fibers, Trans. IECE Japan E65 (1982),166-172

/5/ J.W.Fleming,D.L.Wood, Refractive index dispersion and related properties in fluorine doped silica, Appl. Opt. 22 (1983),3102-3104

/6/ J.W.Fleming,J.W.Shiever, Thermal History Dependence of Refractive Index Dispersion of Fused Silica, J. Am. Ceram. Soc. 62 (1979),526

/7/ M.J.Adams, An Introduction to Optical Waveguides, Interscience, Chichester 1981

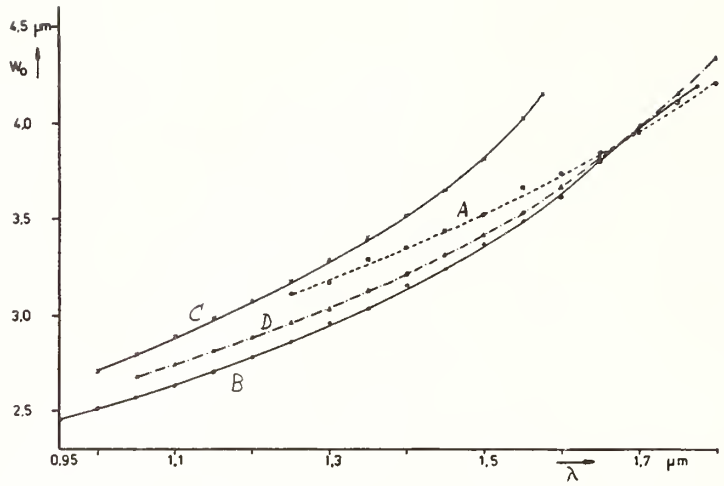

Fig. 1: Measured spot size w_o versus wavelength λ for fibers A, B, C and D

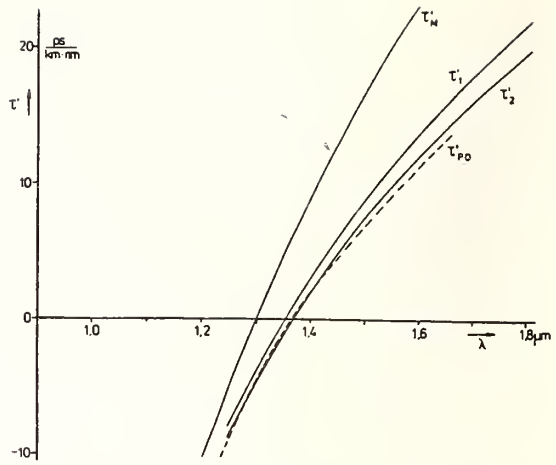

Fig. 2: Dispersion of fiber A versus wavelength (τ'_M = material dispersion, τ'_{PD} = dispersion from pulse delay measurement, τ'_1 = disp. from spot size measurement, τ'_2 = disp. from spot size measurement without profile disp.)

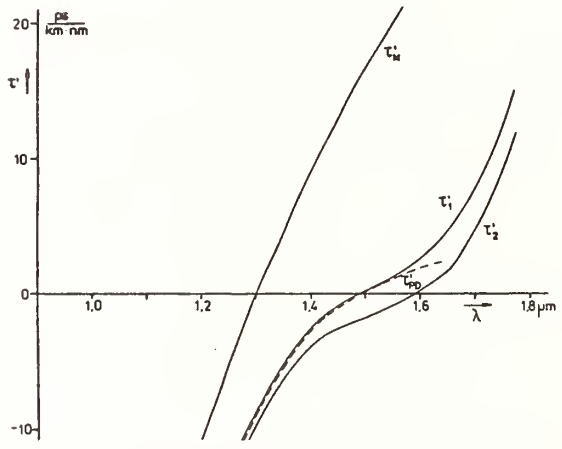

Fig. 3: Dispersion of fiber B versus wavelength (notation as in Fig. 2)

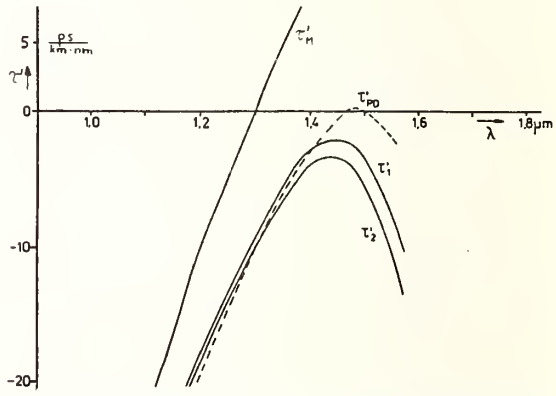

Fig. 4: Dispersion of fiber C versus wavelength (notation as in Fig. 2)

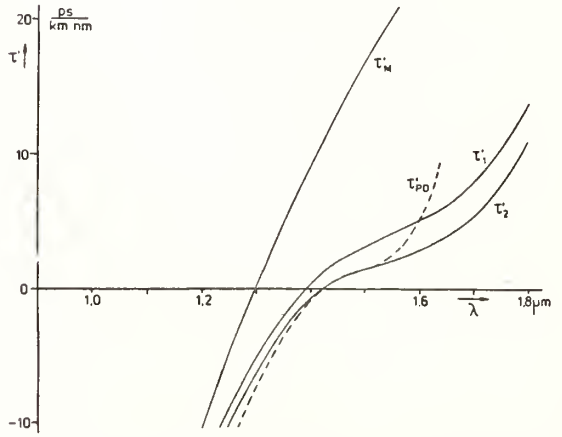

Fig. 5: Dispersion of fiber D versus wavelength (notation as in Fig. 2)

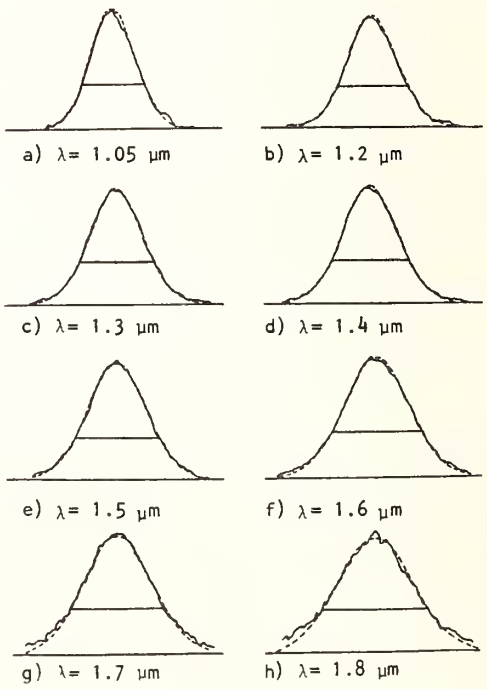

Fig. 6: a) - h) Measured autocorrelation curves of the field function of fiber D and corresponding Gaussian fit at different wavelength

Field Dispersion Measurements - A Swept Frequency Technique

R. Rao
Valtec, West Boylston, Massachusetts

Introduction

As transmission rates increase and WDM systems become operational, it is likely that the dispersion characteristics of long spans of single mode cable will have to be checked after installation. This will require dispersion measurement equipment capable of making field measurements.

Dispersion in single mode fibers is caused by the material and waveguide properties of the fiber. For long lengths of fiber, it can be determined from measuring the relative group delay through the fiber as a function of wavelength. Present laboratory techniques for doing this measurement are unsuitable for field use due to their complexity and equipment size.[1, 2] A variation of the fiber Raman system discussed in Reference [1] and a single frequency phase measurement[3, 4] have been suggested for field use. In this paper a swept frequency measurement system is described where group delay is determined from frequency domain data. This system has been developed specifically for field use and uses typical multimode frequency domain bandwidth test equipment.

Theory

The time shift Γ at a wavelength λ with respect to a reference wavelength which occurs due to the wavelength dependent group delay is given by the equation: $\Gamma = A + B\lambda^2 + C\lambda^{-2}$, where A, B and C are the fit parameters. The dispersion and zero dispersion wavelengths are obtained from this equation:

$$D(\lambda) = d\Gamma/d\lambda = 2B\lambda - 2C\lambda^{-3} \quad (1)$$

$$\lambda_0 = (C/B)^{1/4} \quad (2)$$

At least three wavelengths are required to find A, B and C.

Two lasers at different wavelengths are modulated in phase, combined, and launched into a fiber as one composite signal. The input and output signals may be described as

$$\text{Input:} \quad S_i(t) = A_i(\lambda_1)\,\text{Cos}\,(\omega t) + B_i(\lambda_2)\,\text{Cos}\,(\omega t) \quad (3)$$

$$\text{Output:} \quad S_o(t) = A_o(\lambda_1)\,\text{Cos}\,(\omega t) + B_o(\lambda_2)\,\text{Cos}\,(\omega[t+\Gamma]) \quad (4)$$

where $A_i(\lambda_1)$, $B_i(\lambda_2)$ and $A_o(\lambda_1)$, $B_o(\lambda_2)$ are the peak amplitudes of each component at the input and output respectively,

λ_1 is the reference wavelength, and $\omega = 2\pi f$ corresponds to the modulating frequency. In general, the peak amplitudes are also a function of the modulating frequency but this is being ignored here for the sake of simplicity in the discussion. From $S_0(t)$ the output spectra can be shown to be described by

$$S_0(\omega) = A_0(\lambda_1) + B_0(\lambda_2) \cos(\omega \Gamma) \quad (5)$$

The two signals at the output are 180^0 out of phase when the time shift, Γ is

$$\Gamma = nT_n + \frac{1}{2}T_n \text{ for } n = 0, 1, 2, 3 \text{ etc.} \quad (6)$$

where T_n is the period of the modulating frequency.

Substituting $T_n = \frac{1}{f_n}$ and simplifying we find

$$\Gamma = \frac{2n+1}{2f_n} \quad (7)$$

and

$$\Gamma = \frac{1}{f_{n+1} - f_n} = \frac{1}{\Delta f} \quad (8)$$

Minimas occur in the amplitude spectra of the output signal at frequencies where the signals are 180^0 out of phase. Γ is determined by locating consecutive frequencies at which this condition occurs.

Figure 1 schematically represents the measurement system. Three lasers with wavelengths at 1318 nm, 1265 nm and 1213 nm are used. For a measurement the 1265 or 1213 laser is modulated simultaneously with the 1318 laser. The lasers, drive electronics necessary to modulate two of the lasers in phase and optical couplers required to couple the signals comprise a field transportable transmitter. The receiver is a longwave analog receiver with a germanium APD.

Results

At present, data is taken manually by tuning the spectrum analyzer center frequency to out of phase frequencies. These frequencies are most easily discerned with the analyzer in the logarithmic mode. Typically measurements are made between 10 MHz to 500 MHz where the system has the best phase linearity. Each laser's phase is adjusted so that the maximum phase deviation between any two lasers is 5^0 at about 500 MHz. A fixed phase offset is added to the 1265 laser in order to bring 1318/1265 minimas to within 500 MHz and enable shorter lengths of cable ($\simeq$ 8 km) to be measured. $A_0(\lambda_1)$ is variable to allow adjustment of the amplitude of $S_0(\omega)$.
Figures 2a and 2b show the signals from 25 km of single mode fiber obtained by simultaneously modulating the 1318/1213 and 1318/1264 lasers respectively.

The separation of successive minima are clearly defined and agree to within 1 MHz. Γ is determined by averaging the minima separation Δf between 10 MHz and 500 MHz. Dispersion and zero dispersion wavelengths were computed from the delay data generated by a fiber Raman system and the swept frequency system for several fiber links of varying lengths. The agreement is better than .2 psec/nm/km for dispersion in the 1.20 nm to 1.55 nm region and 2 nm for the zero dispersion wavelengths (Table 1). The close agreement between the systems indicate that the error is small and accurate results are obtainable using three wavelengths for a measurement. Delay and dispersion curves computed from successive minima are shown in Figure 3. A detailed analysis of computed dispersion error as a function of frequency separation error is being done at present.

Conclusion

In conclusion, several features of the method are noted which make it especially suitable for field use.

1. Large dynamic ranges required for long lengths of cable are obtainable (>30 dB) because of the superior SNR of frequency domain techniques.
2. The technique enables measurements over widely varying lengths of cable without ignoring 360^{o} phase shifts which is possible with a single frequency phase measurement. Additionally, the laser wavelengths can be spaced far apart increasing the relative delay, reducing the effects of laser wavelength instabilities and thereby enhancing measurement accuracy.
3. A trigger signal or reference is not required for the spectrum analyzer as is required for time domain or a single frequency phase measurement.
4. All the equipment, except for the single mode laser transmitter, may be used for field multimode bandwidth measurements.

Acknowledgement

The author wishes to thank Dr. W. Meixner and Dr. I. Aggarwal for useful discussions and encouragement and, Dr. R. Sierra for Raman fiber dispersion measurements.

References

1. L.G. Cohen and C. Lin, Appl. Opt. 16, 3136 (1977)
2. K. Daikoku and A. Sugimura , Electron. Lett. 14, 326 (1978)
3. C. Lin, A.R. Tynes, A. Tomita, P. L. Liu, and D.L. Philen, Bell Syst. Tech. J. 62, 457 (1982)
4. P.J. Vella, P.M. Garet-Jones, and R.S. Lowe, Tech. Digest, Topical Meeting in Optical Fiber Communication (Optical Society of America, New Orleans, LA (1984), Paper TUN15

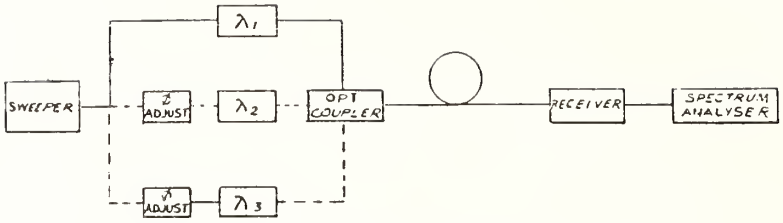

FIGURE 1. Swept frequency measurement system. λ_1 is modulated simultaneously with λ_2 or λ_3.

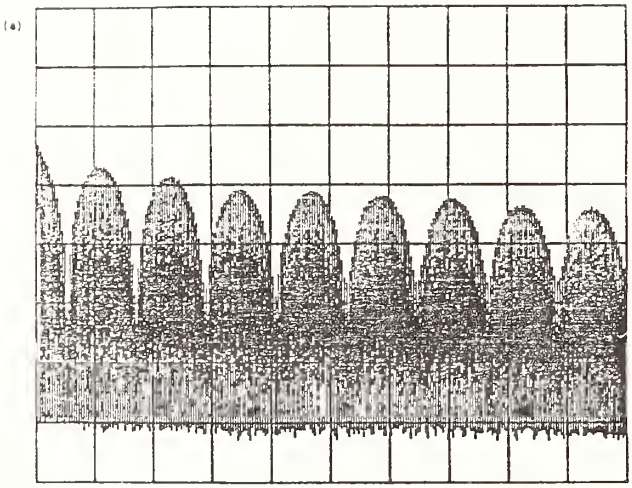

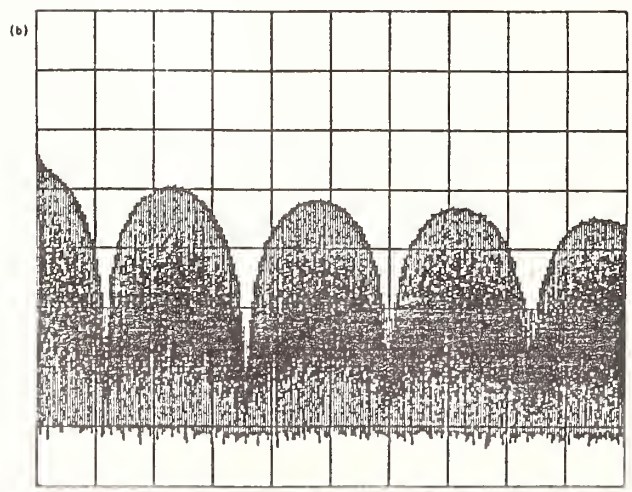

FIGURE 2. Frequency Spectra from 25 km of Fiber with (a) 1318/1213 Modulation (b) 1318/1265 Modulation

Scale: Vertical 10 dB/div
Horizontal 50 MHz/div. Center Frequency 250 MHz

λ	Dispersion (PS/nm-km) Swept Frequency	Fiber Raman
1.285	-4.4	4.2
1.300	3.1	-3.0
1.330	-0.7	-0.6
1.390	3.6	3.7
1.500	10.4	10.3
1.550	13.0	12.9
	Zero Dispersion Wavelength	
λ_0	1.339 μm	1.338 μm

TABLE 1 A comparison of dispersion and zero dispersion wavelength data obtained using the swept frequency system and a fiber Raman system.

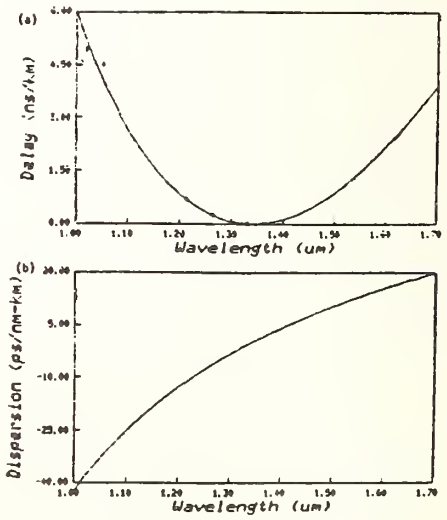

FIGURE 3. (a) Delay vs. λ and (b) dispersion vs. λ as computed from swept frequency system data

INDEX OF AUTHORS

NBS-114A (REV. 2-8C)

U.S. DEPT. OF COMM. BIBLIOGRAPHIC DATA SHEET (See instructions)	1. PUBLICATION OR REPORT NO. NBS SP-683	2. Performing Organ. Report No.	3. Publication Date October 1984

4. TITLE AND SUBTITLE

Technical Digest - Symposium on Optical Fiber Measurements, 1984

5. AUTHOR(S)

G. W. Day and D. L. Franzen

6. PERFORMING ORGANIZATION (If joint or other than NBS, see instructions)

NATIONAL BUREAU OF STANDARDS
DEPARTMENT OF COMMERCE
WASHINGTON, D.C. 20234

7. Contract/Grant No.

8. Type of Report & Period Covered

9. SPONSORING ORGANIZATION NAME AND COMPLETE ADDRESS (Street, City, State, ZIP)

Sponsored by the National Bureau of Standards in cooperation with the IEEE Optical Wave Guide Communications Committee and the Optical Society of America

10. SUPPLEMENTARY NOTES

Library of Congress Catalog Card Number: 84-601092

☐ Document describes a computer program; SF-185, FIPS Software Summary, is attached.

11. ABSTRACT (A 200-word or less factual summary of most significant information. If document includes a significant bibliography or literature survey, mention it here)

This volume contains summaries of 31 papers presented at the Symposium on Optical Fiber Measurements held October 2-3, 1984, at the National Bureau of Standards, Boulder, Colorado. Subjects include measurements on singlemode fiber, multimode fiber, fiber designed for sensing applications, instrumentation, field measurements, and standards.

12. KEY WORDS (Six to twelve entries; alphabetical order; capitalize only proper names; and separate key words by semicolons)

fiber optics; fiber optics-multimode; fiber optics-singlemode; instrumentation; measurements; optical fiber sensors

13. AVAILABILITY

☒ Unlimited

☐ For Official Distribution. Do Not Release to NTIS

☒ Order From Superintendent of Documents, U.S. Government Printing Office, Washington, D.C. 20402.

☐ Order From National Technical Information Service (NTIS), Springfield, VA. 22161

14. NO. OF PRINTED PAGES 148

15. Price

☆U.S. GOVERNMENT PRINTING OFFICE: 1984-780-574/9435

NBS TECHNICAL PUBLICATIONS

PERIODICALS

JOURNAL OF RESEARCH—The Journal of Research of the National Bureau of Standards reports NBS research and development in those disciplines of the physical and engineering sciences in which the Bureau is active. These include physics, chemistry, engineering, mathematics, and computer sciences. Papers cover a broad range of subjects, with major emphasis on measurement methodology and the basic technology underlying standardization. Also included from time to time are survey articles on topics closely related to the Bureau's technical and scientific programs. As a special service to subscribers each issue contains complete citations to all recent Bureau publications in both NBS and non-NBS media. Issued six times a year. Annual subscription: domestic $18; foreign $22.50. Single copy, $5.50 domestic; $6.90 foreign.

NONPERIODICALS

Monographs—Major contributions to the technical literature on various subjects related to the Bureau's scientific and technical activities.

Handbooks—Recommended codes of engineering and industrial practice (including safety codes) developed in cooperation with interested industries, professional organizations, and regulatory bodies.

Special Publications—Include proceedings of conferences sponsored by NBS, NBS annual reports, and other special publications appropriate to this grouping such as wall charts, pocket cards, and bibliographies.

Applied Mathematics Series—Mathematical tables, manuals, and studies of special interest to physicists, engineers, chemists, biologists, mathematicians, computer programmers, and others engaged in scientific and technical work.

National Standard Reference Data Series—Provides quantitative data on the physical and chemical properties of materials, compiled from the world's literature and critically evaluated. Developed under a worldwide program coordinated by NBS under the authority of the National Standard Data Act (Public Law 90-396).

NOTE: The principal publication outlet for the foregoing data is the Journal of Physical and Chemical Reference Data (JPCRD) published quarterly for NBS by the American Chemical Society (ACS) and the American Institute of Physics (AIP). Subscriptions, reprints, and supplements available from ACS, 1155 Sixteenth St., NW, Washington, DC 20056.

Building Science Series—Disseminates technical information developed at the Bureau on building materials, components, systems, and whole structures. The series presents research results, test methods, and performance criteria related to the structural and environmental functions and the durability and safety characteristics of building elements and systems.

Technical Notes—Studies or reports which are complete in themselves but restrictive in their treatment of a subject. Analogous to monographs but not so comprehensive in scope or definitive in treatment of the subject area. Often serve as a vehicle for final reports of work performed at NBS under the sponsorship of other government agencies.

Voluntary Product Standards—Developed under procedures published by the Department of Commerce in Part 10, Title 15, of the Code of Federal Regulations. The standards establish nationally recognized requirements for products, and provide all concerned interests with a basis for common understanding of the characteristics of the products. NBS administers this program as a supplement to the activities of the private sector standardizing organizations.

Consumer Information Series—Practical information, based on NBS research and experience, covering areas of interest to the consumer. Easily understandable language and illustrations provide useful background knowledge for shopping in today's technological marketplace.

Order the **above** *NBS publications from: Superintendent of Documents, Government Printing Office, Washington, DC 20402.*

Order the **following** *NBS publications—FIPS and NBSIR's—from the National Technical Information Service, Springfield, VA 22161.*

Federal Information Processing Standards Publications (FIPS PUB)—Publications in this series collectively constitute the Federal Information Processing Standards Register. The Register serves as the official source of information in the Federal Government regarding standards issued by NBS pursuant to the Federal Property and Administrative Services Act of 1949 as amended, Public Law 89-306 (79 Stat. 1127), and as implemented by Executive Order 11717 (38 FR 12315, dated May 11, 1973) and Part 6 of Title 15 CFR (Code of Federal Regulations).

NBS Interagency Reports (NBSIR)—A special series of interim or final reports on work performed by NBS for outside sponsors (both government and non-government). In general, initial distribution is handled by the sponsor; public distribution is by the National Technical Information Service , Springfield, VA 22161, in paper copy or microfiche form.

U.S. Department of Commerce
National Bureau of Standards

Washington, D.C. 20234
Official Business
Penalty for Private Use $300

POSTAGE AND FEES PAID
U S DEPARTMENT OF COMMERCE
COM-215

SPECIAL FOURTH-CLASS RATE
BOOK